

Managing Manganese: The Corporate Duties of MntR in Regulating Metal Ion
Homeostasis

A Thesis
Presented to
The Established Interdisciplinary Committee for
Biochemistry and Molecular Biology
Reed College

In Partial Fulfillment
of the Requirements for the Degree
Bachelor of Arts

Vilmante Kodyte

May 2024

Approved for the Committee
(Biochemistry and Molecular Biology)

Shivani Ahuja

Acknowledgements

My growth as a scientist and thinker, in addition to this thesis, would not have been possible without the dedication and endless support of my thesis advisor, Shivani Ahuja. Thank you for your encouragement and the doors you have opened for me. From professing my first in-person science lecture at Reed to letting me whisk off away to study biochemistry in Scotland, you have made my experience learning this discipline so special. Thank you for welcoming me into your research, trusting me to frolic around in the lab over my junior summer while you were away (I swear we behaved), and for being ever-present and patient during the tumultuous, slam-into-the-wall moments that inevitably arise during undergraduate research. Your mentorship will stay with me long after Reed.

Thank you to Arthur Glasfeld for being the goofiest chemistry professor I have gotten the chance to study under. And, of course, for all of the endless emails I have sent, asking about a step of a protocol (or the whole thing), and you always being willing to lend a hand in support. I dearly miss you, and thank you for making my organic chemistry experience a little less daunting.

Thank you to Meg Scharle, who completely opened the door to the field that is the next chapter of my academic life. Your class changed the way I view the obligations I hope to one day have as a future clinician. I got the chance to see you passionately lead changes at the faculty level to make our community a better place, a more encouraging academic space for students to thrive and have their achievements be recognized. Thank you for your advocacy and for listening to what I had to say. Your unwavering support and excitement leave me bewildered with the sheer luck I have in getting to meet you and study under you.

To Lexi Neame, for inspiring me to develop my seedling interests into practical and interesting ideas. For your enthusiasm to always be learning something new, and for your grounded, say-it-like-it-is attitude. You are one of

the most brilliant professors I have gotten the chance to learn from. Thank you for your belief in me, which, at times, I was losing sight of.

To Anand Vaidya, for inspiring me to think critically about scientific work in a way I have never conceived of before. For exemplifying the way I would love to teach one day. To Anna Ritz, for inspiring my curiosity for cancer science and for your insane ability to distill complicated computational methods and math down to digestible bits. Your seminar class was one of my favorite classes at Reed. Thank you for such a fun writing project and for your endless happy-go-lucky charm. To Nicole James, for being the professor I feel the most comfortable making a mistake in front of. Your kindness and your willingness to keep the student experience at the core of your teaching has been so inspiring. Thank you for your dedication, patience, and absolute kindness.

To my pool hall crew, for growing and learning the top tier hustling sport with me through these years. I have spent countless Thursday nights in those four walls, and it's been so cherishing to see you all grow your love for the game. Maya and Eden, for crushing pool management. And to the pool hall, in general. You were my favorite place to waste time. You were the place I found my favorite person.

Thank you to the communities I have had the chance to be a part of, since the start and only recently. To my pre-health Reedies, you can do Reed and go to medical school. Don't let anyone tell you otherwise! The trenches end, if only briefly, and you'll be so wickedly smart at the end of this. Keep pushing; I believe in you. To my frisbee mates, thank you for an incredible semester. I wish I would have joined earlier!

To my dear friends. Emilie, you have been my go-to since day 1. Thank you for this crazy journey we have been on together, taking us across the sea even. I wish you the brightest future and I am cheering you on as you one day get to don that white coat. I hope to see you there. Ethan and Rainie, y'all are hilarious. Thank you for always helping me feel grounded and inspiring me with your insane science brains. Aidan and Milo, you both were the best OWLs I could have trained with. I am so grateful for our friendship through the years, and the next Guinness is on me! To Cam, thank you for being a good friend to me, for all of the poker nights, and for your pool hall comradery. Maybe one day

our paths in Boston will cross. Mattia, for being so stupidly silly and brilliant, all wrapped in one. You never failed to give a listening ear, and it's been amazing to know someone like you.

Thank you to my lab mates for answering my endless questions and all around making thesis a more joyful experience. Especially you, Mack. You were my rock in more ways than may be obvious. Thank you for being my lab neighbor and buddy.

Thank you to my parents, who have been cheering me on since day one. For encouraging me to push my limits, since you knew I was always capable and could achieve more. To my family across the water, I miss you, I love you, I wish you were here, or I was there.

To the Kleins, for welcoming me with the most open arms. To Josh, for making me feel like I am the luckiest girl in the world. I love you and I love the life we have built together. I am so excited to move worlds with you (again).

To Sweetpea, for your exorbitant fluff and sassy attitude. You brought a smile to my face every time I took a break from writing. Welcome to the family. I'm sorry I pick you up so often. May you find that paper ball under the couch one day.

And thank you to the person reading this. This thesis has helped me realize how capable I am, how much I have learned during this experience and during my time at Reed, and to really, *really* have a full introduction finished by the due date Shivani assigned me. Write early, write everything down. And never lose sight of why you're doing this.

List of Abbreviations

ABC transporter	ATP-Binding Cassette Transporter
CDF	Cation-Diffusion Facilitator
CFSE	Crystal Field Stabilization Energy
FSEC	Fluorescence Size Exclusion Chromatography
IPTG	Isopropyl- β -D-Thiogalactopyranoside
MntR	Manganese Transcription Regulator
NRAMP	Natural Resistance-Associated Macrophage Protein
PCR	Polymerase Chain Reaction
PLL	Poly-L-Lysine
RNAP	RNA Polymerase
ROS	Reactive Oxygen Species
SEC	Size Exclusion Chromatography
SOD	Superoxide Dismutase

Table of Contents

Introduction	1
Use of Metals in the Biological Chemistry of Living Systems.....	2
Role of Mn ⁺² in Bacteria.....	2
Role of Mn ⁺² in Combatting ROS Burst during Bacterial Pathogenesis.....	3
Metalloregulators.....	6
MntR: Structure and Function	9
MntR, a Mn ⁺² sensing protein.....	13
Transcriptional Role of MntR.....	15
Transcription	16
MntR binds to mneP promoter region.....	20
Mutations to MntR.....	22
Tyrosine to Alanine at Site 22.....	23
Aspartic acid to Alanine at Site 27	25
Tyrosine to Alanine at Site 57.....	29
Size Exclusion Chromatography	31
Mass Photometry	31
Thesis Aims.....	35
Methods	37
Site-directed Mutagenesis of MntR plasmid pSMT3.....	37
Growth Conditions for MntR Mutants	40
Expression testing of MntR mutants using FSEC	41
Large Scale Purification of Mutant MntR.....	43
Mass Photometry experiments to determine complex formation	44
Results and Discussion	47
Mutagenesis, Amplification, and Purification.....	47
FSEC of MntR Mutants	47
Tyr57Ala MntR Purification	49
Tyr22Ala MntR Purification	55

Asp27Ala MntR Purification	59
Mass Photometry and FSEC of Wild Type or Mutant MntR, and DNA	63
Tyr57Ala – MntR DNA coordination.....	66
Tyr22Ala—Inter-dimer stabilization	69
Asp27Ala – Intra-dimer coordination.....	71
Proposed mechanism of MntR activation of mneP expression.....	75
Conclusions and Future Directions.....	79
Appendix A: MntR Mutagenesis Reaction Protocols	81
Bibliography	85

List of Tables

Table 1. Amino acid sequence of the MntR encoding region of the pSMT3 plasmid	37
Table 2. Primer Sequences for MntR Mutagenesis Reactions.....	38
Table 3. List of sample components used for mass photometry experiments.....	45
Table 4: TALON Co ⁺² IMAC Protein Concentrations for Tyr57Ala MntR Purification.....	51
Table 5: Reverse Ni ⁺² NTA IMAC Protein Concentrations for Tyr57Ala MntR Purification (First Attempt)	53
Table 6: Reverse Ni ⁺² NTA IMAC Protein Concentrations for Tyr57Ala MntR Purification (Second Attempt)	54
Table 7: TALON Co ⁺² IMAC Protein Concentrations for Tyr22Ala MntR Purification.....	57
Table 8: Reverse Ni ⁺² NTA IMAC Protein Concentrations for Tyr22Ala MntR Purification.....	58
Table 9: TALON Co ⁺² IMAC Protein Concentrations for Asp27Ala MntR Purification.....	61
Table 10: Reverse Ni ⁺² NTA IMAC Protein Concentrations for Asp27Ala MntR Purification.....	62
Table A1. Q5 Site Directed Mutagenesis PCR Reagents	81
Table A2. Q5 Site Directed Mutagenesis PCR Thermocycler Conditions	81
Table A3. KLD Incubation Reaction Reagents and Protocol	81
Table A4. Qiagen MiniPrep Protocol for Plasmid Purification	82
Table A5. Sanger Sequencing Reaction Components	83

List of Figures

Figure 1. Schematic showing process of bacterial spore formation.....	2
Figure 2. Superoxide dismutase reaction to neutralize superoxide anions.	5
Figure 3. Depicting Irving-William Series relationship and trends between transition metal ions.	8
Figure 4. Color-coded Structure of MntR homodimer.	9
Figure 5. Mn(II) mediated DNA-binding of MntR.	10
Figure 6. Metal-binding sites A and C in MntR.....	11
Figure 7. Asp8Met mutation in MntR Site A metal-binding site.	12
Figure 8. MntR bound to P84 DNA sequence.....	16
Figure 9. Structure of <i>B. subtilis</i> RNA Polymerase bound to DNA.	17
Figure 10. Process of transcription by RNA Polymerase.	18
Figure 11. LacL binds to the Lac operator to repress transcription of downstream genes.....	19
Figure 12. RNAP bound to DNA duplex, occupied by four MntR dimers.	21
Figure 13. Comparison of DNA P106 and P84 constructs.	22
Figure 14. Amino acid structures of tyrosine and alanine.	23
Figure 15. Tyrosine residues at site 22 of MntR.....	24
Figure 16. Tyr22 ion-dipole interaction with Glu59.....	25
Figure 17. Amino acid structure of aspartic acid.	26
Figure 18. Aspartic acid residues at site 27 of MntR.....	27
Figure 19. Asp27 engages in a series of salt bridges.	28
Figure 20. Tyrosine residues at site 57 of MntR.....	29
Figure 21. Tyr57 is situated within the DNA minor groove.....	30
Figure 22. Mass Photometry data collection example.	33

Figure 23. Illustration of site-directed mutagenesis PCR.	39
Figure 24. FSEC Chromatogram for Histidine fluorescence of MntR mutants pre- and post-IPTG induction.....	48
Figure 25. SDS-PAGE gel showing SUMO-Tyr57Ala MntR complex following TALON Co ⁺² IMAC column purification	50
Figure 26. SDS-PAGE gel showing uncleaved SUMO-Tyr57Ala MntR following TALON Co ⁺² and Reverse Ni ⁺² IMAC column purifications.....	52
Figure 27. SDS-PAGE gel showing cleaved Tyr57Ala MntR following second Reverse Ni ⁺² IMAC column purification	55
Figure 28. SDS-PAGE gel showing SUMO-Tyr22Ala MntR complex following TALON Co ⁺² IMAC column purification	56
Figure 29. SDS-PAGE gel showing cleaved Tyr22Ala MntR following second Reverse Ni ⁺² IMAC column purification	59
Figure 30. SDS-PAGE gel showing SUMO-Asp27Ala MntR complex following TALON Co ⁺² IMAC column purification	60
Figure 31. SDS-PAGE gel showing cleaved Asp27Ala MntR following second reverse Ni ⁺² IMAC column purification	63
Figure 32. Mass photometry chromatogram showing differences in complexing between P84 DNA duplex and WT mutant or MntR mutant.	64
Figure 33. FSEC chromatogram showing complexing behavior between P84 DNA duplex and WT MntR.	65
Figure 34. Mass photometry chromatogram showing complexing behavior between P84 DNA duplex and Tyr57Ala MntR mutant.	66
Figure 35. FSEC chromatogram showing complexing behavior between P84 DNA duplex and Tyr57Ala MntR mutant.	67
Figure 36. Mass photometry chromatogram showing complexing behavior between P84 DNA duplex and Tyr22Ala MntR mutant.	69
Figure 37. FSEC chromatogram showing complexing behavior between P84 DNA duplex and Tyr22Ala MntR mutant.	70

Figure 38. Mass photometry chromatogram showing complexing behavior between P84 DNA duplex and Asp27Ala MntR mutant using PLL-coated plates.	71
Figure 39. Mass photometry chromatogram showing complexing behavior between P84 DNA duplex and Asp27Ala MntR mutant on normal glass plates.	73
Figure 40. FSEC chromatogram showing complexing behavior between P84 DNA duplex and Asp27Ala MntR mutant.	74
Figure 41. Proposed mechanism of <i>mneP</i> activation by MntR.	76

Abstract

Manganese homeostasis is essential for bacterial virulence. Manganese transcription regulator (MntR) from *Bacillus subtilis* controls the transcription of both Mn⁺² importers (MntH and MntABCD) and exporters (MneP and MneS), and the molecular mechanism for this delicate dual control is of great interest. Each monomer of MntR (142 residues, 16.7 kDa) binds two Mn⁺², which greatly increases its affinity for DNA. It has been shown that MntR binds cooperatively to four binding sites upstream of the transcription start site to induce the expression of manganese efflux transporters. Furthermore, the first MntR binding site overlaps with the RNA Polymerase recognition sequence, suggesting that some interaction between these two proteins likely contributes to the specified activation of MneP expression by MntR.

To better understand both cooperative binding and transcriptional activation, three mutations were made to highly conserved residues in MntR. These mutations aimed to disrupt intra-dimer stability, inter-dimer coordination, and MntR:DNA complexation. Mass photometry was used to investigate the oligomeric state of the assembled complexes, consisting of (mutant or wild type) MntR and a DNA duplex containing four MntR binding sites. Preliminary data suggest that inter-dimer and MntR:DNA contacts are essential for a 4 MntR:1 DNA complex to form, and this is the most stable minimum oligomer state for this complex.

Future investigations should aim to study complex formation between MntR, RNA Polymerase, an adjoining sigma factor, and a DNA duplex containing the RNA Polymerase binding site and transcription start site, in addition to the four MntR binding sites. These studies should seek to identify possible oligomeric states, using both mass photometry and cryo-EM as possible techniques. This will help further elucidate the mechanism of transcriptional activation by MntR.

Introduction

Metals are essential micronutrients for nearly all forms of life. The careful regulation of the kind of ions and their concentration within and between cells is a vital factor in maintaining homeostasis. In the bacteria *Bacillus subtilis* (*B. subtilis*), which is used as a model organism for studying how bacteria regulate the homeostasis of metal ions, manganese (Mn^{+2}) is one metal that is maintained as a cation in the reducing environment at concentrations up to 0.5 mM. Broadly, Mn^{+2} is used by up to 40% of enzymes of the bacterial cytoplasm (Helmann, 2014). The impact of Mn^{+2} levels is widespread across the cell, playing central roles in photosynthesis, nitrogen fixation, and other steps in elemental cycling. Crucially, the ability to sequester metal ions from the environment and export excess ions is vital to the pathogenesis of various bacterial species (Huang et al., 2017). Therefore, the study of metal ion homeostasis is an essential task in seeking to better understand bacterial survival and virulence. This thesis aims to elucidate this process by studying a bacterial manganese transcription regulator (MntR), a highly conserved metalloregulatory protein. While MntR has been shown to regulate Mn^{+2} homeostasis through transcription of both Mn^{+2} importers (MntH and MntABCD) and exporters (MneP and MneS), how this is molecularly achieved is unclear. Through mutagenesis experiments and mass photometry experiments, the present thesis helps to elucidate the molecular mechanism of transcription activation of Mn^{+2} exporters by MntR.

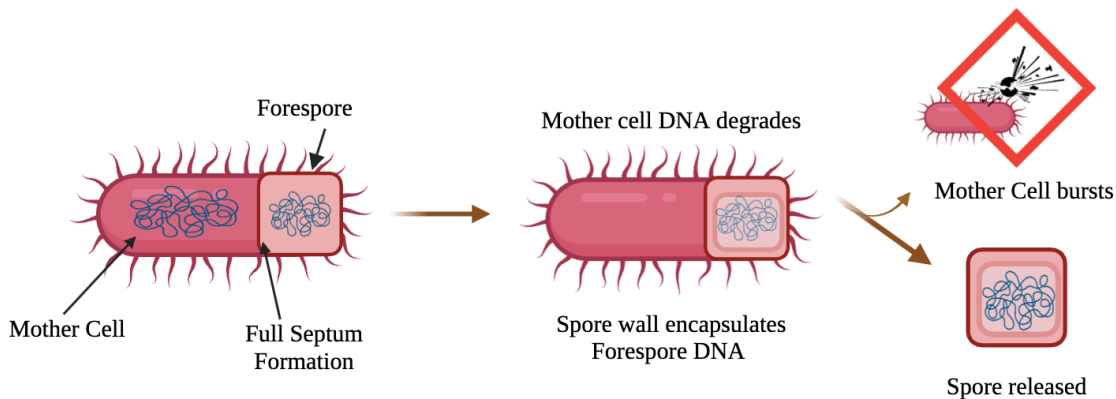
Use of Metals in the Biological Chemistry of Living Systems

All cells use transition metals (e.g., manganese, iron, zinc, and copper) to regulate essential functions for life. Mn^{+2} is one such metal-ion that is required for central metabolism, oxidative stress resistance, replication, and elemental cycling.

Role of Mn^{+2} in Bacteria

Mn^{+2} supports many essential functions in bacterial cellular physiology. Foremost, Mn^{+2} influences *B. subtilis* spore composition, structure, and germination. Spores are considered the most dormant form of bacteria. They have thick cell walls and minimally undergo metabolism and cellular respiration. Producing spores is one survival mechanism bacteria utilize in response to stress conditions.

Figure 1. Schematic showing process of bacterial spore formation.



Classic bacterial cell division is generally symmetric, where each sister cell receives a relatively equal amount of nutrients, organelles, and a full copy of the genome. However, in response to stressful conditions, bacteria cells will switch to asymmetric cell division, spurred by varying concentrations of regulatory proteins in the bacterial cytoplasm, causing a polar septum to form on one side of the bacterium (Kysela et al., 2013). In switching from symmetric to asymmetric cell division, SpoIIE serine phosphatase influences polar septum formation from

the initial medial composition, which changes the direction of synthesis of peptidoglycan, a predominant structure comprising the bacterial cell wall. Mn⁺² accumulated in the forespore serves as a cofactor for SpoIIE serine phosphatase. Separately, this phosphatase also activates σ^F , a transcription factor that initiates the transcription of key genes in the forespore, by dephosphorylating SpoIIAA (Partridge et al., 1991). As such, it has been suggested that Mn⁺² also regulates σ^F activation by SpoIIE (Jacubovics et al., 2001).

Following septation, the forespore environment drops by 1 unit in pH, which causes the dissociation of the essential Mn⁺² cofactor from 3-phosphoglycerate mutase (Jacubovics et al., 2001). The developing *Bacillus* forespore then accumulates 3-phosphoglyceric acid, which is metabolized shortly following germination. The budding endospore begins to form inner and outer layers of the spore coat, which requires manganese-cofactored superoxide dismutase. Following a rapid increase in pH, the spore begins to germinate, activating 3-phosphoglycerate mutase and mobilizing 3-phosphoglyceric acid reserves. Mn⁺² and increased levels of Mn⁺² dependent pyrophosphatases stimulate protease production as the spore exits the bacterial cytoplasm, following a burst of metabolic activity.

Role of Mn⁺² in Combatting ROS Burst during Bacterial Pathogenesis

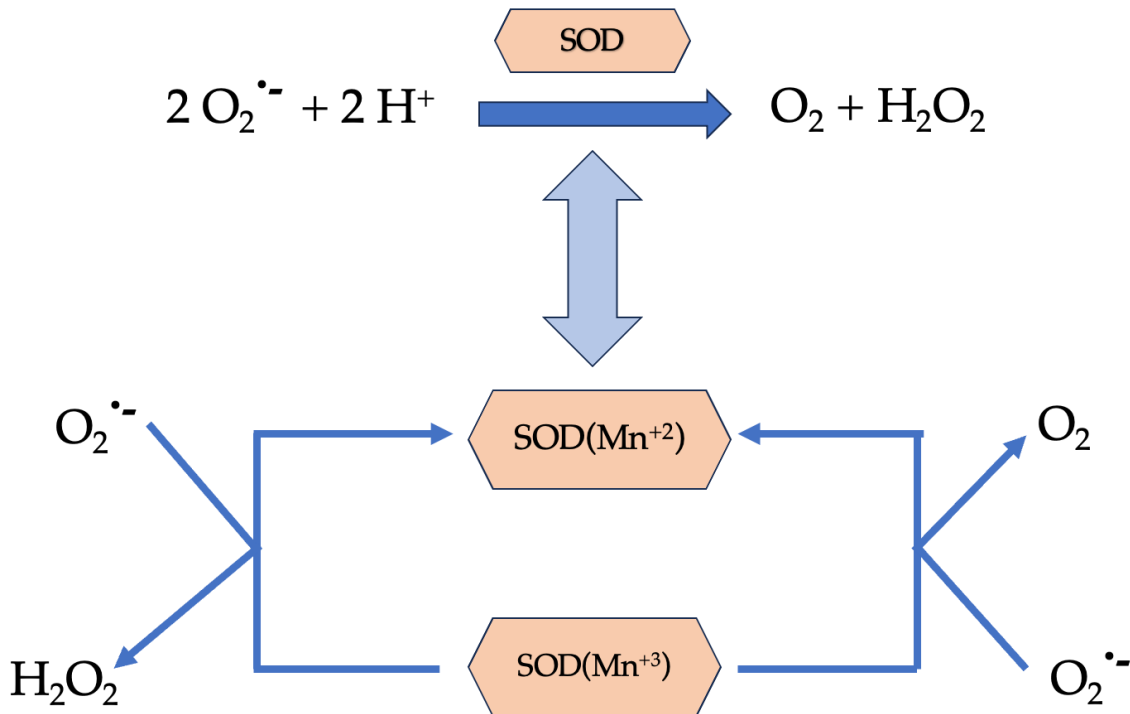
Mn⁺² also detoxifies reactive oxygen species (ROS), which otherwise would threaten the viability of the bacterial cell. ROS, such as O₂^{•-}, H₂O₂, and hydroxyl radicals, can arise endogenously, through aerobic respiration, or exogenously, through human immune cells, or both (Gozzi et al., 2017). In aerobic respiration, flavoproteins in the mitochondria of human cells can transfer one electron at a time in a reaction, which may be leaked to oxygen, the final electron acceptor in the Krebs cycle. Ultimately, the monovalent reduction of oxygen produces ROS (Turrens, 2003). The mitochondrion simultaneously exhibits various antioxidant defenses to help eliminate superoxide anions and hydrogen peroxide, but ROS may escape these strategies.

Host immune cells also execute a process termed oxidative burst, where they trap pathogens in the phagosome and inundate the pathogens with ROS. Oxidative burst damages biomolecules like proteins and DNA. For instance, changing the intracellular environment to an oxidative state thereby oxidizes cysteine residues of proteins. They can then create disulfide linkages amongst cysteine residues, which leads to protein aggregation and cell death (Tikhomirova et al., 2024).

Furthermore, ROS species can directly produce single strand and double strand breaks in bacterial DNA. Upon creating single strand breaks, ROS incite what is known as the SOS pathway, which activates genes that contribute to DNA damage repair. Through nucleotide excision repair, homologous recombination, and translesional DNA synthesis, SOS activation often leads to increased rates of spontaneous mutation, primarily due to the upregulated activity of error-prone polymerases, as well as chromosome rearrangements. Therefore, all bacteria have developed a mechanism in defending against ROS, namely through superoxide dismutase(s) (SOD), catalases and peroxidases.

The most well-established Mn-sensing strategy to minimize oxidative stress is MnSOD, to which Mn^{+2} serves as a primary cofactor. SOD catalyzes the conversion of superoxide radicals into molecular oxygen and hydrogen peroxide.

Figure 2. Superoxide dismutase reaction to neutralize superoxide anions.



Alternatively, several lactic acid bacteria incorporate a high concentration of Mn⁺² in place of MnSOD, since Mn-containing compounds can react with ROS without generating deleterious free radical species like free Fe⁺² does (Inaoka et al., 1999). The exact mechanism for how high intracellular Mn⁺² levels scavenge O₂^{·-} is not fully understood, but it does seem to require considerably higher levels of Mn⁺² than MnSOD otherwise would. While many *E. coli* incorporate multiple other SOD activities to defend against ROS, *B. subtilis*, most streptococci, and enterococci seem to only use MnSOD (Inaoka et al., 1999). Furthermore, one explanation for reduced virulence of bacteria that have impaired Mn⁺² uptake systems is their inability to minimize oxidative stress (Jacubovics et al., 2001).

Metalloregulators

As a divalent cation, manganese is present at overall average concentrations in bacteria that may approach 0.5 mM in the reducing environment of the cell's cytoplasm (Helmann, 2014). Although essential for growth and survival, too high of a concentration of essential metals can be toxic. And yet, bacteria sequester metal ions that are crucial for enzyme function and for key reactions to occur. Nutritional immunity is a strategy executed by hosts to starve bacteria of essential metal ions. As such, a co-evolution of metal ion sequestration strategies has emerged for both host and bacterial defenses (Murdoch et al., 2022). The ability to delicately balance the levels of manganese, as well as other metals inside the cell, is a critical aspect to a host's nutritional immunity and bacterial virulence and is regulated by metal sensory proteins called metalloregulators or metalloenzymes (Huang et al., 2017; Helmann, 2014). Insights into how bacteria regulate intracellular levels of manganese and other key metals in response to availability and demand is of great interest.

Foremost, nearly all forms of life require iron (Fe^{+2}), and where the need for iron has been abolished, living organisms have an absolute requirement for manganese. For example, in *Borrelia burgdorferi*, manganese has replaced iron in all essential metabolic functions (Glasfeld et al., 2003). Lactobacilli also have shown little evidence for requiring iron (Helmann, 2014). Conversely, *Escherichia coli* (*E. coli*) have an iron-centric metabolism but conditionally import manganese in response to oxidative stress. Therefore, the relationship between these two ions and their metalloregulatory systems can reveal a great deal about the nutritional requirements and how bacteria may adapt to stressful conditions. *B. subtilis* requires both Fe^{+2} and Mn^{+2} for growth and survival and has served as the main model organism for structural biochemical studies of metalloregulatory proteins and their mechanisms (Errington et al., 2020).

Metalloregulators are proteins that reversibly interact with specific metal ions to control gene expression. The most well studied metalloregulators are dimers with each subunit containing an amino-terminal helix-turn-helix DNA-binding domain and an adjacent metal-binding domain (Que et al., 2000). *B.*

subtilis contains at least four distinct metal ion dependent sensors, of which MntR is the only one known to specifically regulate manganese homeostasis.

Manganese cations are predominantly bound to metalloenzymes, regulators, and low molecular-weight species, such as citrates and phosphates. Ions may also be present unbound in trace amounts within aqueous solution of the bacterial cell (Kang et al., 2023). The atomic radius of Mn⁺² (0.80 Å) in aqueous solution lies between that of Mg⁺² (0.65 Å) and Ca⁺² (0.99 Å), which helps to explain why these cations may be interchangeable in metal binding sites of various proteins (Jacobovics et al., 2001). One challenge of metalloregulatory proteins in maintaining metal-ion homeostasis is to prevent mismetalation.

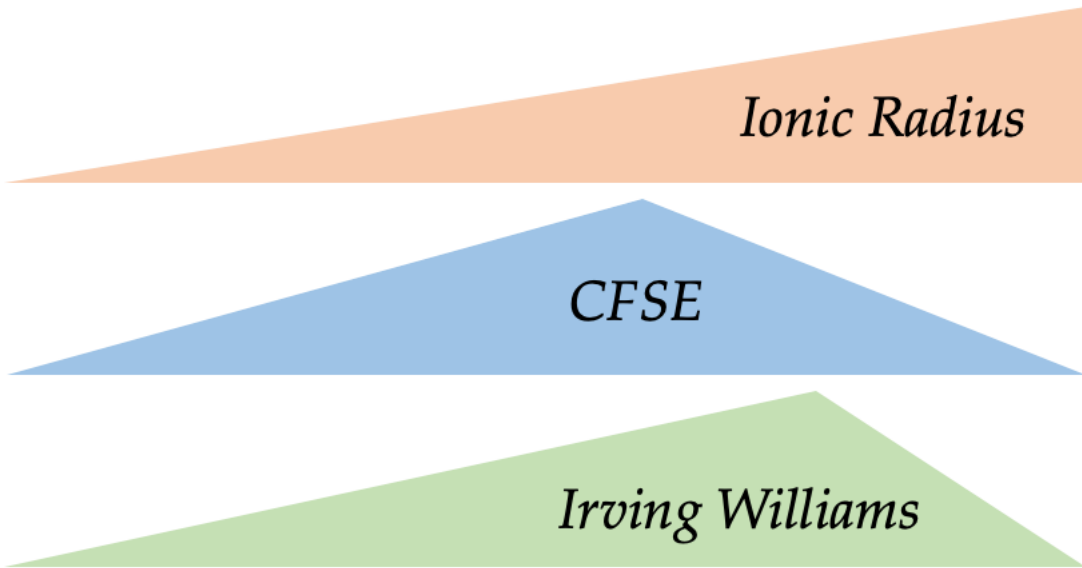
The Irving Williams Series is a set of relationships between first-row transition metals indicating the relative stabilities of metal ion complexes when an aqueous ion is replaced by any ligand. Both the atomic radius and the crystal field stabilization energy contribute to the relationship (Figure 3). As atomic radius decreases across the periodic table, atoms are more stable, because the distance between the positively charged nucleus and the external valence electrons is increasingly smaller. This increasing attractive force stabilizes the metal complex. Crystal field stabilization energy (CFSE) refers to the energy that emerges when a metal ion approaches a charged ligand, breaking the *d* and *f* orbital degeneracies (Martin, 1987). Although Cu⁺² has a lower CFSE compared to Ni⁺², Cu⁺² takes on a tetragonal configuration that contributes to increased stability during complexation.

The Irving-Williams series can provide insight in how mismetalation can occur in proteins, insofar as it suggests that certain metal ions have a higher affinity for metal-binding sites within proteins compared to others. Due to environmental metal ion concentration, metal ion availability, and metal-binding site specificity, proteins may bind an alternative metal ion rather than one that it would have bound given natural conditions. This can cause mismetalation and cause the protein to fail to function properly or perform less efficiently.

Figure 3. Depicting Irving-William Series relationship and trends between transition metal ions.

Irving-Williams Series

Mn^{+2} Fe^{+2} Co^{+2} Ni^{+2} Cu^{+2} Zn^{+2}



First-row metal ions increase in ionic radius across the periodic table. Copper has the most stable complex formation, as indicated by the Irving Williams relationship in row two. Nickel has the maximum crystal field stabilization energy of the ions.

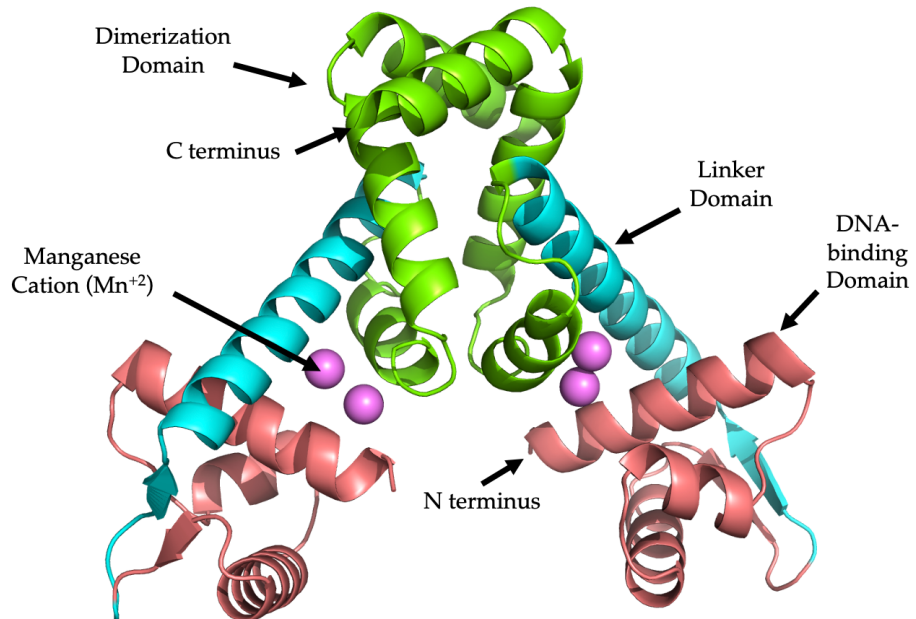
The cell exerts control over the binding affinity of metals by modulating their concentration and sequestering them from unbound states (Osman et al., 2019). This regulatory mechanism allows the cell to adjust the concentration of different metal ions based on their binding affinity, ensuring that a weaker-binding metal is more abundant and less likely to be out-competed by a stronger-binding metal, preventing mismetalation. Consequently, bacterial cells can be presumed to achieve a high degree of individual regulation for each metal ion species, facilitated by metal-sensing transcription regulators.

MntR: Structure and Function

MntR of *B. subtilis* is the key regulator of Mn⁺² homeostasis by transcriptionally repressing key Mn⁺² uptake systems and activating the transcription of key Mn⁺² efflux systems. The transcription regulator is a 142 residue, 16.7 kDa protein that exists as a homodimer in solution, stable over nearly a whole pH point (pH range 7.2 – 8.0) (Lieser et al., 2003). MntR consists of three domains (Figure 4).

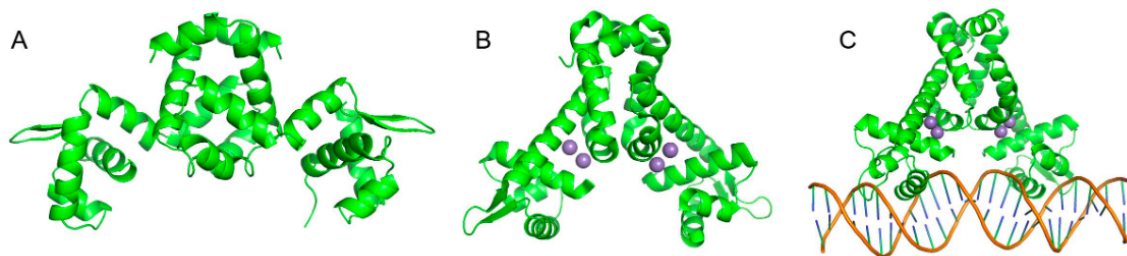
The C terminus (shown in green below in Figure 4) is found in the dimerization domain, which is responsible for facilitating the dimerization between two MntR monomers to form the homodimer (two identical monomers non-covalently bound together). The N terminus (shown in salmon red below in Figure 4) is found in the DNA-binding domain, which is the least rigid domain and can rotate 30 degrees at the Tyr75 residue site in the metal-free conformation state (Dewitt et al., 2007) (Figure 5).

Figure 4. Color-coded Structure of MntR homodimer.



Dimerization domain is shown in green. Linker domain is shown in cyan. DNA-binding domain is shown in salmon pink.

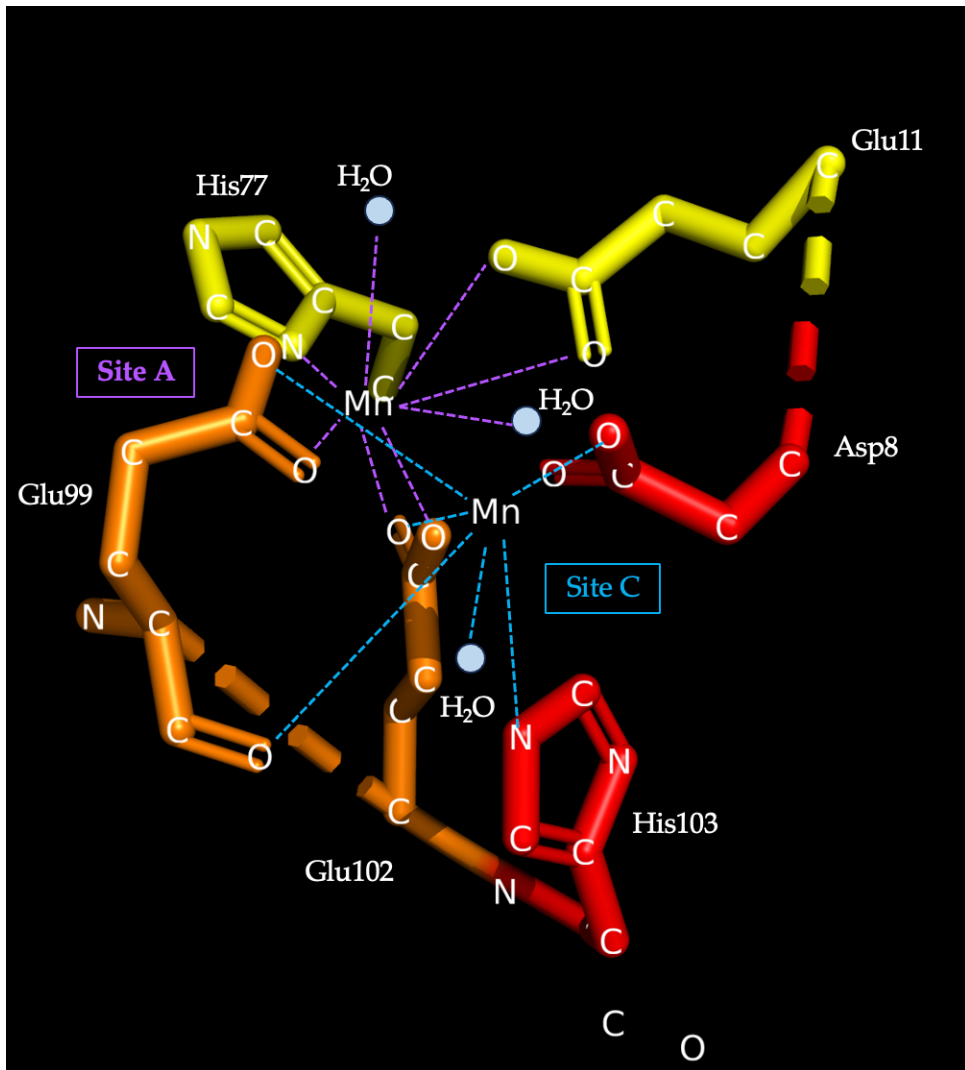
Figure 5. Mn(II) mediated DNA-binding of MntR.



Unpublished crystal structure of un-metallated MntR, courtesy of Arthur Glasfeld.

The metal-binding region of the monomer, which binds to two Mn^{+2} approximately 4.4 Å apart, is located in the linker domain (shown in cyan in Figure 4) and consists of sites A and C (Figure 6). Mn^{+2} at site A interacts with Glu11, His77, Glu99, Glu102, and a water molecule in a pseudo-heptacoordinate geometry. The Mn^{+2} at site C interacts with Asp8, Glu99, Glu102, and His103, the backbone carbonyl of Glu99, and a water molecule in the octacoordinated geometry (Figure 6) (Kriegman, 2006). The location of the polar water molecules in Site C remains ambiguous. Notably, when MntR binds other metals, such as Cd^{+2} , this binuclear complexation remains preserved. When Zn^{+2} binds to MntR, it does so only at Site A, and MntR does not reveal enhanced binding to DNA. The data presented by Kriegman et al. suggest that this specified binuclear binding is what underpins MntR's activation.

Figure 6. Metal-binding sites A and C in MntR.

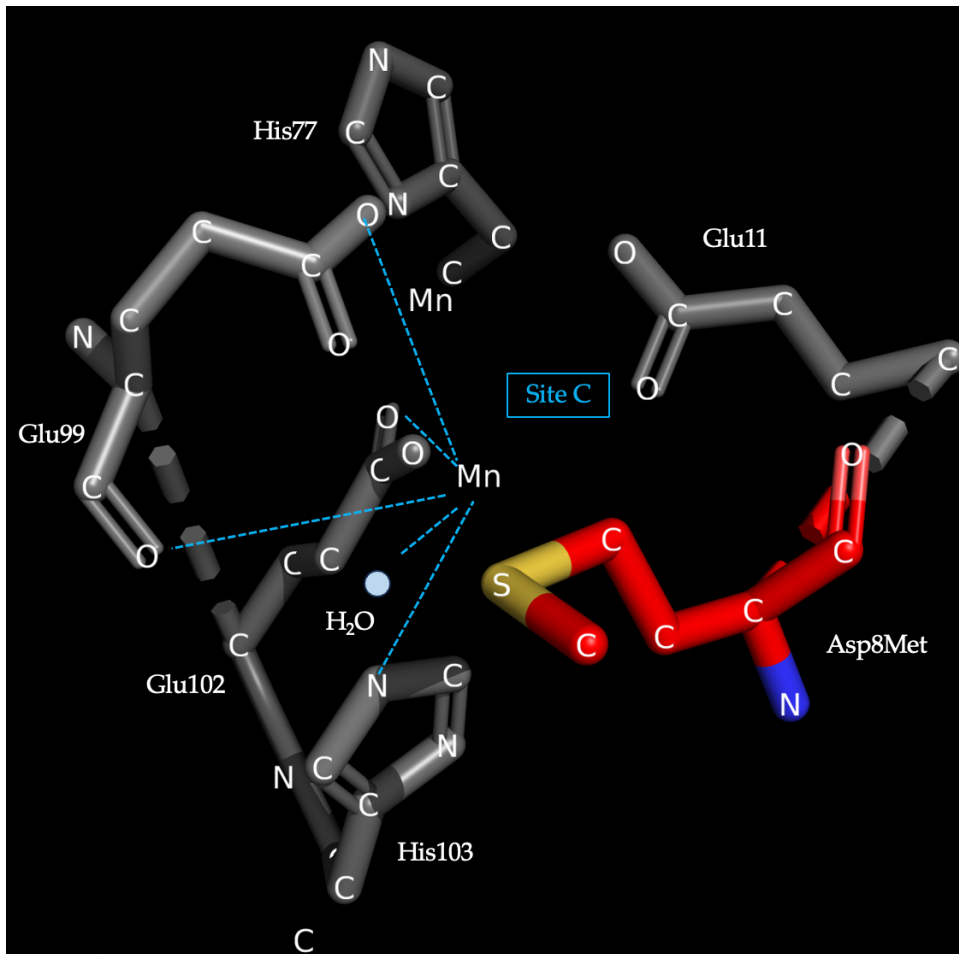


Site A (interactions shown in purple) features a pseudo-heptacoordinate geometry. Site C (interactions shown in blue) features an octacoordinated geometry. Polar solvent water molecules are shown as light blue spheres. Yellow amino acids (His77 and Glu11) are only engaged in the Site A metal-binding site. Orange residues (Glu99, Glu102) engage in interactions with both Sites A and C. Red amino acids (His 103 and Asp8) are only involved in interactions with Site C. One MntR monomer features both A and C metal-binding sites.

In its apo form, MntR binds DNA weakly, but this interaction becomes significantly stronger upon MntR's binding of two Mn^{+2} ions per monomer. MntR can also bind other metals with low affinity, like Ni^{+2} , Cu^{+2} , and Zn^{+2} . However, MntR only binds DNA with high affinity when bound to either Mn^{+2} or Cd^{+2} (Lieser et al., 2003). One possible reason for this is that MntR contains

carboxylate residues at sites that coordinate metal ions. Glasfeld and Guedon (2003) determined the crystal structures of wild-type MntR and a Asp8Met mutant, which features a methionine residue at position 8 instead of an aspartic acid (Figure 7) (Glasfeld et al., 2003). They found that a binuclear manganese cluster is responsible for MntR's metal ion selectivity.

Figure 7. Asp8Met mutation in MntR Site A metal-binding site.



Grey amino acids represent wild type MntR metal-binding residues present in Sites A and C. Colored residue (Met8) represents the mutated amino acid residue methionine from an aspartic acid, implicating metal-binding ability only in Site C. Asp8Met mutation does not affect metal-binding of Site A.

Two Mn^{+2} ions are bridged by carboxylate side chains and a solvent molecule in the MntR wild type. Figure 7 above shows what the coordination would look like if Mn^{+2} bound at Site C. By replacing the carboxylate with a sulfur atom ligand in the Asp8Met mutant, the researchers noticed that the

resultant crystal structure only bound one manganese ion in site A (Glasfeld et al., 2003). The side chain of Met8 seems to orient the sulfur atom away from the metal-binding position in site C, although the other metal-binding site remains unaffected and retains its ability to bind a Mn⁺². Asp8Met notably was activated non-specifically by both Fe⁺² and Mn⁺² *in vivo*, which suggests that the mutant lost Mn⁺² specificity in the binding site A. Nonetheless, the Asp8Met mutant was still able to repress transcription in response to manganese. Therefore, it seems that binuclear manganese clustering is not essential for MntR activation but plays an important role in establishing selectivity for Mn⁺².

MntR, a Mn⁺² sensing protein

MntR has been identified as the central Mn⁺² sensing protein in *B. subtilis*, due to its ability to bind biologically relevant Mn⁺² and regulate the expression of Mn⁺² importers and exporters (Que et al., 2000). At high manganese concentrations, one dimer of MntR first binds four manganese ions and then binds to the operators upstream of the coding regions of *mntH* and *mntABCD* operons, repressing the expression of MntH and MntABCD Mn⁺² importers.

Specifically, in the presence of Mn⁺², MntR functions to both repress the proton-coupled transporter MntH, a proton-coupled symporter protein belonging to the natural resistance associated macrophage protein (NRAMP) family that broadly regulates the transfer of metal ions, and the *mntABCD* operon, which encodes an ATP-binding cassette (ABC) transporter protein. This transporter protein consists of three proteins: the ATP-binding protein MntA, the permease MntB (which catalyzes the diffusion of particles in the direction of a concentration gradient), and the metal binding protein MntC (Coady et al., 2015). By repressing MntH, MntR stops the synthesis of the MntH importer, thereby slowing the intake of Mn⁺² into the cell.

As Mn⁺² levels continue to rise, MntR also induces the expression of cation-diffusion facilitator (CDF) efflux pumps MneP and MneS, leading to a greater Mn⁺² effluence from the cell into the environment. While both MneP and

MneS regulate concentrations of free Mn⁺² inside the bacterium, MneP is understood to be the primary transporter and MneS aids in a supportive fashion.

Mutants deficient in *mntR* or both *mneP* and *mneS* are highly sensitive to elevated levels of Mn⁺². Que and Helmann et al. (2000) studied the phenotypes of various *mntR/mneP/mneS/mntH* mutants using disk diffusion assays. By applying 10 uL of particular mutant strains onto galactose LB agar plates with 8 mm filters, the researchers studied the effects of the mutation on sensitivity to metals and hydrogen peroxide by measuring the zone of inhibition (mm) (Que et al., 2000). A zone of inhibition measures the extent to which bacteria can grow on the plate medium. A smaller zone of inhibition indicates more growth, since less bacteria have died in response to the given stress variable.

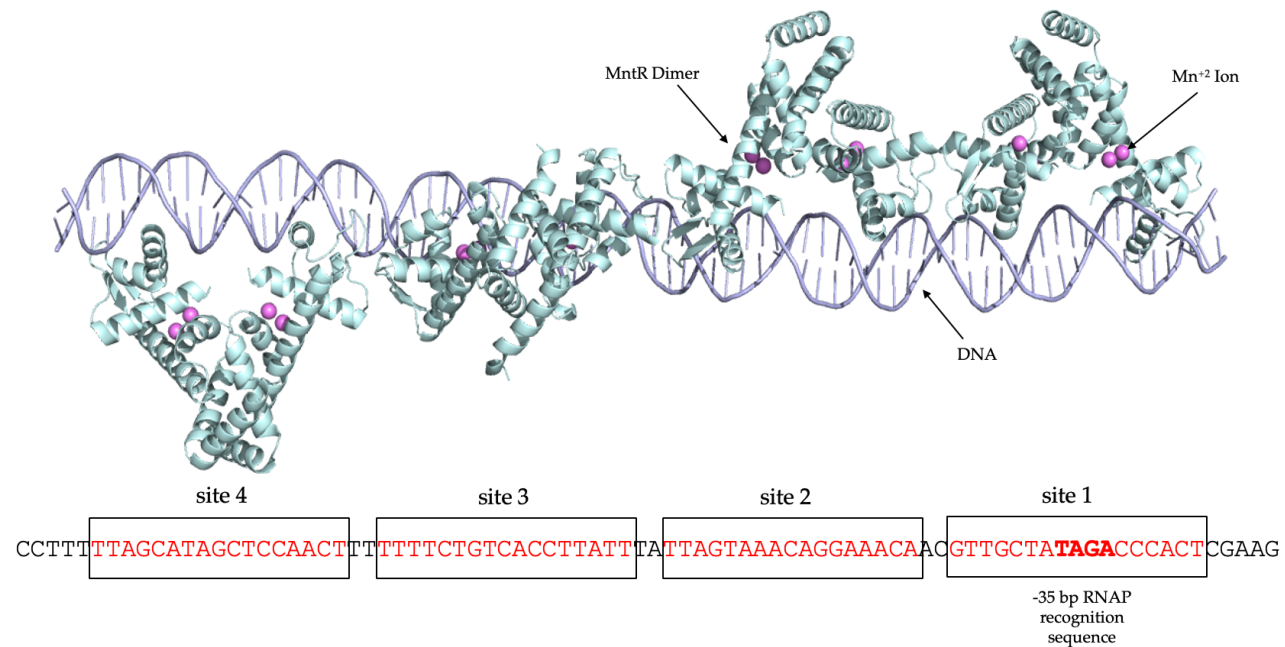
In response to excess (1 M) Mn⁺², the *mntH* mutant was characterized by the lowest zone of inhibition, and the *mntR* and *mntA* mutants were characterized by the highest zone of inhibition. This result validates the suggested roles of these respective proteins. When MntH, which imports manganese into the bacterium, is unable to be synthesized due to a *mntH* gene knockout, the bacteria can still grow relatively well due to other manganese import systems, such as MntABCD. Notably, the authors suggest that MntH and MntABCD may correspond to low- and high-affinity systems for Mn⁺² uptake, which explains why the zone of inhibition for the *mntH* mutant separately was lower than that of the joint mutant *mntHmntA*.

When both importers are deleted, the bacteria cell no longer can intake Mn⁺² into the cell, resulting in a higher zone of inhibition for this double mutant. MntR is unable to be produced due to a *mntR* knockout, and the bacteria greatly struggle to survive due to two reasons: constitutive expression of the importers MntH and MntABCD, and the inability to synthesize appropriate Mn⁺² export proteins, such as MneP and MneS. Additionally, because MntR is not being synthesized, it also does not bind excess Mn⁺², as it would in its typical mechanism to regulate and sense the metal-ion's intracellular concentration, which fails to help reduce the extent of manganese's toxic effect at high concentrations.

Transcriptional Role of MntR

MntR binds DNA to regulate the expression of Mn⁺² importer and exporter proteins by affecting transcription. At high concentrations of internal Mn⁺² (> 6 uM), each subunit of the MntR homodimer binds two Mn⁺², which increases the affinity MntR has for DNA. The dissociation constant (K_d) of wild type MntR bound to Mn(II) was determined to be 16.0 nM for the *mntH* operator site and 30.4 nM for *mntA* operator site (Lieser, 2003; Golynskiy, 2005). Upon binding Mn⁺², the DNA recognition helix rotates 30 degrees, facilitating contact between the DNA duplex and MntR (Helmann, 2014; Dewitt et al., 2007). MntR then facilitates the expression of the *mneP* promoter sequence. The exact mechanism for this specific regulation is still unclear. Using the synthesized P84 DNA sequence, previous thesis work (Fu, 2021; Shi, 2022) have successfully solved the complex structure between MntR and the *mneP* promoter sequence, confirming that eight MntR proteins (4 MntR dimers) bind to the *mneP* promoter sequence (Figure 8).

Figure 8. MntR bound to P84 DNA sequence.



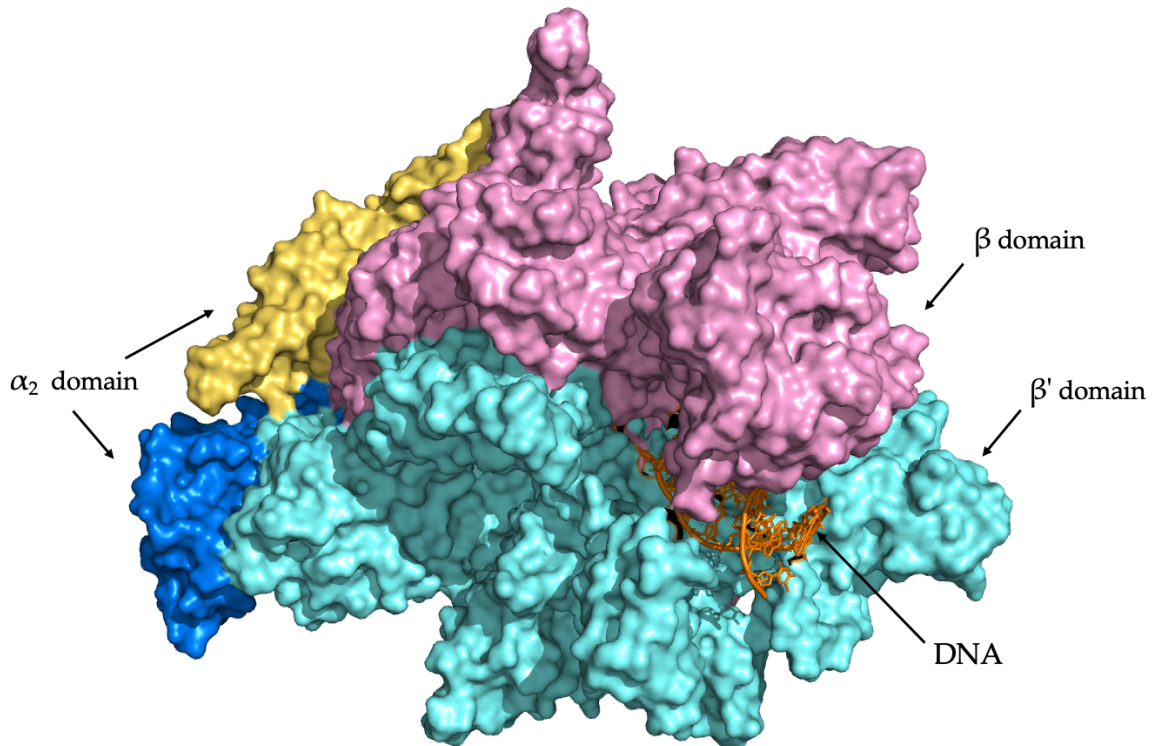
Before discussing the nuances of the MntR-*mneP* structure, the process of transcription is briefly discussed below.

Transcription

Transcription is the process of converting DNA, the basic genomic information in a cell, to messenger RNA, which can be further read and processed by a ribosome to produce proteins. RNA Polymerase (RNAP) is the key enzyme in the process of transcription. It binds to a promoter region, the region which precedes the operator region, the genetic sequence which actually contains the instructions for protein synthesis. RNAP unwinds a small section (~ 10 nucleotides long) of the circular double-stranded DNA to a single-stranded form. RNAP attaches one of four ribonucleotide triphosphates – adenine guanine, cytosine, or uracil – to a DNA template base to form a Watson-Crick base pair. A linear RNA strand is thereby built in the 5' to 3' direction.

In contrast to eukaryotic transcription, bacterial transcription is accomplished using only one RNA polymerase. *B. subtilis* RNAP weighs ~400 kDa and features a complex structure comprised on four minimal moieties that resemble a crab claw (Figure 9). The core enzyme consists of the $\alpha_2 \beta \beta'$ complex. The alpha subunit primarily interacts with transcription factors that further regulate genetic expression, while the two beta subunits clamp the DNA substrate (Newing et al., 2000). This complex is universally conserved in sequence, structure, and function across all living systems.

Figure 9. Structure of *B. subtilis* RNA Polymerase bound to DNA.

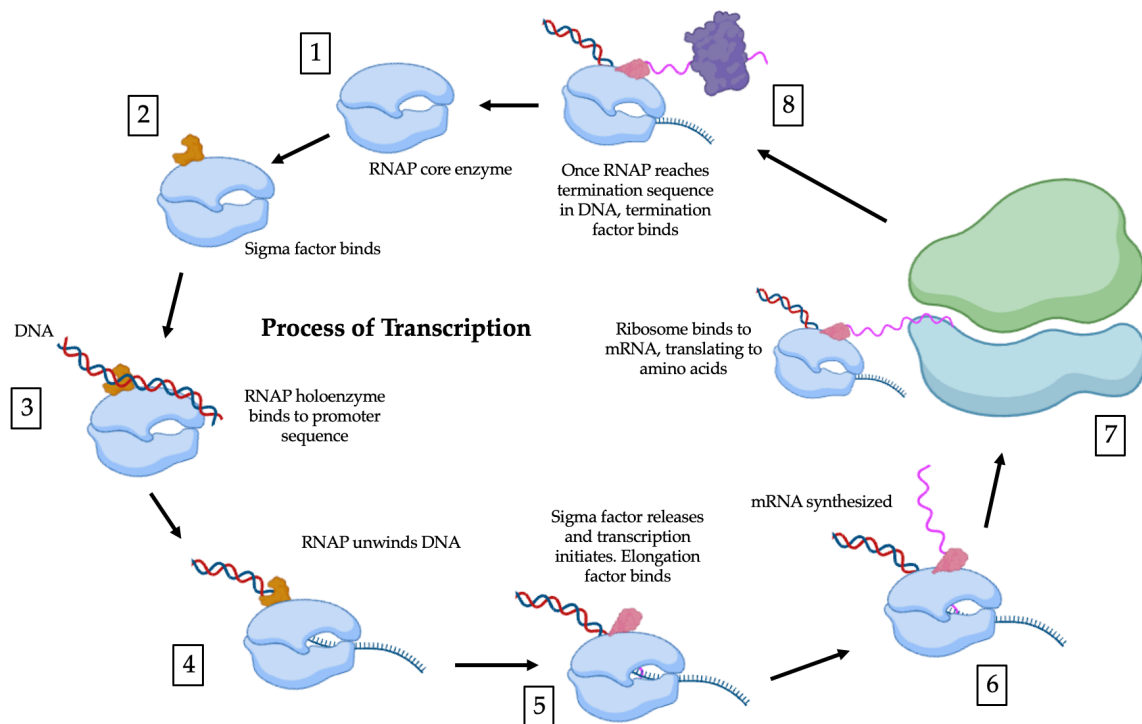


Yellow and blue represent the α_2 moieties, pink represents β , cyan represents β' , and orange represents DNA. (Model reproduced from Newing et al. (2000) without permission; PDB number: 6WVJ)

Because bacteria only feature one type of polymerase, a variety of sigma factors that bind to RNAP help to direct the polymerase to specific DNA promoter regions. *B. subtilis* encodes at least 17 sigma factors, of which only sigma factor alpha is the only essential and most abundant during bacterial

growth (Helmann, 2003). Other factors are less abundant during growth but show greater importance during sporulation. Upon binding to sigma factors, the core enzyme becomes the functional holoenzyme, which then binds to a specific promoter site (Figure 10). The interaction between sigma factor alpha and the core RNAP complex is quite strong, with a dissociation constant estimated to be $\sim 10^{-9}$ M (Jun et al., 2013). Nonetheless, once RNAP has bound to the DNA to begin the elongation phase, the sigma factor disassociates from the core enzyme. This paradoxical nature can be explained by the unique architecture of sigma factor alpha, which contains four highly conserved, flexibly linked domains: sigma1.1, sigma2, sigma3, and sigma4. These domains independently and simultaneously bind to different parts of the core enzyme. While each linkage is relatively weak, the simultaneous binding of each sigma domain creates a high-affinity interaction between the sigma factor and RNAP. Upon RNAP binding to the DNA template, the sigma domain-core interaction undergoes stepwise structural transitions which releases each sigma domain individually from the core enzyme.

Figure 10. Process of transcription by RNA Polymerase.

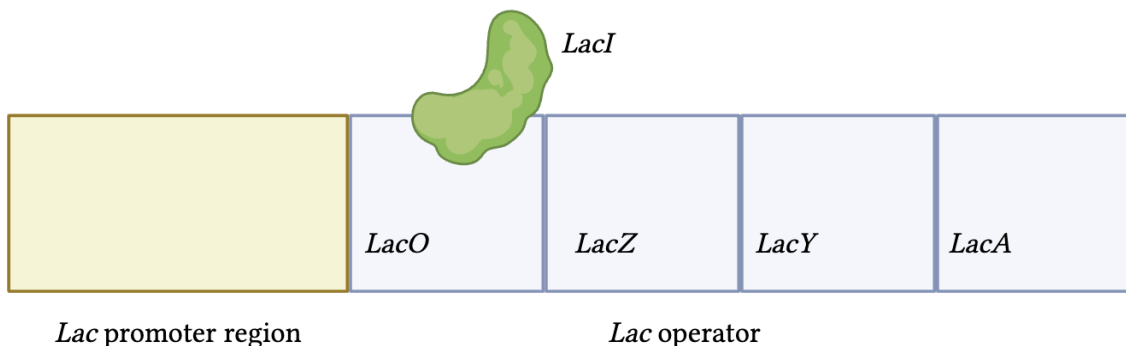


Transcription factors, molecules that either facilitate RNAP's ability to bind to the DNA or block it, can also bind DNA to regulate gene expression in response to environmental cues. Indeed, transcription factors account for approximately 6% of the total gene count in *B. subtilis* (Seshasayee et al., 2011). The genomes of organisms in symbiosis with their hosts feature significantly lower transcription factor gene content, which is consistent with the minimal need for sensing and adapting to changing environments. *Mycobacterium leprae*, for example, only encode 42 transcription factors, consisting of only 2.4% of gene count.

Role of lacL in regulating expression

The T7 expression system, naturally performed in bacteria, is widely used in microbiology and biochemistry to manipulate native protein expression machinery. The system depends upon the natural activity of the *lacO* operator (Figure 11). *Lac* genes (*LacO*, *LacZ*, *LacY*, and *LacA*) encode for proteins that degrade lactose for energy when glucose supply is low in the bacterial cell.

Figure 11. LacI binds to the Lac operator to repress transcription of downstream genes.



Schematic showing the *Lac* promoter (yellow) and operator (blue) regions. *LacO*, *LacZ*, *LacY*, and *LacA* genes encode for protein that degrade lactose for energy. LacI binds to *LacO* and prevents RNAP from transcribing the downstream *Lac* genes.

At high glucose concentrations, the bacterium uses glucose as its main energy source. LacI, a transcription factor, binds to *LacO* to repress transcription of *Lac* genes. At low glucose concentrations, the bacterium switches to using lactose to access energy. Allolactose is produced as a byproduct of the cleavage of lactose into glucose and galactose. Allolactose binds to LacI, popping it off of the *Lac* operator, allowing for RNAP to transcribe *Lac* genes, which encode for proteins that degrade lactose for energy the bacterium can use (Swint-Kruse et al., 2013). Downstream lays the T7 promoter, where the T7 RNA polymerase binds to initiate transcription of the downstream genes, hence the name of the system.

As will become relevant in the Methods, this system can be used in the construction of plasmids, containing genes of interest that encode for proteins we would like to over-express. Isopropyl β -D-1-thiogalactopyranoside (IPTG) is an analog of allolactose that is added to bacterial cultures that serves the same function as allolactose in re-initiating transcription. The advantage of this reagent is that it cannot be metabolized, unlike allolactose, which allows for genes of interest, downstream of *LacO*, to be continuously transcribed into mRNA and subsequently translated into protein.

*MntR binds to *mneP* promoter region*

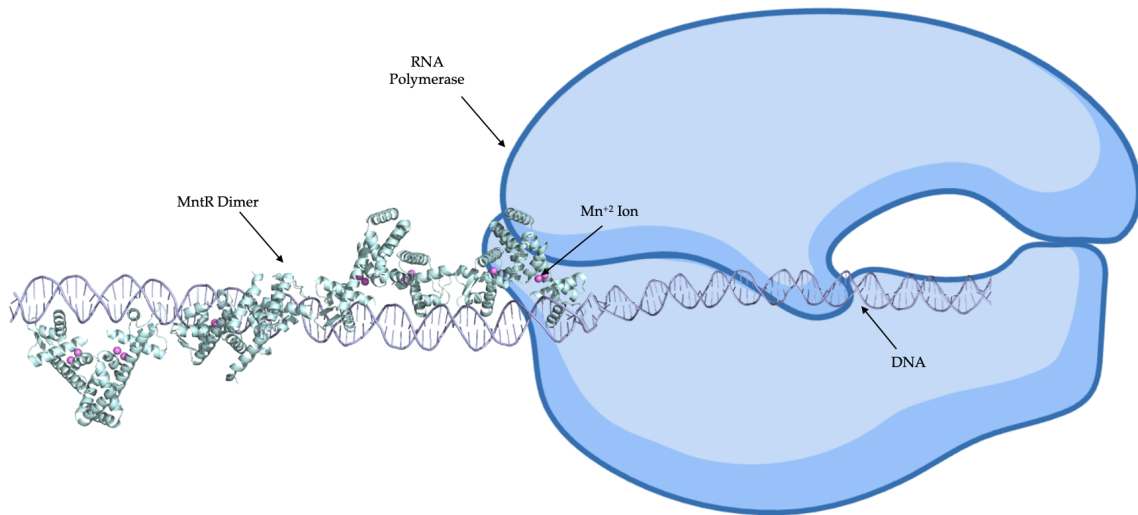
MntR functions as a transcription regulator and binds to promoters that express either Mn⁺² importers or exporters depending on intracellular Mn⁺² content relative to the environment. The focus of this thesis is to elucidate the molecular mechanism for how MntR binds to the *mneP* promoter region to activate the transcriptional expression of the Mn⁺² exporter MneP.

Helmann et al. (2017) had previously hypothesized that the *mneP* promoter sequence contains three MntR binding sites. However, previous thesis work (Shi, 2021) has produced a cryo-EM structure of four MntR dimers bound to the *mneP* promoter sequence (Figure 8). Interestingly, it seems that MntR binding site 1 overlaps with the RNAP binding site, suggesting an interaction between RNAP

and MntR that allows for this specialized expression of *mneP* (Figures 12 and 13).

The Helmann lab also investigated the effect of varying stoichiometries in the complex (e.g., 8 MntR:1 DNA, versus 6 or 4 MntR: 1 DNA) have on the expression of the *mneP* operator. Using a truncated lacZ fusion containing only one, two, or three MntR binding sites, the authors found that three binding sites should be filled before the *mneP* operator is transcribed (Huang et al., 2017). Upon discovery of a fourth MntR binding site, it can be concluded that at least three of the four MntR binding sites should be filled to activate expression of *mneP*. This demonstrates that only at high Mn⁺² concentrations do MneP proteins get synthesized, enabling the bacterial cell to export Mn⁺².

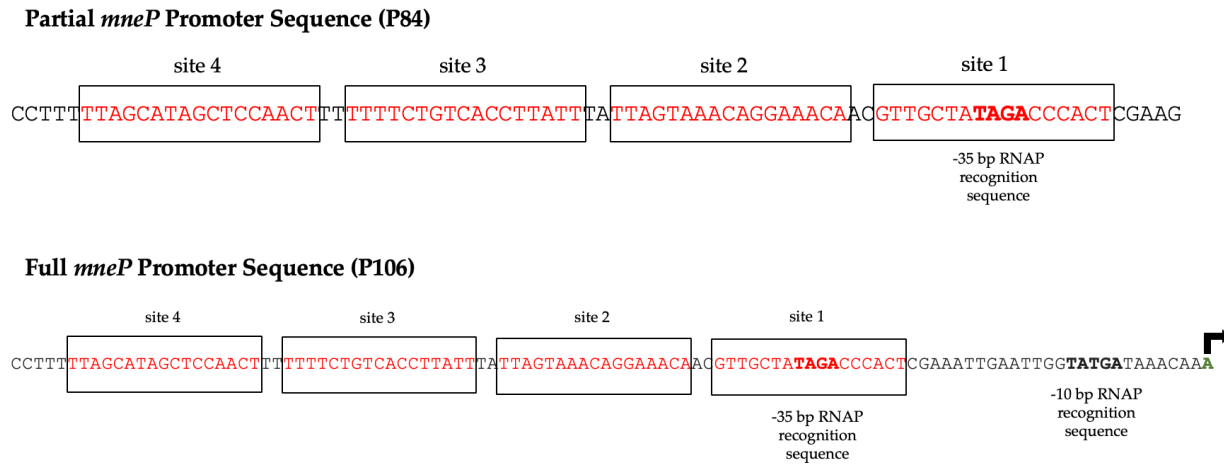
Figure 12. RNAP bound to DNA duplex, occupied by four MntR dimers.



RNA Polymerase (RNAP) binds to MntR binding site 1 to initiate expression of Mn⁺² exporter MneP by transcribing the *mneP* operator region.

The P106 DNA construct has since been synthesized. This sequence contains, in addition to the four MntR binding sites, the RNAP binding site and the transcription start site for *mneP* (Figure 13).

Figure 13. Comparison of DNA P106 and P84 constructs.



Top: Partial *mneP* promoter sequence (P84) only contains four MntR binding sites, as well as one of the RNAP recognition sequences. Bottom: Full *mneP* promoter sequence (P106) contains the four MntR binding sequences, both (-35, -10) RNAP recognition sequences, and the transcription start site (denoted with an arrow) for the *mneP* operator region.

Ultimately, the P106 construct can be used in complexation experiments to evaluate how MntR and RNAP interact at binding site 1 and what the molecular mechanism could be for MntR activation to help execute *mneP* expression.

Mutations to MntR

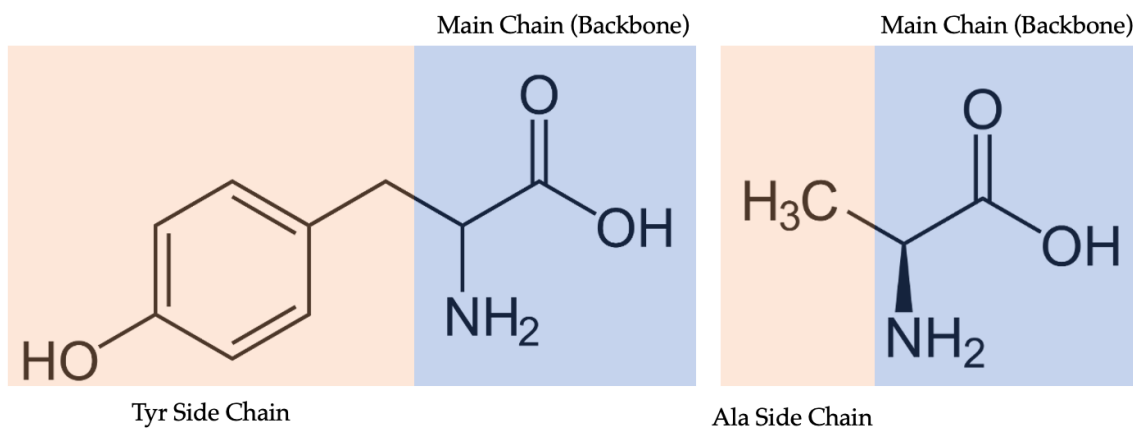
The primary focus of this thesis is to generate mutations to highly conserved residues in wild-type MntR. These residues, discussed in detail below, seem to uphold intra-dimer, inter-dimer, and MntR-DNA contacts that we hypothesize allow for MntR to specifically activate *mneP* expression. By mutating these residues through site-directed mutagenesis, the aim is to firstly, validate the cryo-EM model of MntR in complex with the promoter region of *mneP*; secondly, to understand if the activation of *mneP* is driven by the allosteric modulation of MntR's binding affinity to the binding sites; and thirdly, to understand the mechanism of activation of *mneP* by MntR.

Specifically, three different mutations are studied in this thesis.

Tyrosine to Alanine at Site 22

Tyrosine and alanine are two examples amino acids, which are the building blocks of proteins. Amino acids consist of an amine-carboxylate backbone, and they exhibit specificity through their side chains. A variety of functional groups exist which can make an amino acid hydrophobic (water-avoidant), electro-static (possessing an ionic charge), polar (possessing electronegative atoms), or non-reactive (containing inert methyl groups). Alanine is one such amino acid which contains a non-polar side chain. The covalent bonds between carbon and hydrogen in the methyl side chain are highly stable and uncharged, and therefore this side chain only engages in weak van der Waals interactions with other amino acid residues.

Figure 14. Amino acid structures of tyrosine and alanine.

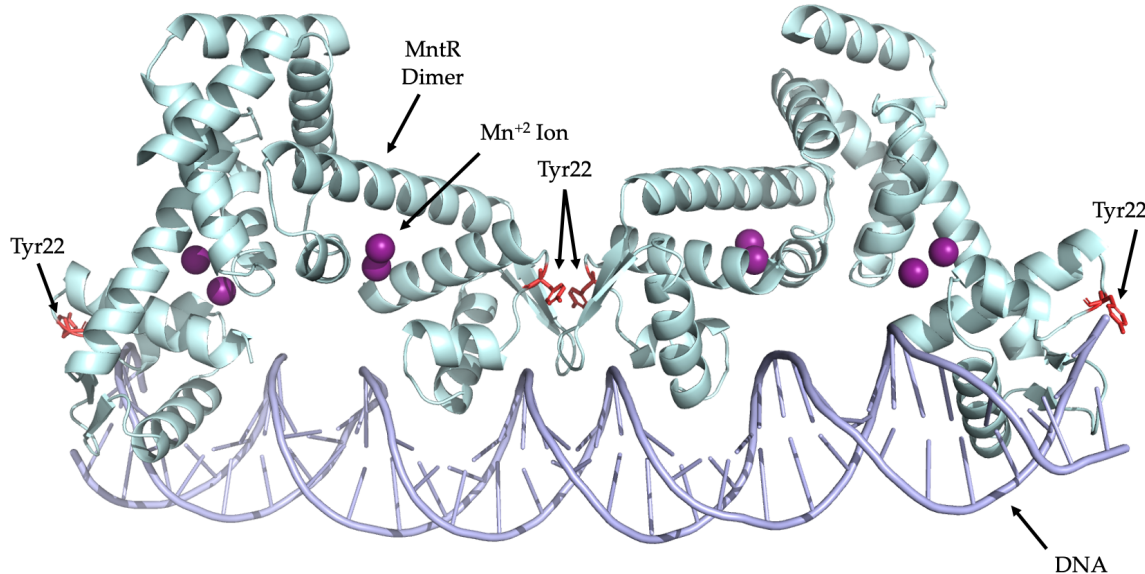


Left: Tyrosine. Note the reactive hydroxyl group bonded to an aromatic ring in the structure. Right: Alanine. The methyl group bonded to the amino acid backbone is non-reactive.

Alanine stands in contrast with tyrosine, which contains a reactive hydroxyl group bonded to a highly stable aromatic ring. Due to the length of the ring, tyrosine residues may be able to engage in otherwise longer-range interactions with other residues. The hydrogen and oxygen atoms in the hydroxyl group are highly polar, suggesting a high capacity for dipole-dipole and hydrogen bonding with other electronegative atoms if properly aligned.

Tyrosine is one residue that is mutated for this thesis. At site 22, it appears that tyrosine (Tyr22) may play an important role in supporting the complexation between two MntR dimers (Figure 15).

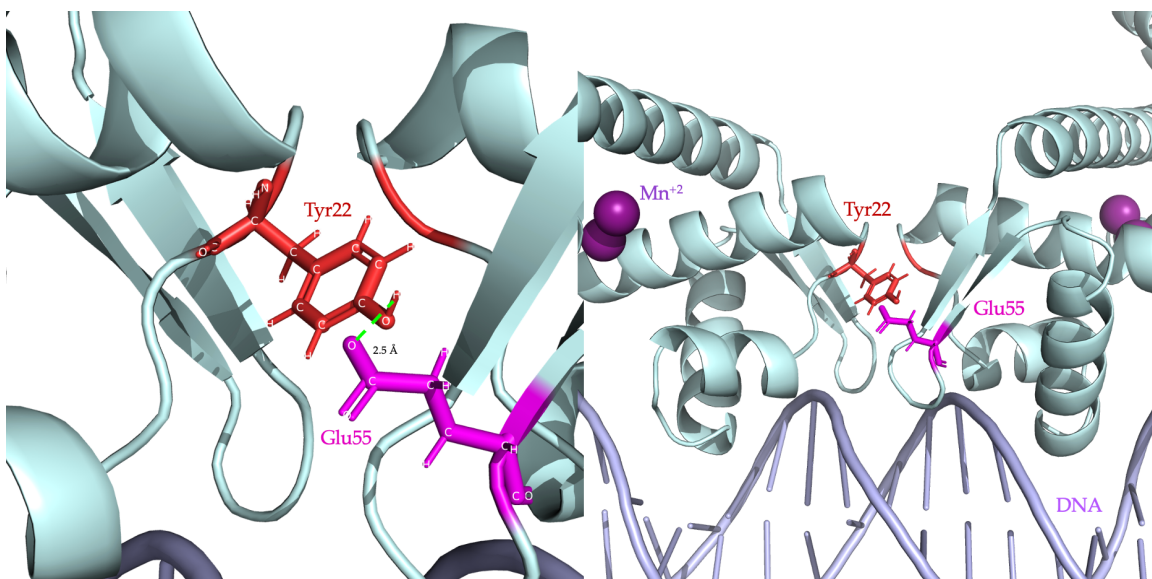
Figure 15. Tyrosine residues at site 22 of MntR.



Tyrosine residues (red) at site 22 of each MntR monomer in the 4 MntR-p84 DNA complex structure. Manganese ions shown in purple. Notably, this residue appears at the linkage site between the two MntR dimers, suggesting a potential stabilizing role for the 2 MntR dimer complex.

Tyrosine was mutated to an alanine, which effectively removes the capacity for tyrosine to engage in dipole interactions with other electronegative side chains, as well as prevents the capacity for interacting with residues relatively further away. Modeling suggests that Tyr22 forms an ion-dipole interaction with a glutamic acid residue on a different MntR monomer, at position 55 (Figures 16). The electropositive hydrogen of the tyrosine side chain hydroxyl group (dipole) interacts with the negatively charged oxygen atom (ion) of glutamic acid's side chain hydroxyl group (pK_a 4.15).

Figure 16. Tyr22 ion-dipole interaction with Glu59.



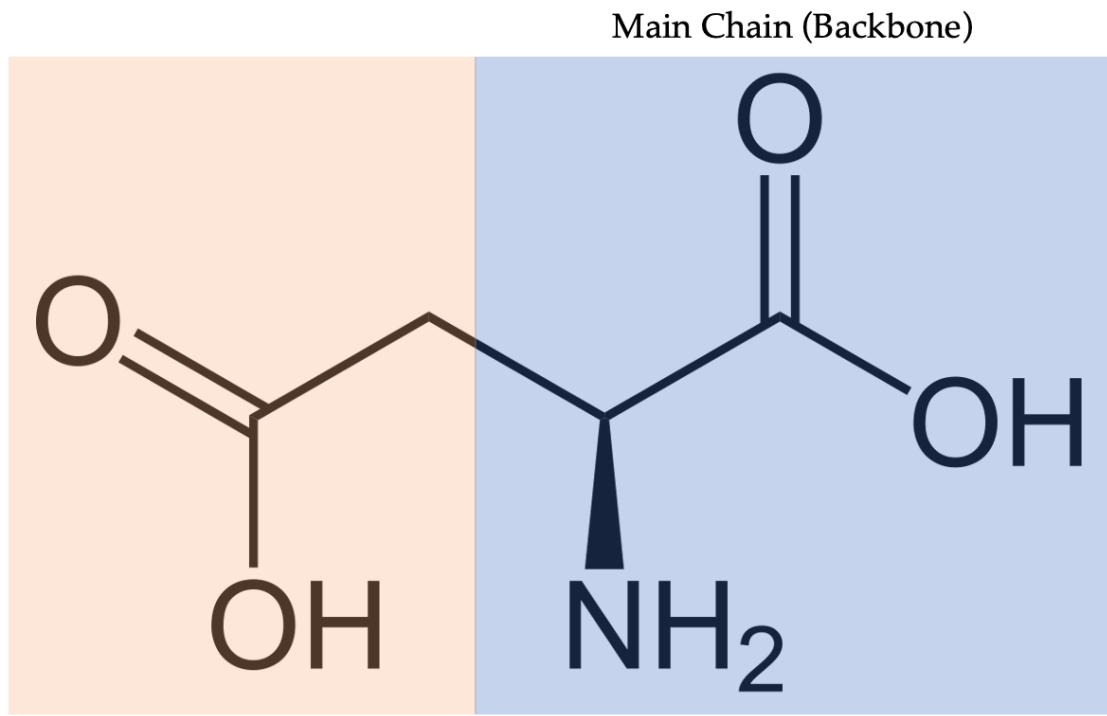
Left: Tyrosine at site 22 (red) engages in ion-dipole interaction over a 2.5 Å distance with glutamic acid at site 55 (pink). Right: The interaction between the tyrosine and glutamic acid residues is across two monomers of MntR, each belonging to separate MntR dimers. Manganese ions shown in purple.

By mutating tyrosine to alanine at this position, the aim is to disrupt the stabilizing interaction that supports the complexation of two MntR dimers together. Alanine does not have the reach to interact with the atoms in the glutamic acid side chain, nor does it have the polar capacity to engage in hydrogen bonding or dipole-dipole interactions. It may be possible that van der Waals forces can maintain an interaction between these two residues, but this thesis hypothesizes that the subsequent interaction will not be sufficient for the two MntR dimers to anchor together, which may be required for the dimers to bind to the DNA in a stable way.

Aspartic acid to Alanine at Site 27

Aspartic acid is another amino acid that, at site 27 of the MntR protein structure sequence, seems to enhance intra-dimer stabilization.

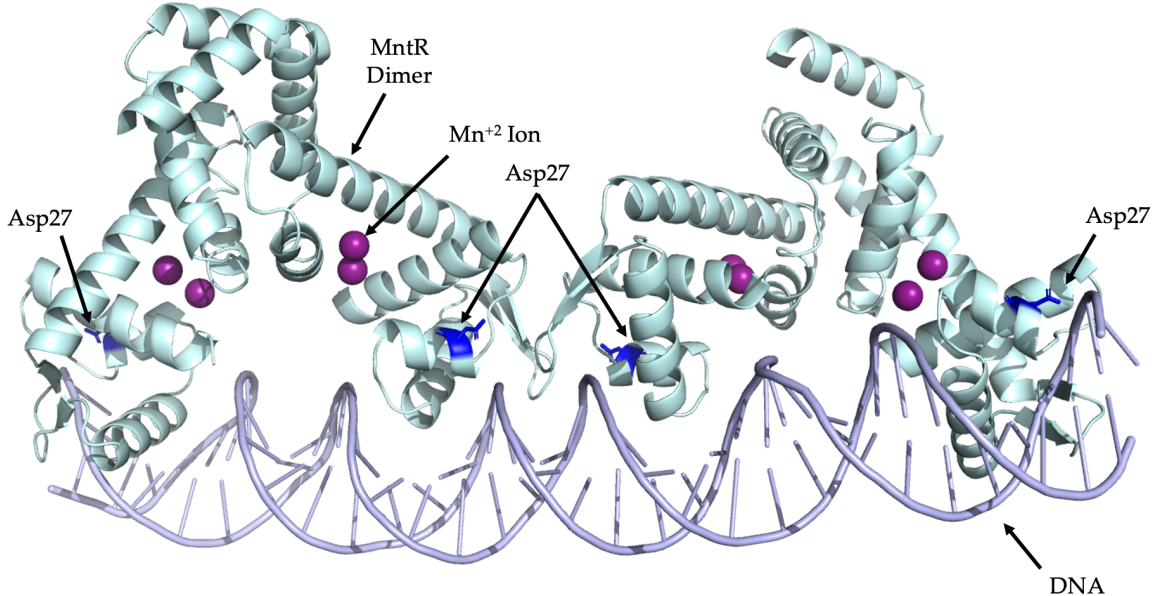
Figure 17. Amino acid structure of aspartic acid.



Aspartic acid contains a highly reactive carboxylic acid functional group attached to the backbone. The side chain carboxylate carbon is electropositive due its bond with two electronegative oxygen atoms. The hydroxyl group is also highly reactive, with the capacity for hydrogen bonding.

At site 27, aspartic acid (Asp27) engages in a variety of stabilizing interactions.

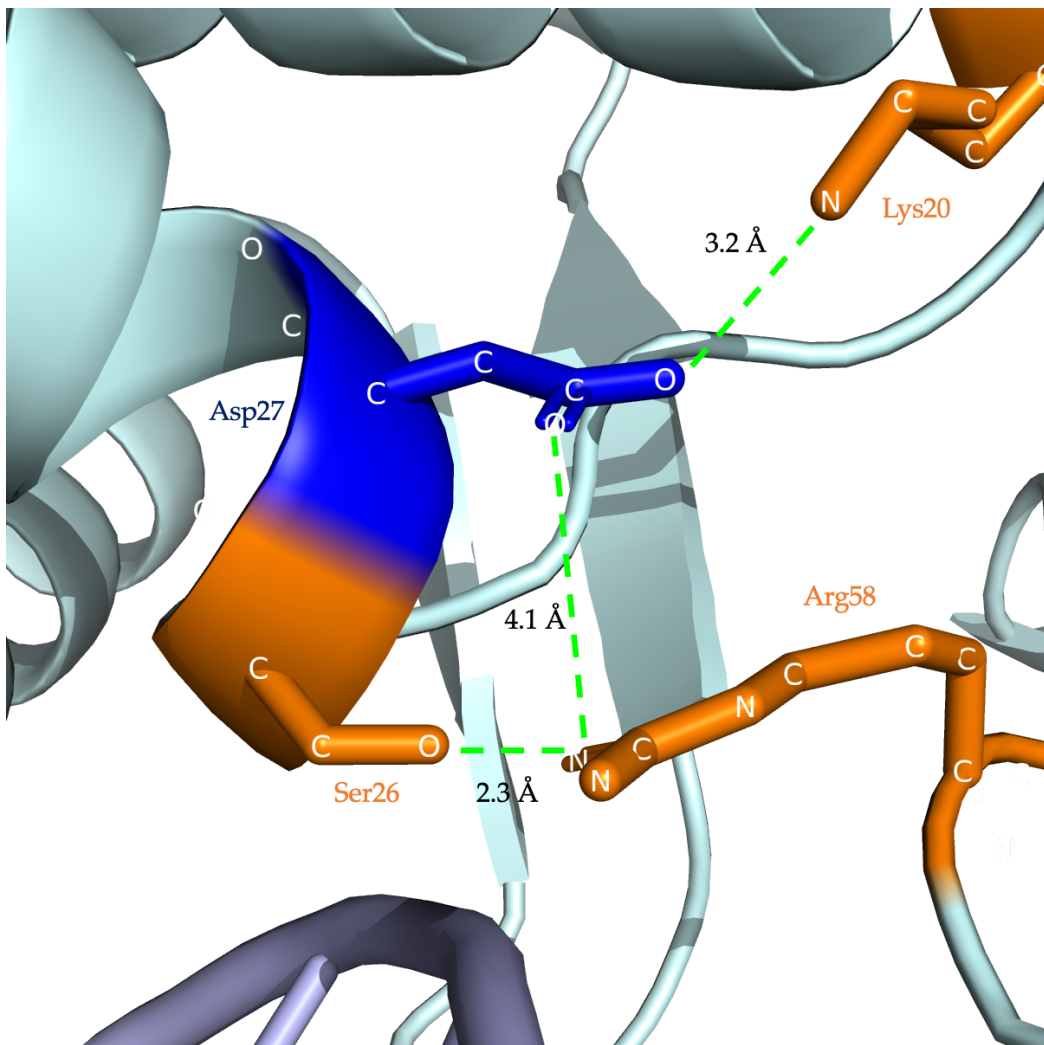
Figure 18. Aspartic acid residues at site 27 of MntR.



Aspartic acid residues (blue) at site 27 of each MntR monomer in the 4 MntR-p84 DNA complex structure. Manganese ions shown in purple. This residue engages in a variety of stabilizing interactions with other residues in the MntR proteins.

Aspartic acid at site 27 contributes to an interlocking network of salt bridge interactions (Figure 18).

Figure 19. Asp27 engages in a series of salt bridges.



Aspartic acid at site 27 (blue) engages in salt bridges with lysine at site 20 and arginine at site 58.

The carboxylate side chain on the aspartic acid (pK_a 3.7) engages in a salt bridge with the nitrogen on the lysine (20) side chain (pK_a 10.7). The carboxylate also engages in a salt bridge with the guanidino side chain amino nitrogen (pK_a 12.1) on the arginine (58) of the neighboring MntR monomer of a separate dimer. Arg58 further interacts with serine (26) through a salt bridge. Collectively, intra-dimer stability is achieved through a woven fabric of interactions with Asp27.

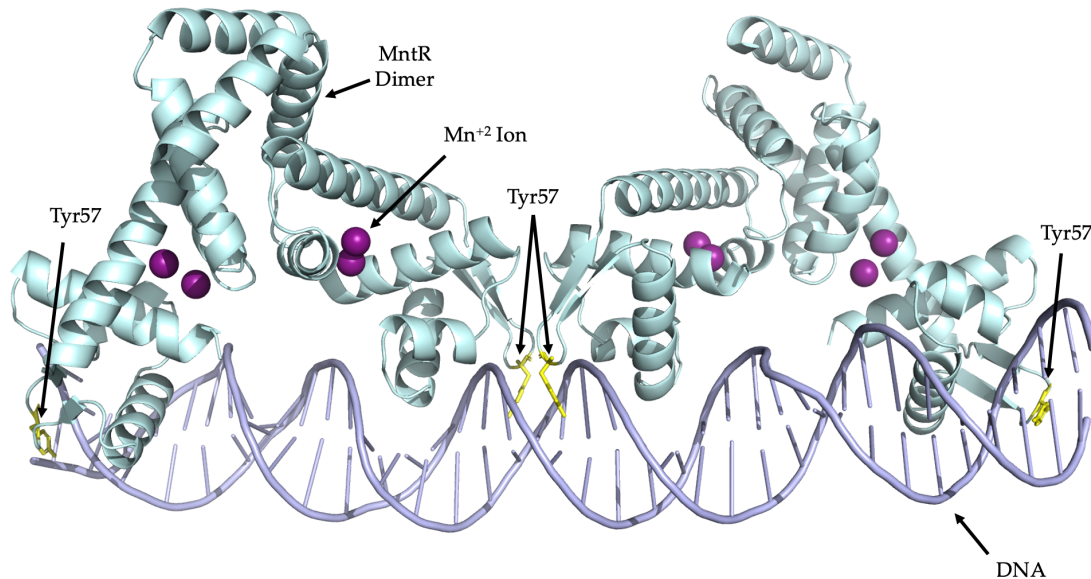
An Asp27Ala mutation would interrupt the salt bridge interactions aspartic acid engages in. The electrostatic interactions that take place require the electronegative oxygen atoms on the carboxylate side chain of the aspartic acid to engage with the positively charged alkylammonium (Lys20) and guanidino

(Arg58) side chains. A mutation to alanine would result in only weak van der Waals forces interconnecting these residues, significantly weakening intra-dimer stability.

Tyrosine to Alanine at Site 57

Tyrosine is also located at site 57 of the MntR protein structure sequence and is of interest due to its potential stabilizing role in the MntR binding to the DNA.

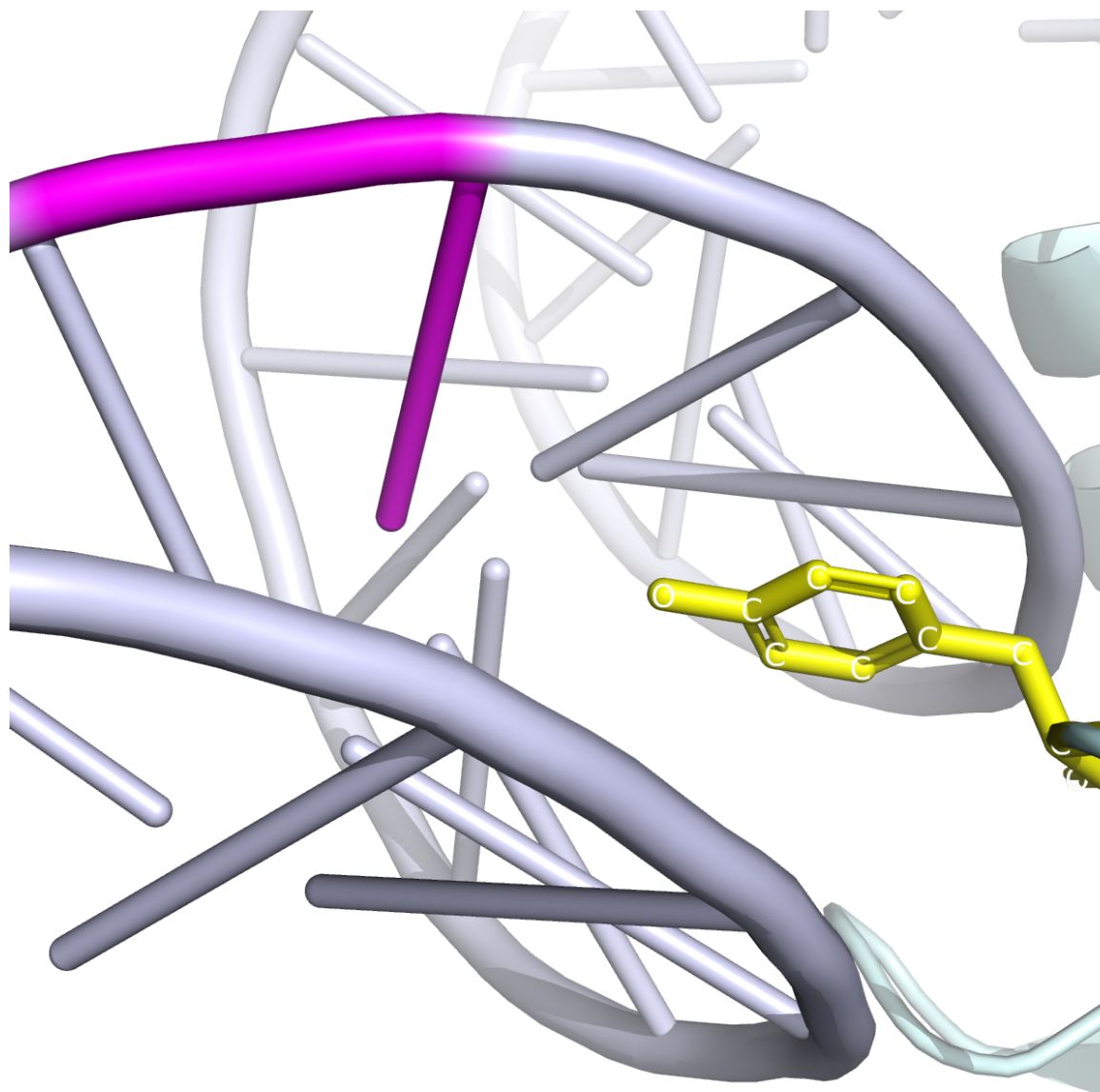
Figure 20. Tyrosine residues at site 57 of MntR.



Tyrosine residues (yellow) at site 57 of each MntR monomer in the 4 MntR-p84 DNA complex structure. Manganese ions shown in purple. This residue engages in stabilizing interactions with the duplex DNA.

Tyrosine stabilizes the interaction between the DNA-binding domain of the MntR monomer and the minor groove of the DNA duplex (Figure 21).

Figure 21. Tyr57 is situated within the DNA minor groove.



Tyrosine at site 57 (yellow) is situated within the minor groove of the DNA.

The hydroxyl hydrogen of the Tyr57 side chain likely engages in hydrogen bonding or pi-pi aromatic ring stacking with the DNA base pair located at this position (position 41 in our model). This interaction stabilizes the binding of MntR to DNA. Therefore, a Tyr57Ala mutation would greatly disrupt this interaction, because the alanine side chain, which contains a nonpolar methyl group, is unable to engage in hydrogen bonding, due to the absence of an electron donor or acceptor in the alanine side chain, nor can it engage in pi-pi stacking due to the absence of an aromatic ring in the side chain.

Size Exclusion Chromatography

Size exclusion chromatography (SEC) is a bread-and-butter method in biochemistry for separating and purifying proteins or nucleic acids, providing insights into sample heterogeneity based on size. A sample is loaded onto a chromatographic column that contains porous beads with a defined pore size, capturing smaller molecules inside the beads where they interact with the stationary phase. Larger molecules pass around the beads and move through the column more quickly. Therefore, larger molecules elute quicker than smaller molecules, which interact with the stationary phase inside the beads and take longer to pass through the column. SEC produces a size distribution of the molecules in a sample, allowing for characterization of monomers, oligomers, aggregates, and impurities.

A fluorescence detector can also be combined with a SEC set-up, which allows for the detection of fluorescence labeling molecules, like GFP tags, to be identified in a heterogenous sample. In this thesis, fluorescence SEC (FSEC) is used to measure the expression and complexing behavior of mutant MntR. MntR possesses a histidine tag, a series of six histidine amino acid residues. A fluorescent dye was added to mutant MntR lysates that binds to these residues and absorbs at 494 nm and emits light at 520 nm. Purified mutant MntR was measured using tryptophan absorbance at 280 nm and emission at 350 nm. This data is analyzed on a chromatogram, where, by comparing peak positions to known standards or controls, a species identity can be assigned. The relative amplitude indicates the quantity of that species in the sample.

Mass Photometry

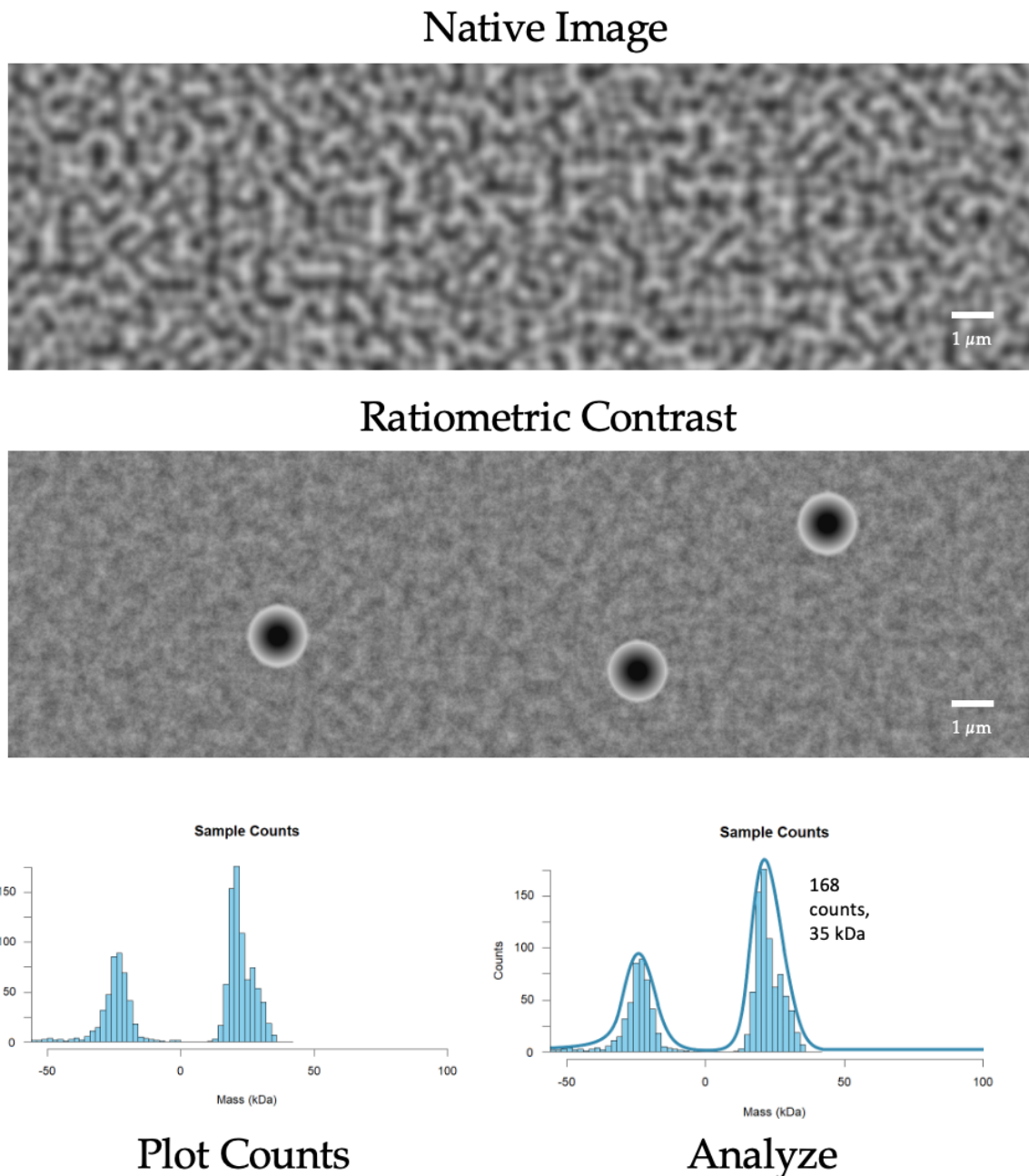
Mass photometry is an analytical technique used to assess the molecular heterogeneity of a sample in solution under equilibrium conditions. This information can be used to determine the molecular weight and oligomeric state of a variety of macromolecules, including protein and DNA. For example, a protein sample of interest is first suspended in a buffer and then deposited on a glass microscope slide. Then, a detector measures the interference between light

scattered by single particles as they absorb onto the glass and the light reflected by the glass surface. Because particles are in solution, they come off the glass and may re-absorb, and these counts are categorized separately in the generated chromatogram, as shown below. Data is taken as a one-minute movie and processed using ratiometric imaging, which helps distinguish molecular size from background noise. Particles with a molecular weight larger than 30kDa exhibit a signal intensity that is directly proportional to its refractive index and mass. Calculated masses are fitted to a Gaussian curve and analyzed as a chromatogram. This technique produces accurate information for the mass of macromolecules from 30 kDa to 5Mda, making this a versatile technique and especially practical for investigating oligomeric state and complexing behavior.

To measure different DNA sizes, poly-L-lysine coated glass plates can be used during data collection. DNA exhibits a long and wavy structure, making it difficult for the entire molecule to bind to the glass plate for detection. Because DNA is negatively charged, glass plates coated in positively charged poly-lysine residues attract the DNA and facilitate binding. A drawback of using these plates is increased background noise. Because light now must also diffract through the poly-lysine coating, the interference pattern produced when the light hits the particles may be skewed, producing noise in the dataset.

The below figure shows the images one might expect during calibration and data collection.

Figure 22. Mass Photometry data collection example.



The native image shows a lot of background noise in addition to the molecules in solution, which come in and out of the detection range as they land and come off the glass. Ratiometric processing is applied to produce frames with contrast, enabling clearer visualization of particles moving through the field. Each particle is counted once, as it adheres to the glass slide. If the particle comes

off, the processing software categorizes this as part of the background noise. These counts do show up in the chromatogram to the left of the plot's origin. A Gaussian curve is applied to each peak. Using the protein calibration standards, molecular weight can be attributed to each peak, which can also indicate oligomeric status and the fraction of particles in each oligomeric state.

Thesis Aims

This thesis seeks to address the molecular mechanism of activating *mneP* transcriptional expression by the Mn⁺² sensor MntR.

The binding interaction between MntR and DNA is studied by producing mutations to MntR at three conserved residue sites. Through site-directed mutagenesis, three mutations were performed to MntR. Tyrosine (sites 22 and 57) and aspartic acid (site 27) were mutated to alanine residues. Tyr22Ala on one MntR dimer removes the ion-dipole interaction with a residue on a separate MntR dimer. This mutation therefore may prevent the stabilization of multiple MntR dimers complexing together. Modeling further suggests that Tyr57 helps to coordinate the DNA binding domain of MntR to the minor groove of the DNA. Therefore, mutating this residue should also result in the complex not being able to form, because the MntR and DNA cannot bind together with enough affinity. Finally, Asp27 contributes to intra-dimer stability. Asp27Ala therefore may result in MntR being unable to successfully form a complex if the dimer itself is unstable, impeding its ability to first coordinate with other MntR dimers or first bind to the DNA.

Mass photometry and FSEC are used to identify how these mutations to the MntR protein impact its complexation with the P84 DNA, which contains the four predicted MntR binding sites and the *mneP* promoter region, and was used to elucidate the cryo-EM structure of MntR. Specifically, Tyr22Ala is meant to interrupt the inter-dimer contacts between two MntR dimers. Asp27Ala is intended to disrupt intra-dimer stabilization within each MntR dimer. And Tyr57Ala aims to de-stabilize the interaction between the MntR monomers of each dimer with the minor groove in the DNA duplex. These mutations will help elucidate the mechanism for the specialized binding of MntR to regulate the expression of the Mn⁺² efflux transport proteins, MneP, and contribute to a better understanding of the molecular mechanisms underlying this type of homeostasis management as a virulence factor.

Methods

Site-directed Mutagenesis of MntR plasmid pSMT3

A polymerase chain reaction (PCR) was performed to generate three mutant MntR-encoding genetic sequences for each mutation. Primers, single-stranded DNA sequences, were designed using NEBasechanger to introduce a mutation to alanine residues at sites 22, 27, and 57 in the MntR-encoding genetic sequence of the pSMT3 plasmid (Table 1).

Table 1. Amino acid sequence of the MntR encoding region of the pSMT3 plasmid.

TPSMEDYIEQIYMLIEEKGYARVSDIAEALAVHPSSVTKMVKLDKDEYLYEKYRGL
VLTSKGKKIGKRLVYRHELLEQFLRIIGVDEEKIYNDVEGIEHLSWNSIDRIGDLVQ
YFEEDDARKKDLKSIQKKTEHHN

¹Highlighted residues were separately mutated.

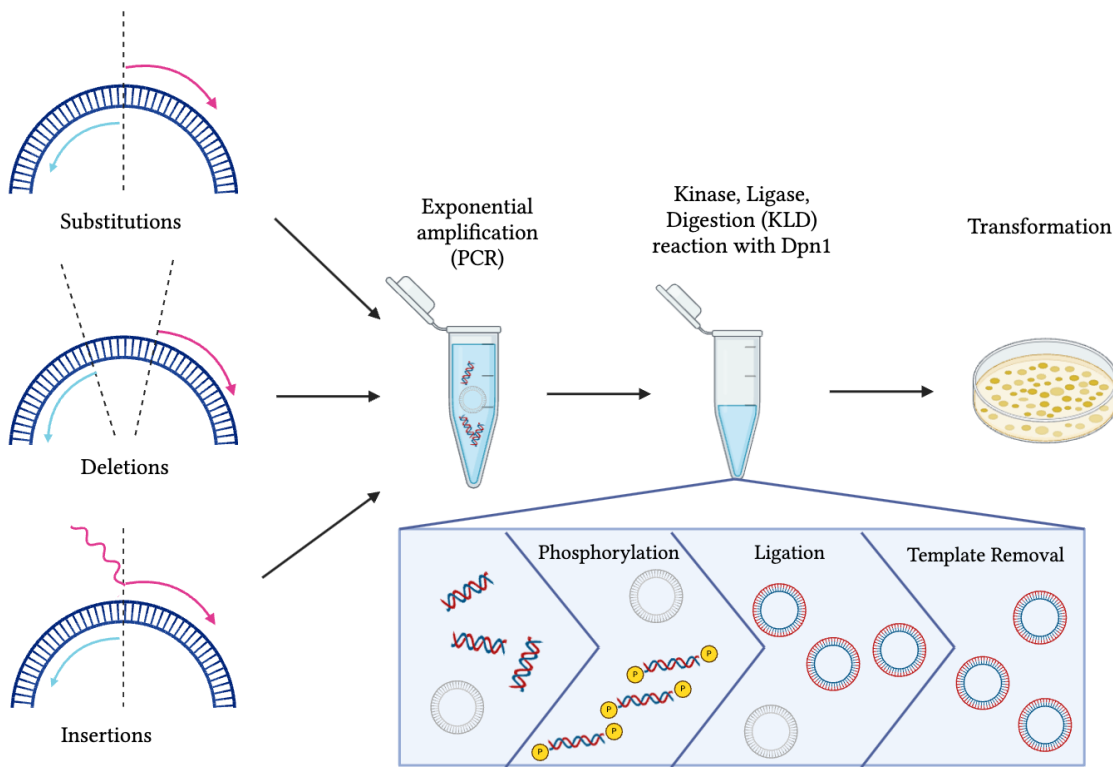
Double-stranded plasmid DNA is first denatured at a high temperature (approximately 94-98 °C), unwinding the double helix. The temperature within the thermocycler then drops to allow primers to anneal to the complimentary sequences of the DNA. The forward primers consist of changes in three base pairs that, following transcription and translation processes, encode for the amino acid mutation in the MntR protein. The mutation containing region of DNA is then extended by DNA Polymerase (Q5 Hot Start High-Fidelity DNA Polymerase) following an increase in temperature (approximately 72 °C), which allows the DNA polymerase to synthesize new DNA nucleotides following the template DNA. These steps – denaturation, annealing, and extension – are repeated many times to allow for exponential amplification of the target sequence. The resultant product is a double-stranded DNA molecule that contains the mutant MntR genetic sequence. The primers used for each mutant are listed in Table 1. A full protocol containing the reagents and thermocycler conditions can be found in Tables A1-2 (Appendix A) .

Table 2. Primer Sequences for MntR Mutagenesis Reactions

Primer Name	Number of base pairs (bp)	Annealing Temperature (°C)	Sequence
Y57A MntR Forward Primer	25	58	TTATGAAAAA gcg CGCGGTCTCGTG
Y57A MntR Reverse Primer	29	59	ATTAAATATTCGTCTTATCTAGTTTG
Y22A MntR Forward Primer	25	56	AGAAAAAGGA gcg GCACGAGTTCC
Y22A MntR Reverse Primer	23	58	TCAATCAGCATATAATCTGTT
D27A MntR Forward Primer	23	64	ACGAGTTCC gcg ATCGCGGAAG
D27A MntR Reverse Primer	23	60	GCATATCCTTTCTTCAATCAG

Next, an incubation reaction with kinase, ligase, and Dpn1 was performed to phosphorylate and ligate the new vector, as well as digest the parent plasmid. Kinase phosphorylates the newly synthesized, linear DNA molecules, which marks them for circularization. Ligase glues the phosphorylated ends of each DNA strand together, creating a circular DNA molecule. Dpn1 digests any unphosphorylated molecules, including the template DNA sequence. Figure 23 illustrates this process (Figures 23). A list of reagents and the protocol can be found in Table A3 (Appendix A).

Figure 23. Illustration of site-directed mutagenesis PCR.



The blue DNA molecule represents the pSMT3 template DNA from which new, mutation-containing DNA molecules are formed. The PCR product contains both newly synthesized linear DNA (blue and red DNA fragments) and template plasmid (grey). Kinase phosphorylates (yellow molecules) the ends of the linear DNA (blue and red). Ligase then circularizes the phosphorylated molecules together. Finally, Dpn1 digests the unphosphorylated template DNA (grey), leaving only the mutated MntR-encoding DNA vector.

The mutant MntR plasmids were then transformed into *E. coli* DH5-alpha competent cells (NEB #C2987H), optimized for plasmid production. Cells were defrosted on ice for 10-15 minutes. 5 uL of KLD product was pipetted into one aliquot (~50 uL) of cell mixture, and this was repeated for each mutant. Tube was flicked gently a few times and allowed to incubate on ice for 30 minutes. Cells were then heat shocked by placing them in a water bath at 42 °C for exactly 30 seconds, followed by an incubation period of 5 minutes on ice. 950 uL of SOC media was pipetted into the cell mixture and placed in a heat shaker at 37 °C for 1 hour, shaking at 300 rpm. Cells were pelleted by a quick spin in the microcentrifuge for a few seconds at 10,000 rpm. The full reaction was pipetted

onto LB/Kanamycin agar petri dish plates, equilibrated at 37 °C, with 3-6 sterile glass beads and incubated at 37 °C overnight. Upon successful growth of colonies, 6 colonies per plate (otherwise stated, per mutant) were picked using a p20 pipette tip and added to separate overnight cultures consisting of 5 mL of LB and 50 uL/mL of kanamycin. The overnight culture was grown overnight at 30 °C for 16 hours, shaking at 220 rpm. The next day, plasmids for each colony of mutant (6 colonies per mutant: 18 total) were recovered following the Qiagen MiniPrep protocol, detailed in Table A4 (Appendix A).

Sequencing reactions were then prepared, following the protocol found in Table A5 (Appendix A). Reactions were sent to Azenta Life Sciences for Sanger sequencing. Mutant plasmid sequences were aligned with the WT pSMT3 plasmid using Benchling.¹ Proper alignments featured the correct nucleotide base substitutions and no disruption to the rest of the plasmid sequence. The plasmids with the sequence-verified mutants of MntR were then transformed into *E. coli* DE3 NiCo21 competent cells (NEB #C2529H), optimized for expression. The transformation protocol was consistent with the one described above, other than that multiple colonies were picked and added to a single overnight starting culture. Glycerol stocks were prepared for each of the three MntR mutants by mixing 500 uL of each overnight culture with 500 uL of sterile 50% glycerol. The cells were mixed well with glycerol and flash frozen in liquid nitrogen and stored at -80 °C for future expression.

Growth Conditions for MntR Mutants

E. coli NiCo21 cells encoding the SUMO-tagged mutant MntR protein were used for the following expression and purification protocols. Saturated overnight culture of the modified *E. coli* was grown in 25 mL LB (0.1 g tryptone, 0.1 g NaCl, and 0.05 g yeast extract in 10 mL water) with 50 uL/mL kanamycin antibiotic. Cells were then grown aerobically at 37 °C by addition of 5 mL of saturated overnight culture, grown with 220 rpm shaking at 37 °C, to 1 L

¹ <https://benchling.com/>

lysogeny broth (LB) medium (10 g tryptone, 10 g sodium chloride, and 5 g yeast), and 50 uL / mL kanamycin. Cells were allowed to grow for 2-3 hours until OD₆₀₀ reached 0.6-0.8. Cells were induced with the addition of 0.12 g IPTG (0.4 mM), with a 10 mL aliquot removed prior to induction for expression testing (described below). After 2-3 hours of incubation, another 10 mL aliquot was removed for expression testing, and cells were then harvested via centrifugation at 6700 xg for 35 minutes at 4°C. The pellets were washed with lysis buffer (25 mM HEPES pH 7.5, 300 mM NaCl, 10 mM imidazole, 5% glycerol) and centrifuged again at 67000 xg for 20 minutes. The resulting pellets were stored at -80 °C until purification.

Expression testing of MntR mutants using FSEC

FSEC was used to check that the *E. coli* containing the mutant MntR plasmids could effectively express mutant MntR protein. The pre-induction and post-induction 10 mL culture aliquots for each mutant were retrieved and centrifuged at 6700 xg at 4°C for 5 minutes. Cells were lysed with 10 mL lysis buffer (25 mM HEPES pH 7.5, 300 mM NaCl, 10 mM imidazole, 5% glycerol) per 1 g of pellet, with the addition of 0.4 g / mL lysozyme, 1 mM MgCl₂, 1 mM PMSF, and 0.1 g DNase. The mixture was vortexed and allowed to incubate on ice for 15 minutes. The resuspended cells (on ice) were then lysed via water bath sonication (1 min on, 5 min off, repeated 3 times). The lysate was then spun down at 100,000 xg in a tabletop ultracentrifuge to clarify the lysate and separate it from the cell debris.

Pre-induction and post-induction samples were prepared for FSEC analysis (2475 FLR Detector, bioSample Manager FTN-R, BioQuaternary Solvent Manager R, Waters). 500 uL of the supernatants from the pre-IPTG and post-IPTG samples were aliquoted into Eppendorf tubes. Z3NTA, a fluorescent dye that targets histidine tags, was added to each sample to a final concentration of 1 uM. The supernatant of each mutant at pre- and post-induction was also used to prepare SDS-PAGE gel samples. 7uL of 5X DNA (no SDS gel loading dye), consisting of two visualizing dyes (bromophenol blue and xylene cyanol), was mistakenly combined with 35 uL of the supernatant sample. 6X SDS loading dye

should be used for SDS-PAGE gels. SDS-PAGE was performed with a 4-20% SDS polyacrylamide gel, run at 25 mA (in the constant current mode) in Tris-Glycine buffer (30 g Tris base, 144 g glycine, and 10 g of SDS in 1L water). Gels were stained with Coomassie Blue (2.5 g Coomassie Brilliant Blue R250, 450 mL methanol, 450 mL milli-Q water, 100 mL glacial acetic acid), destained (900 ml milli-Q water, 900 ml methanol, 200 ml glacial acetic acid), and visualized in natural light conditions.

SEC measures molecular weights of components in the sample and the homogeneity of samples. Samples are injected from a 96 well plate onto a SEC column, which separates the proteins in the lysate by size. In FSEC, the sample then travels to a fluorescence detector, which excites the proteins in the lysate at specific wavelengths and measures the emission. For this experiment, tryptophan (absorbance at 280 nm, emission at 350 nm) and histidine (absorbance at 494 nm, emission at 520 nm) fluorescence were measured. Pure wild type MntR was used as a control, so tryptophan fluorescence would only indicate this species. For the lysate samples, the Z3NTA dye tightly coordinates to the His-tag that only the mutant MntR species possesses. Thus, only proteins containing these residues would be detected. This method was used to evaluate whether the grown *E. coli* expressed mutant MntR, by measuring the relative quantity (indexed by relative fluorescence of His- and Try- residues in the mutant MntR protein) of mutant MntR pre- and post-induction with IPTG.

A Superose-6 (5/150) gel filtration column was utilized for all samples. The entire system, comprising the inject loop, pump, column, and connecting tubes, is stored in 10% ethanol, which was replaced with milli-Q water at the beginning of each day. At the onset of each run, the column underwent equilibration with the buffer in which the sample was prepared. The FSEC running buffer used consisted of 25 mM HEPES pH 7.5, 300 mM NaCl, 10 mM imidazole, and 5% glycerol. Subsequently, 50 uL of samples were injected onto the column at a flow rate of 0.3 mL/min. The fluorescence detector then recorded the absorbance of the samples post-column chromatography relative to the elution volume. FSEC chromatograms were analyzed using PRISM.²

² Software offered by <https://www.graphpad.com/>

Large Scale Purification of Mutant MntR

Mutant MntR was purified from *E. coli* pellets. The pellets were resuspended in lysis buffer (25 mM HEPES pH 7.5, 300 mM NaCl, 10 mM imidazole, 5% glycerol), with 0.4 g / mL lysozyme, 1 mM MgCl₂, 1 mM PMSF, and 0.1 g DNase. The resuspended cells were lysed via sonication (70% amplitude, 6 minutes on total, 20 seconds pulse on, 20 seconds pulse off, 1 minute rest for each 60 second pulse on). The lysate was centrifuged at 16,000 x g for 35 minutes at 4°C. The supernatant was then incubated with 5 mL TALON resin, pre-equilibrated with lysis buffer, for 2 hours under nutation. The lysate-resin slurry was then centrifuged at 1000 x g for 5 min. Most of the supernatant was poured off, and the remaining resin-lysate slurry was loaded onto the column. Flow-through was gravity collected. Ten column volumes (CV) of lysis buffer and 10 CVs of lysis buffer with 20 mM imidazole were then used to wash the column. Lysis buffer with 300 mM imidazole was then used to elute the column using a peristaltic pump, at 1.5 mL / min. Collected fractions were analyzed via SDS-PAGE and by absorption at 280 nm to identify fractions containing MntR-SUMO. SDS-PAGE was performed with a 12% SDS polyacrylamide gel, run at 120 V in Tris-Glycine buffer (30 g Tris base, 144 g glycine, and 10 g of SDS in 1L water). Fractions containing MntR-SUMO were combined and concentrated to a volume <10 mL. 0.5 mg of Ulp protease (2 mg / mL) was added. The mixture was then dialyzed overnight in dialysis buffer (25 mM HEPES pH 7.5, 300 mM NaCl, 10 mM imidazole, 5% glycerol, 1 mM beta mercaptoethanol) at 4C.

The following day, 5 mL of Ni-NTA resin was equilibrated with lysis buffer. Retrieved dialysis and cleaved protein was loaded onto the column dropwise. 5 CVs of lysis buffer were used to clean the walls of the column to ensure maximum protein is bound to the resin. Cleaved MntR was eluted with lysis buffer ranging in imidazole concentration from 20 to 40 mM. Contaminants were washed off of the column using lysis buffer with 300 mM imidazole. Collected fractions were analyzed via SDS-PAGE and by absorption at 280 nm to identify fractions containing mutant MntR. SDS-PAGE was performed with a 12% SDS polyacrylamide gel, run at 200 V in Tris-Glycine buffer (30 g Tris base,

144 g glycine, and 10 g of SDS in 1L water). Fractions containing cleaved MntR were combined, concentrated to a volume <5 mL, and dialyzed overnight in storage buffer (25 mM HEPES pH 7.5, 300 mM NaCl, 10% glycerol at 4C. More detailed expression and purification protocol information for each individual mutant can be found in Appendix A (Appendix A).

Mass Photometry experiments to determine complex formation

The complex of duplex DNA (P84 or P106) and wild type or mutant MntR (Tyr22Ala, Asp27Ala, and Tyr57Ala) was studied using mass photometry. Mass photometry measures the molecular weights of macromolecule species within a sample by measuring the light scattering of single particles as they absorb onto a microscope slide. Such information can provide insights on oligomeric state, heterogeneity of molecules, and mass. Experiments were conducted using the TwoMP mass photometry instrument (Second generation Mass photometer TwoMP0204: AMP version 2024R1.1 and DMP version 2024 R1.0) provided by ReFyne, and data was analyzed using the Refeyn AcquireMP software.

To accurately relate molecular size to the signal intensity, several standards are used. Thyroglobulin is a 660 kDa glycoprotein produced by human follicular cells in the thyroid gland, where it makes up approximately half of the protein content of the gland (Barrett, 1044). Beta amylase, a ~200 kDa enzyme that breaks starch into maltose, was also used as a standard. The protein standard is first suspended in a filtered buffer, usually PBS (137 mM NaCl, 2.7 mM KCl, 10 mM Na₂HPO₄, 1.8 mM KH₂PO₄, milli-Q water) solution that ideally has no impurities, which otherwise can produce significant background noise. Autoclaved water, for instance, often contains precipitants that severely skew the light interference pattern between the glass plate and the proteins in solution.

Complexed samples (consisting of 8 uM WT or mutant MntR and 1 uM P85 DNA) samples were prepared in NB buffer (25mM HEPES pH 7.4, 300mM NaCl, 1mM MnCl₂ in milli-Q water) at 100-fold higher concentration than the expected K_d of MntR for P84 DNA of ~ 2nM to ensure the equilibrium shifted to complete MntR binding to the DNA (Table 3).

Table 3. List of sample components used for mass photometry experiments.

Sample 1 - WT MntR + P84 in 100uL

WT MntR (stock: ~100 uM) 8uM 8.0uL	P84 DNA (stock: 13.5 uM) 1uM 7.4uL	NB Buffer 84.6 uL
--	--	---------------------------------

Sample 2 - Tyr22Ala MntR mutant + P84 in 100uL

Tyr22Ala MntR (stock: 770 uM) 8uM 1.04uL	P84 DNA (stock: 13.5 uM) 1uM 7.4uL	NB Buffer 91.6 uL
--	--	---------------------------------

Sample 3 - Tyr57Ala MntR mutant + P84 in 100uL

Tyr57Ala MntR (stock: 784 uM) 8uM 1.02uL	P84 DNA (stock: 13.5 uM) 1uM 7.4uL	NB Buffer 91.5 uL
--	--	---------------------------------

Sample 4 - Asp27Ala MntR mutant + P84 in 100uL

Asp27Ala MntR (stock: 212 uM) 8uM 3.8uL	P84 DNA (stock: 13.5 uM) 1uM 7.4uL	NB Buffer 88.8 uL
---	--	---------------------------------

For data collection, the above samples were further diluted 50-fold in NB buffer (25mM HEPES pH 7.4, 300mM NaCl, 1mM MnCl₂ in milli-Q water) and then once more diluted 10-fold in PBS (137 mM NaCl, 2.7 mM KCl, 10 mM Na₂HPO₄, and 1.8 mM KH₂PO₄) directly onto the coverslip of the detector. 20 uL of experiment sample (2 uL of MntR-DNA sample and 18 uL of PBS) was loaded onto the detector. Beta-amylase and thyroglobulin were used as protein standards, since these proteins have a similar refractive index to MntR, which ultimately helps to minimize background noise. For both WT MntR and all mutant samples, poly-L-lysine (PLL) plates were used to help better capture the DNA to the plate and minimize background noise.

The 106 bp duplex DNA containing the entire *mneP* promoter region with the four predicted MntR binding sites, the RNA Polymerase binding site, and the transcription start site was commercially synthesized by Integrated DNA Technologies. The 84 bp duplex DNA, which contains part of the *mneP* promoter region (the four predicted MntR binding sites) was prepared by Alex Fu, as previously described (Fu, 2021). The individual DNA oligomers for the P84 duplex were synthesized by Integrated DNA Technologies. The buffer used to suspend these DNA consisted of 25mM HEPES pH 7.4, 300mM NaCl, 1mM MnCl₂ in milli-Q water. Experiments performed sought to identify complex formation between wild type MntR and P84 DNA, as well as identify changes in complex formation between mutant MntR (Tyr22Ala, Asp27Ala, and Tyr57Ala) and P84 duplex DNA.

Results and Discussion

Mutagenesis, Amplification, and Purification

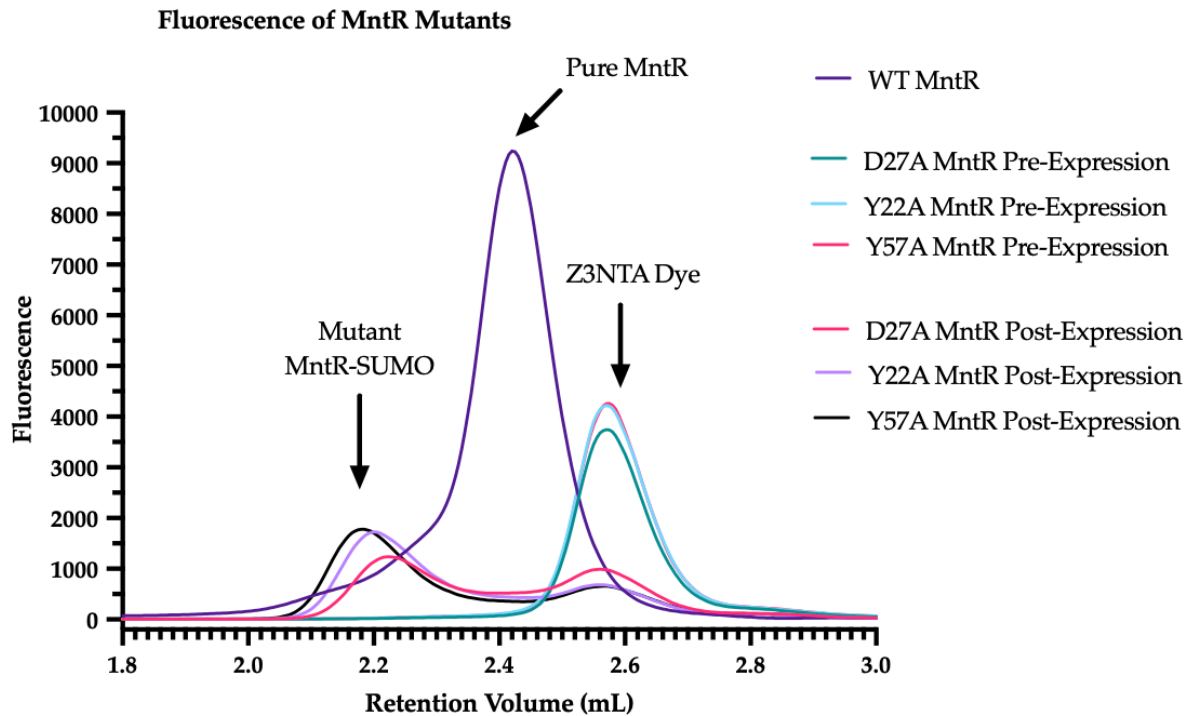
The three MntR mutants, Tyr22Ala, Asp27Ala, and Tyr57Ala were successfully produced in the pSMT3 vector. To check that the intended mutation occurred following site directed mutagenesis, the sequence of the mutated plasmid was compared to the wild-type MntR-encoding plasmid sequence. For the Tyr22Ala and Tyr57Ala mutations, one successfully mutated plasmid was found out of the six transformants that were screened for each mutant. And for the Asp27Ala mutation, two successfully mutated plasmids were found out of the six transformants that were screened.

The mutant plasmids were cloned and amplified by transforming them into DH5-alpha *E. coli*. Then the mutant plasmids were transformed in NiCo21 (DE3) *E. coli* for recombinant expression of the mutant proteins. Cells expressing the mutant MntR protein were grown up and cell pellets were harvested as detailed in the method above.

FSEC of MntR Mutants

FSEC was used to study the expression of mutant MntR following transformation of the plasmid containing the mutant-MntR encoding genetic sequence into *E. coli* cells. SEC measures molecular weights of components in the sample and the homogeneity of samples. In FSEC, the sample also travels to a fluorescence detector, which excites the proteins in the lysate at specific wavelengths and measures the emission. This method produces chromatograms, details of which can be analyzed to evaluate the components of a solution.

Figure 24. FSEC Chromatogram for Histidine fluorescence of MntR mutants pre- and post-IPTG induction.



Cell Lysates: Excitation at 494 nm, Emission at 520 nm

WT MntR Control: Excitation at 280 nm, Emission at 350 nm

Each sample is of one MntR mutant pre-IPTG and post-IPTG induction. WT MntR is used as a control. Z3NTA dye was measured using histidine fluorescence at an excitation wavelength of 494 nm and an emission wavelength of 520 nm. WT MntR was measured using tryptophan fluorescence at an excitation wavelength of 280 nm and an emission wavelength of 350 nm. These samples were run on a Superdex-6 5/150 column in FSEC running buffer at pH 7.5.

The chromatogram above shows successful expression of mutant MntR (Figure 24). Wild type MntR is used as a control to demonstrate where the size of pure MntR should appear (~2.4 mL). The peak is much larger compared to other peaks because this sample was prepared at a higher concentration.

The right-most species on the chromatogram (~2.6 mL) represents the pre-induction mutant MntR samples. Because IPTG had not yet been added to the cultures when these samples were collected, LacI, the protein that binds to the *lac* promoter to prevent transcription, remains bound and associated with the *Lac*

operator. Therefore, the MntR-encoding genetic sequence is not transcribed into RNA, which is necessary for the protein to be translated. The reason for the peaks at ~2.6 mL corresponds to the free Z3NTA dye, which is of a much smaller size compared to the free MntR dimer. Z3NTA dye, which targets His-tags, does not bind to the His-tag of the mutant MntR (since it was not translated pre-induction). Smaller molecules come off the column later, relative to molecules of a larger size, because they get stuck in the beads. Therefore, this species is found on the right of the chromatogram, corresponding to the three pre-expression mutant MntR samples.

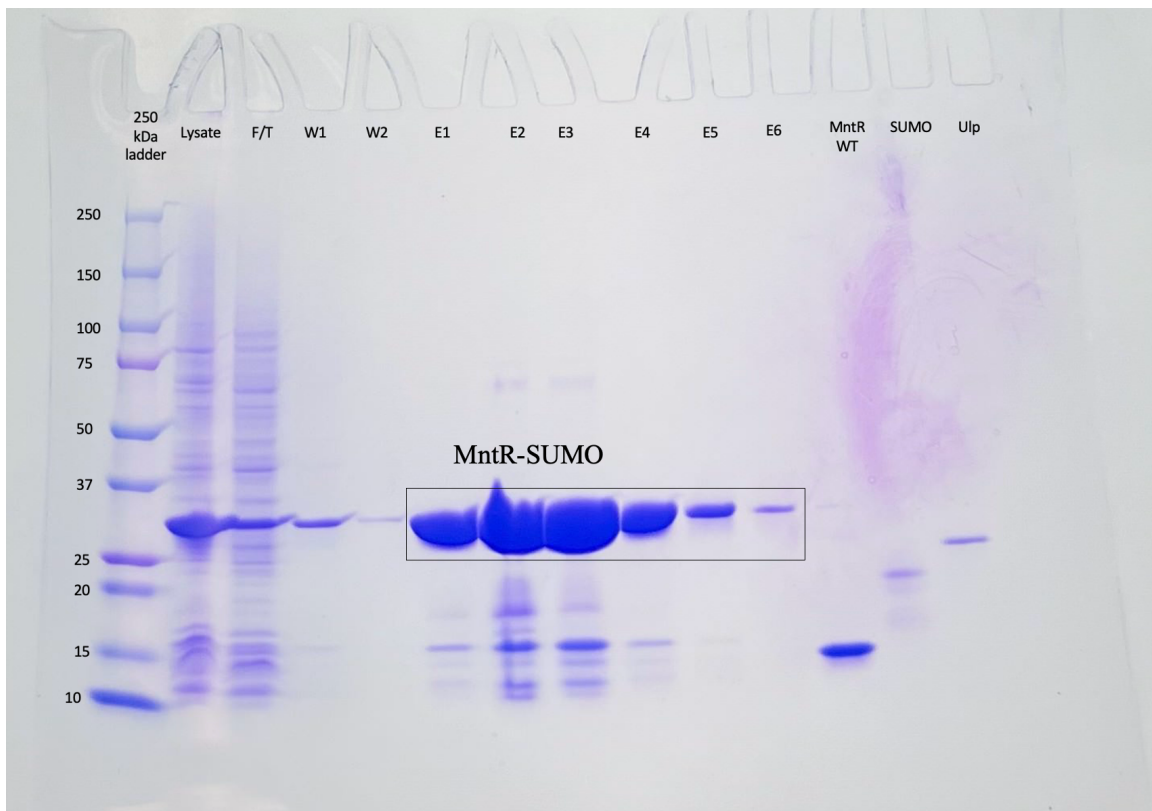
The left-most species on the chromatogram (~2.2 mL) represents the post-expression mutant MntR samples. IPTG had been added, and bacteria were permitted to produce mutant MntR for 2-3 hours. IPTG knocks off LacI, permitting transcription of genetic sequences encoded in the *lac* operator, including the sequence corresponding to the His-tagged mutant MntR. This sequence is transcribed into RNA by RNAP, producing messenger RNA, which is then translated into amino acids by the ribosomes. As such, the peak at 2.2 mL represents the largest species, His-tagged/SUMO-tagged mutant MntR. Z3NTA dye coordinates with the His-tag on the mutant MntR protein, allowing us to detect this species via fluorescence. This peak is shifted to the left of the Wild Type MntR. This is due to the fact that the control used is purified MntR which is no longer covalently linked to the sizable (~12 kDa) SUMO tag (cleaved during the purification protocol). Because the post-expression mutant MntR has not yet been purified, it still possesses the SUMO tag, increasing the size of the full species. Therefore, the species evades the holes in the SEC column's beads, traveling through the column faster and being detected soonest. Therefore, this species is found on the left of the chromatogram, corresponding to the three post-expression mutant MntR samples.

Tyr57Ala MntR Purification

To purify SUMO-tagged Tyr57Ala MntR, 4.5 g of *E. coli* cell pellet containing the expressed protein was resuspended in a lysis buffer and sonicated to separate mutant MntR from the rest of the cell mass. The SUMO-mutant MntR

fusion protein (~ 29 kDa) was successfully purified from the lysate via TALON Co⁺² metal affinity column chromatography (Figure 25). Table 4 shows the relative concentration of protein collected in each fraction (Table 4). The fractions (E1-E4) containing the protein of interest were pooled.

Figure 25. SDS-PAGE gel showing SUMO-Tyr57Ala MntR complex following TALON Co⁺² IMAC column purification



Tyr57Ala MntR-SUMO complex appears at ~29 kDa in elution fractions 1-5.

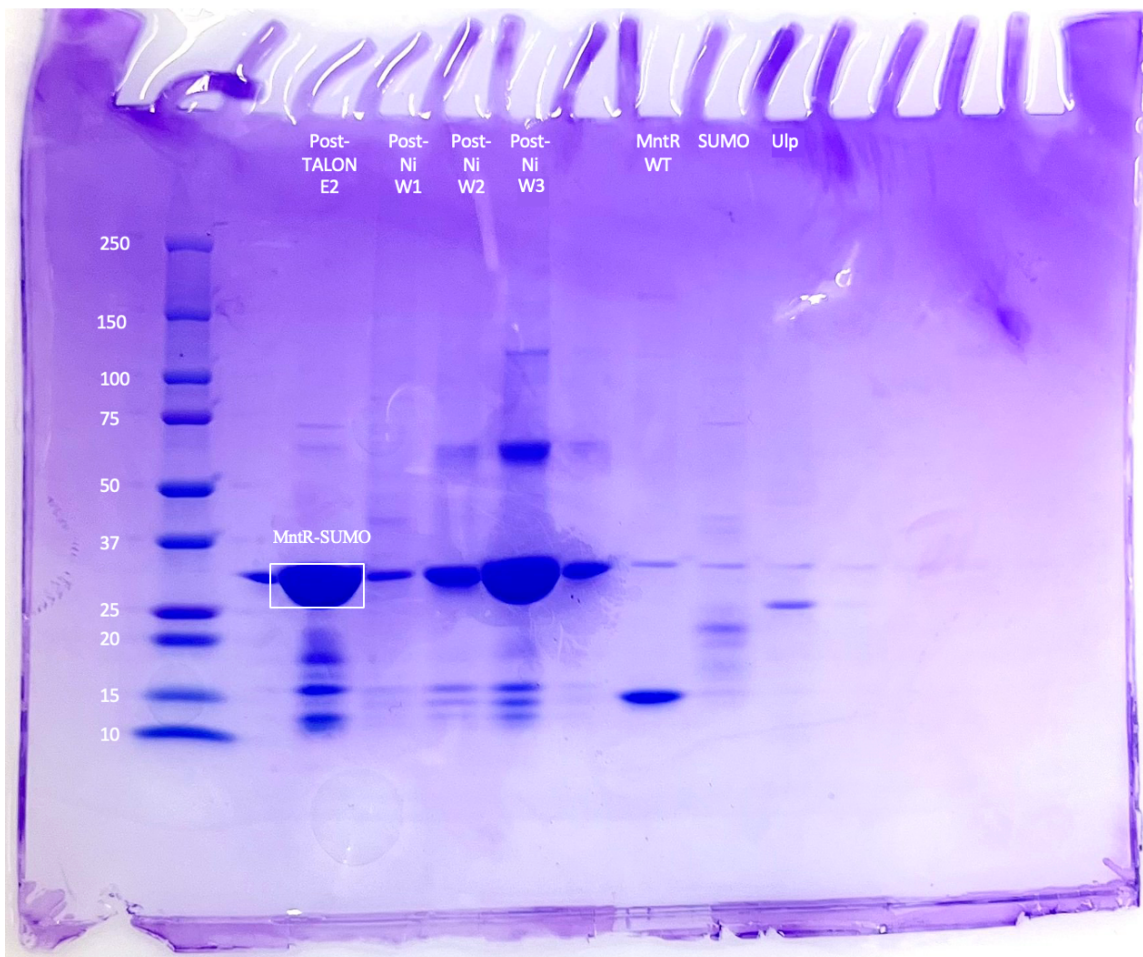
Table 4: TALON Co⁺² IMAC Protein Concentrations for Tyr57Ala MntR Purification

Step	Imidazole (mM)	ND ¹ (mg/mL)	260/280
Flow-through	10	31.17	
Wash 1 (10 CV)	10	2.51	-
W2 (10 CV)	20	0.39	-
Elution 1 (1 CV)	300	1.90	0.49
E2 (1 CV)	300	3.71	0.52
E3 (1 CV)	300	1.08	0.52
E4 (1 CV)	300	0.47	0.76
E5 (1 CV)	300	0.17	0.49
E6 (1 CV)	300	0.13	0.14

¹ND: Nanodrop. This measurement indicates the relative concentration of proteins in the sample based on tryptophan fluorescence (280 nm).

The next step was to cleave the SUMO tag off the mutant protein using a protease called Ulp while dialyzing the purified protein in a dialysis buffer (25 mM HEPES pH 7.5, 300 mM NaCl, 10 mM imidazole, 5% glycerol, 1 mM beta mercaptoethanol). Mistakenly, the Ulp protease was added to the dialysis buffer instead of the pooled protein fraction inside the dialysis cassette. The following morning, 6 mL of the dialyzed protein was retrieved at a concentration of 4.45 mg/mL (26.7 Tyr57Ala MntR-SUMO total). An attempt to purify the uncleaved MntR-SUMO protein complex was made, unsuccessfully. Because Ulp (~ 28 kDa) was added to the dialysis buffer, it could not diffuse into the dialysis cassette, which consists of a port size of < 3 kDa. Therefore, Ulp could not access the SUMO-bound Tyr57Ala MntR inside the cassette, and cleavage did not take place. Figure 26 below shows the uncleaved complex following Reverse Ni⁺² metal affinity column chromatography (Figure 26). Table 5 shows that the entire complex came off the column in the first wash step (Table 5).

Figure 26. SDS-PAGE gel showing uncleaved SUMO-Tyr57Ala MntR following TALON Co⁺² and Reverse Ni⁺² IMAC column purifications



Cleaved Tyr57Ala MntR should appear at ~17 kDa. The SUMO tag features a molecular weight of 12 kDa but can appear on the SDS-PAGE gel anywhere between ~15-17 kDa (Hilgarth, 2005).

Table 5: Reverse Ni⁺² NTA IMAC Protein Concentrations for Tyr57Ala MntR Purification (First Attempt)

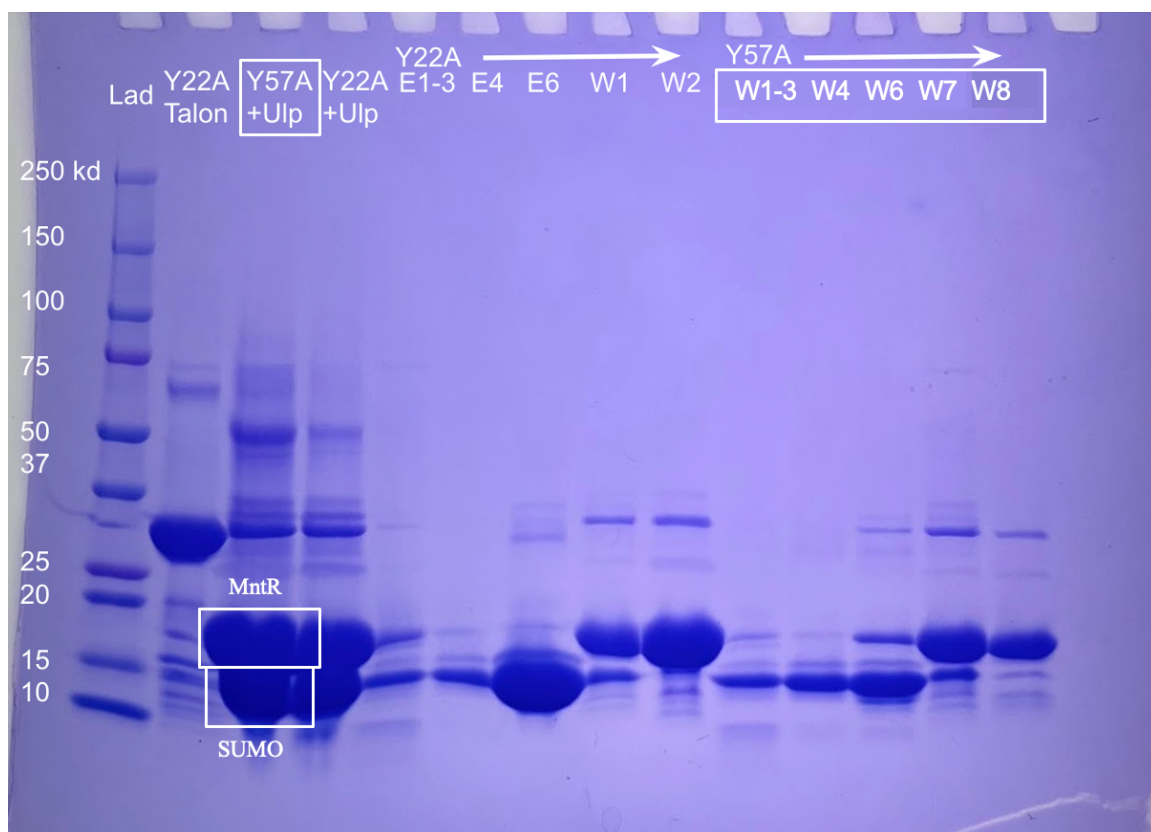
Step	Imidazole (mM)	ND (mg/mL)	260/280
Flow-through	10	1.60	0.83
Wash 1 (1 CV)	10	0.59	0.88
W2 (1 CV)	10	0.11	0.86
W3 (1 CV)	10	0.04	0.29
W4 (1 CV)	10	0	-4.5
W5 (1 CV)	10 -> 300	0.01	-0.61
W6 (1 CV)	300	0.39	0.59
W7 (1 CV)	300	3.29	0.55
W8 (1 CV)	300	1.10	0.58
W9 (1 CV)	300	0.36	0.67
W10 (1 CV)	300	0.21	0.86
W11 (1 CV)	300	0.18	0.83

That evening, 0.2 mg of 2 mg/ml Ulp was correctly added to the pooled protein solution. The solution was dialyzed once more to remove imidazole from the buffer. The next day, Tyr57Ala MntR was purified away from SUMO via Ni⁺² metal affinity column chromatography (Table 6). Fractions (W1-W7) containing pure Tyr57Ala MntR were pooled and dialyzed overnight in storage buffer (Figure 27).

Table 6: Reverse Ni⁺² NTA IMAC Protein Concentrations for Tyr57Ala MntR
Purification (Second Attempt)

Step	Imidazole (mM)	ND (mg/mL)	260/280
Flow-through	10	0.13	1.07
Wash 1 (1 CV)	10	0.58	0.76
W2 (1 CV)	10	0.24	0.6
W3 (1 CV)	20	0.16	0.48
W4 (1 CV)	20	0.71	0.48
W5 (1 CV)	40	0.96	0.44
W6 (1 CV)	40	0.99	0.50
W7 (1 CV)	40	0.14	0.45
W8	300	N/A	N/A
W9	300	N/A	N/A

Figure 27. SDS-PAGE gel showing cleaved Tyr57Ala MntR following second Reverse Ni⁺² IMAC column purification



Cleaved Tyr57Ala MntR appears at ~17 kDa and SUMO appears at 15 kDa. Tyr57Ala MntR was obtained at a concentration of 14.2 mg /mL, for a total yield of 14.2 mg from a cell pellet wet weight of 4.5 g from 2 L of bacterial growth.

Tyr22Ala MntR Purification

SUMO-tagged Tyr22Ala MntR was purified by a fellow thesis student, Amelie Andreas. 5.24 g of *E. coli* cell pellet containing the expressed protein was resuspended in a lysis buffer and sonicated to separate mutant MntR from the rest of the cell mass. The SUMO-mutant MntR fusion protein (~ 27 kDa) was successfully purified from the lysate via TALON Co⁺² metal affinity column chromatography (Figure 28). Table 7 shows the relative concentration of protein collected in each fraction (Table 7). The fractions (E1-E3) containing the protein of interest were pooled and concentrated to ~5 mL for a protein concentration of 6.12 mg /mL (total 30.6 mg).

Figure 28. SDS-PAGE gel showing SUMO-Tyr22Ala MntR complex following TALON Co⁺² IMAC column purification



Tyr57Ala MntR-SUMO complex appears at ~29 kDa in elution fractions 1-5. Gel was prepared by Amelie Andreas.

Table 7: TALON Co⁺² IMAC Protein Concentrations for Tyr22Ala MntR Purification

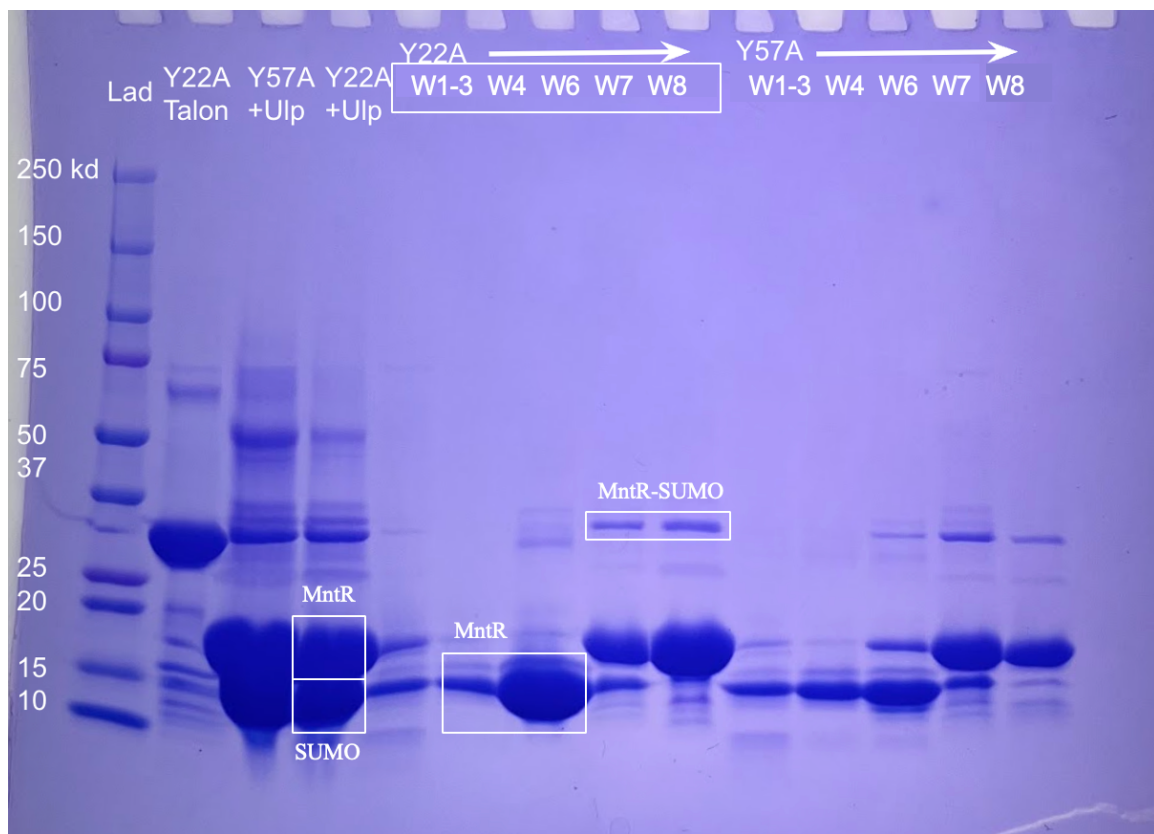
Step	Imidazole (mM)	ND (mg/mL)	260/280	Gel ID
Wash 1 (10 CV)	10	1.02	1.89	Some SUMO-MntR + contaminants
W2 (10 CV)	20	0.17	0.165	Some SUMO-MntR
Elution 1 (1 CV)	300	0.24	0.61	SUMO-MntR + contaminants
E2 (1 CV)	300	2.80	0.54	SUMO-MntR + contaminants
E3 (1 CV)	300	0.27	0.72	SUMO-MntR + some contaminants
E4 (1 CV)	300	0.08	1.11	SUMO-MntR + some contaminants
E5 (1 CV)	300	0.08	1.23	SUMO-MntR + some contaminants

Ulp was added to the pooled protein solution to cleave the SUMO tag off of the mutant MntR protein. The solution was then dialyzed in dialysis buffer overnight. The following morning, 7 mL of the dialyzed protein was retrieved at a concentration of 7.41 mg / mL (51.9 mg Tyr22Ala MntR-SUMO total). Tyr22Ala MntR was then purified away from SUMO via a reverse Ni⁺² metal affinity column chromatography (Table 8). Fractions (W1-W7) containing pure Tyr22Ala MntR were pooled (Figure 29) and dialyzed overnight in storage buffer.

Table 8: Reverse Ni⁺² NTA IMAC Protein Concentrations for Tyr22Ala MntR Purification

Step	Imidazole (mM)	ND (mg/mL)	260/280	Gel ID
Flow-through	10	0.11	0.55	N/A
Wash 1 (1 CV)	10	0.71	0.53	Some cleaved MntR (~17kDa) + contaminants (combined gel samples)
W2 (1 CV)	10	0.43	0.61	
W3 (1 CV)	20	0.12	0.30	
W4 (1 CV)	20	0.17	0.38	Some cleaved MntR + contaminants
W5 (1 CV)	40	1.16	0.48	Majority of cleaved MntR
W6 (1 CV)	40	3.98	0.49	
W7 (1 CV)	40	0.94	0.49	
W8	300	N/A	N/A	Uncleaved MntR, Ulp, SUMO, Some residual uncleaved MntR
W9	300	N/A	N/A	

Figure 29. SDS-PAGE gel showing cleaved Tyr22Ala MntR following second Reverse Ni⁺² IMAC column purification



Cleaved Tyr22Ala MntR appears at ~17 kDa and SUMO appears at 15 kDa. Some uncleaved Tyr22Ala MntR-SUMO came off in the elution steps.

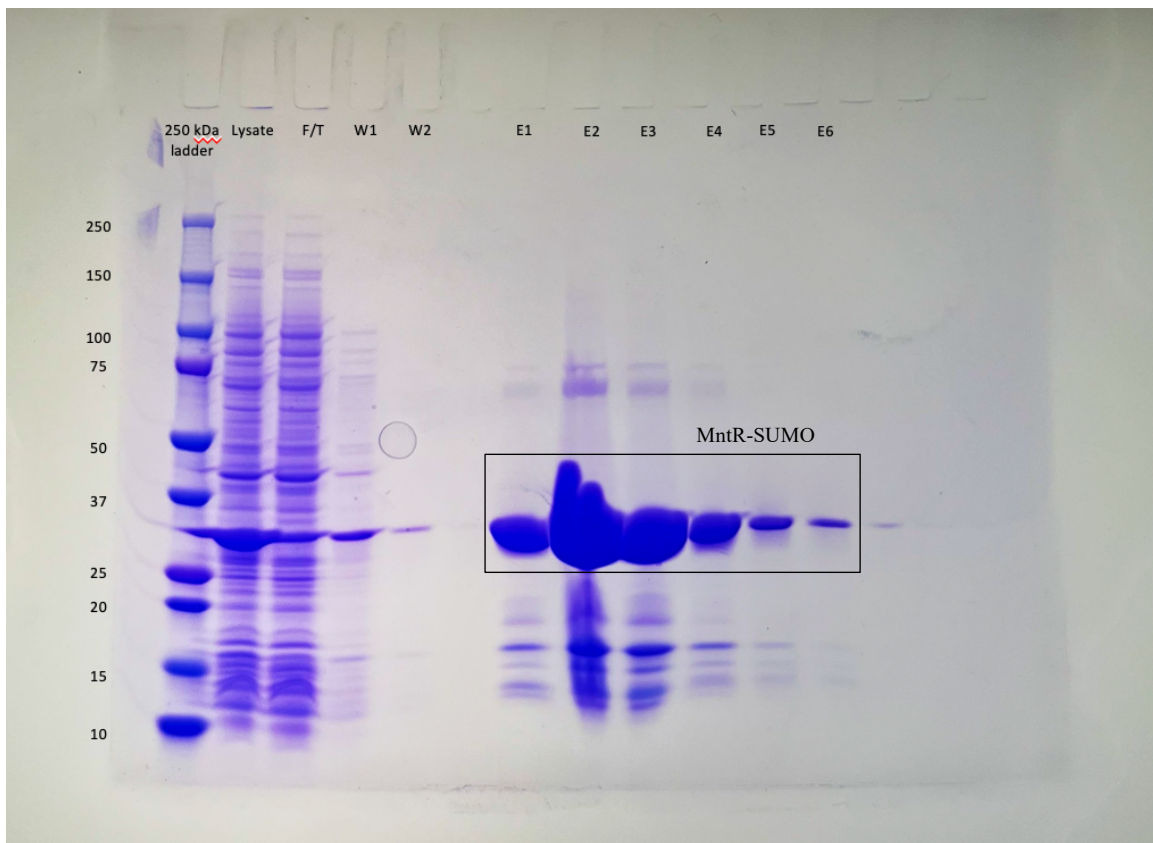
Tyr22Ala was obtained at a concentration of 10.58 mg / mL and flash frozen in liquid nitrogen in 2 1-mL aliquots, for a total yield of 21.16 mg from a cell pellet wet weight of 5.24 g from 2 L of bacterial growth.

Asp27Ala MntR Purification

SUMO-tagged Asp27Ala MntR was purified from 5.20 g of *E. coli* cell pellet containing the expressed protein was resuspended in a lysis buffer and sonicated to separate mutant MntR from the rest of the cell mass. The SUMO-mutant MntR fusion protein (~ 27 kDa) was successfully purified from the lysate via TALON Co⁺² metal affinity column chromatography (Figure 30). Table 9 shows the relative concentration of protein collected in each fraction (Table 9).

The fractions (E1-E4) containing the protein of interest were pooled and concentrated, for a protein concentration of 3.94 mg/mL.

Figure 30. SDS-PAGE gel showing SUMO-Asp27Ala MntR complex following TALON Co⁺² IMAC column purification



Asp27Ala MntR-SUMO complex appears at ~29 kDa in elution fractions 1-6.

Table 9: TALON Co⁺² IMAC Protein Concentrations for Asp27Ala MntR Purification

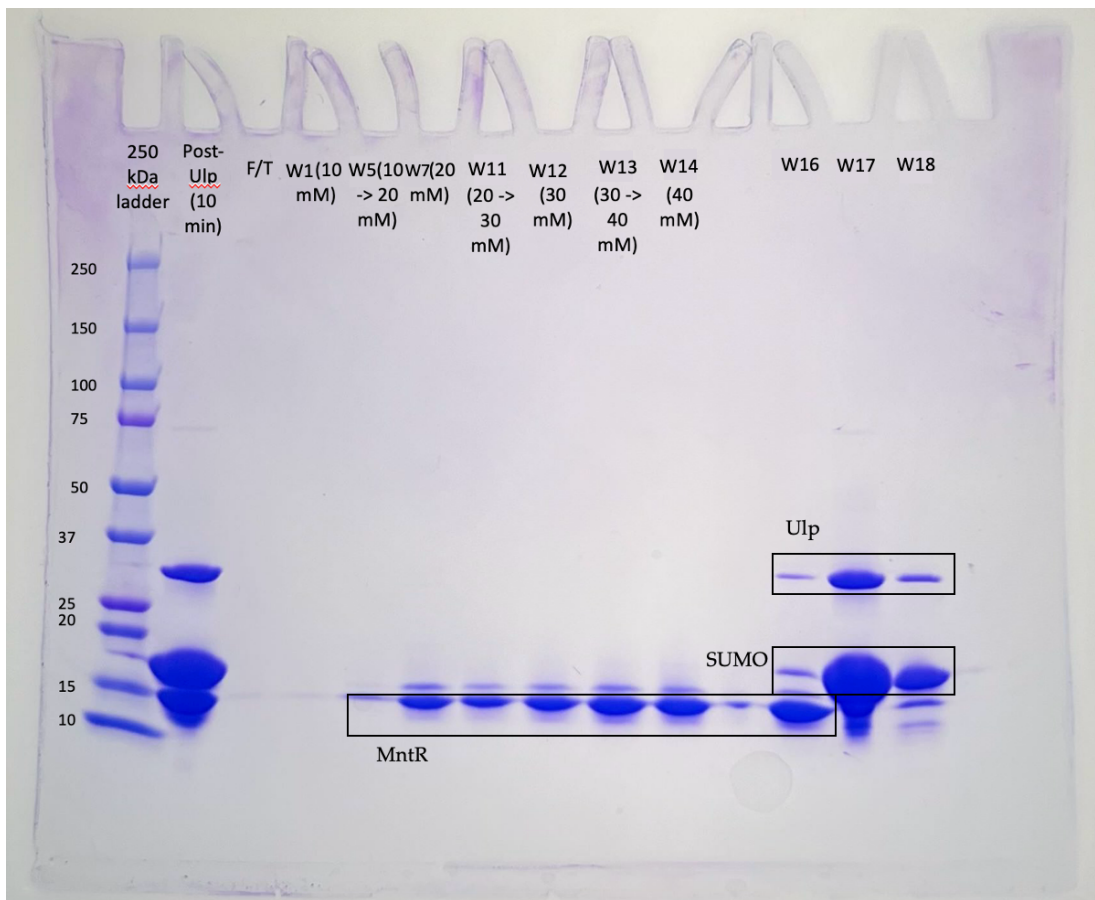
Step	Imidazole (mM)	ND (mg/mL)	260/280
Flow-through	10	Didn't take a ND reading here	-
Wash 1 (10 CV)	10	Didn't take a ND reading here	-
W2 (10 CV)	20	Didn't take a ND reading here	-
Elution 1 (1 CV)	300	0.50	0.37
E2 (1 CV)	300	4.93	0.52
E3 (1 CV)	300	1.95	0.52
E4 (1 CV)	300	0.52	0.60
E5 (1 CV)	300	0.10	0.58
E6 (1 CV)	300	0.03	0.09

0.4 mg of Ulp (100 uL of 2 mg / mL stock) was added to the pooled protein solution to cleave the SUMO tag off of the mutant MntR protein. The solution was then dialyzed in dialysis buffer overnight. The following morning, 5 mL of the dialyzed protein was retrieved at a concentration of 4.14 mg / mL (20.17 mg Asp27Ala MntR-SUMO total). Asp27Ala MntR was then purified away from SUMO via Ni⁺² metal affinity column chromatography (Table 10). Fractions (W7-W14) containing pure Asp27Ala MntR were pooled (Figure 31) and dialyzed overnight in storage buffer.

Table 10: Reverse Ni⁺² NTA IMAC Protein Concentrations for Asp27Ala MntR Purification

Step	Imidazole (mM)	ND (mg/mL)	260/280
Flow-through	10	0.26	0.43
Wash 1 (1 CV)	10	0.09	1.04
W2 (1 CV)	10	0.03	1.50
W3 (1 CV)	10	0.04	0.85
W4 (1 CV)	10	0.06	0.60
W5 (1 CV)	10 -> 20	0.05	0.49
W6 (1 CV)	20	0.19	0.54
W7 (1 CV)	20	0.42	0.52
W8 (1 CV)	20	0.38	0.54
W9 (1 CV)	20	0.34	0.50
W10 (1 CV)	20	0.27	0.45
W11 (1 CV)	20 -> 30	0.30	0.56
W12 (1 CV)	30	0.58	0.49
W13 (1 CV)	30 -> 40	0.82	0.50
W14 (1 CV)	40	0.93	0.48
W15 (1 CV)	40 -> 300	1.13	0.52
W16 (1 CV)	300	1.24	0.59
W17 (1 CV)	300	0.18	0.66
W18 (1 CV)	300	0.04	0.70
W19 (1 CV)	300	0.01	0.32

Figure 31. SDS-PAGE gel showing cleaved Asp27Ala MntR following second reverse Ni⁺² IMAC column purification



Cleaved Asp27Ala MntR appears at ~17 kDa and SUMO appears at ~19 kDa.

Asp27Ala was obtained at a concentration of 10.58 mg / mL and flash frozen in liquid nitrogen in 2 1-mL aliquots, for a total yield of 21.16 mg from a cell pellet wet weight of 5.24 g from 2 L of bacterial growth.

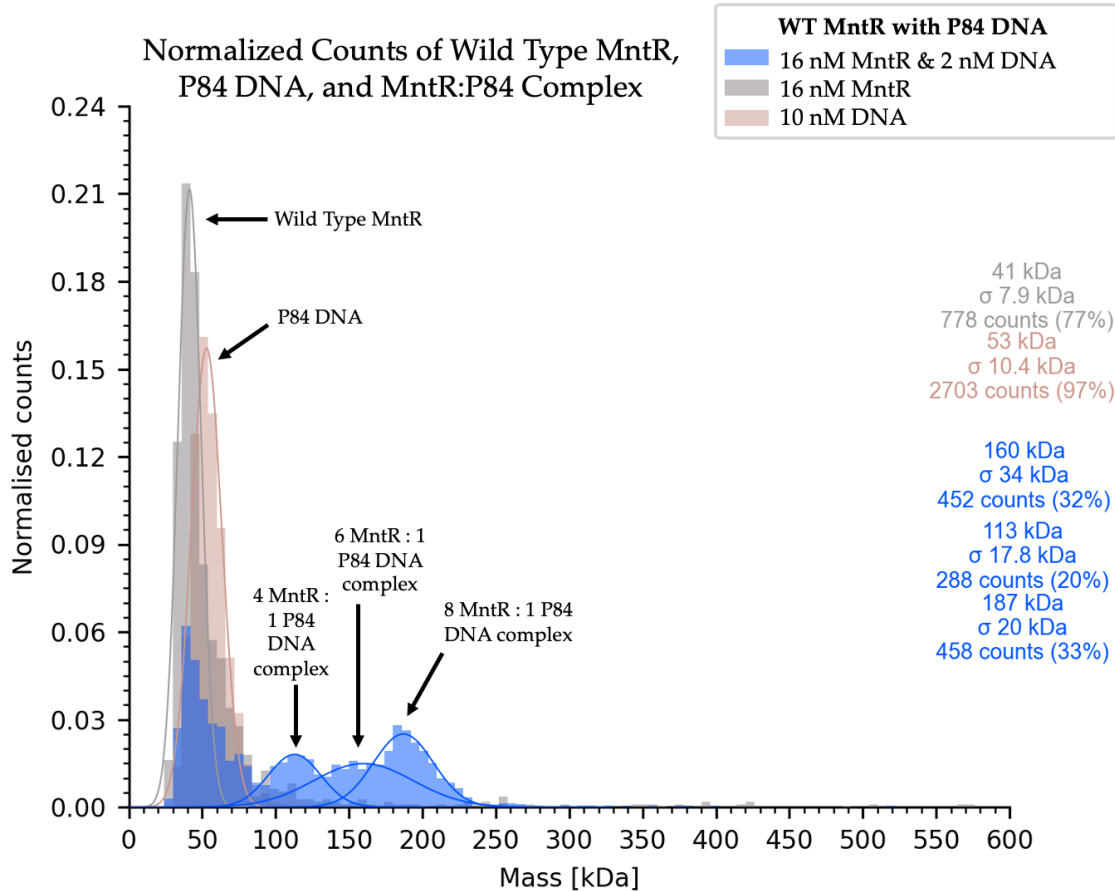
Mass Photometry and FSEC of Wild Type or Mutant MntR, and DNA

The MntR mutants were then complexed with duplex DNA (P84) and studied using mass photometry. Mass photometry measures the molecular weights of macromolecule species within a sample by measuring the light scattering of single particles as they absorb onto a microscope slide. Such

information can provide insights on oligomeric state, heterogeneity of molecules, and their molecular weight.

Samples for mass photometry experiments were prepared at Reed College (as described in the Methods section and Ahuja Lab Protocol SA011324) and kept on ice until arriving to ReFyne.

Figure 32. Mass photometry chromatogram showing differences in complexing between P84 DNA duplex and WT mutant or MntR mutant.

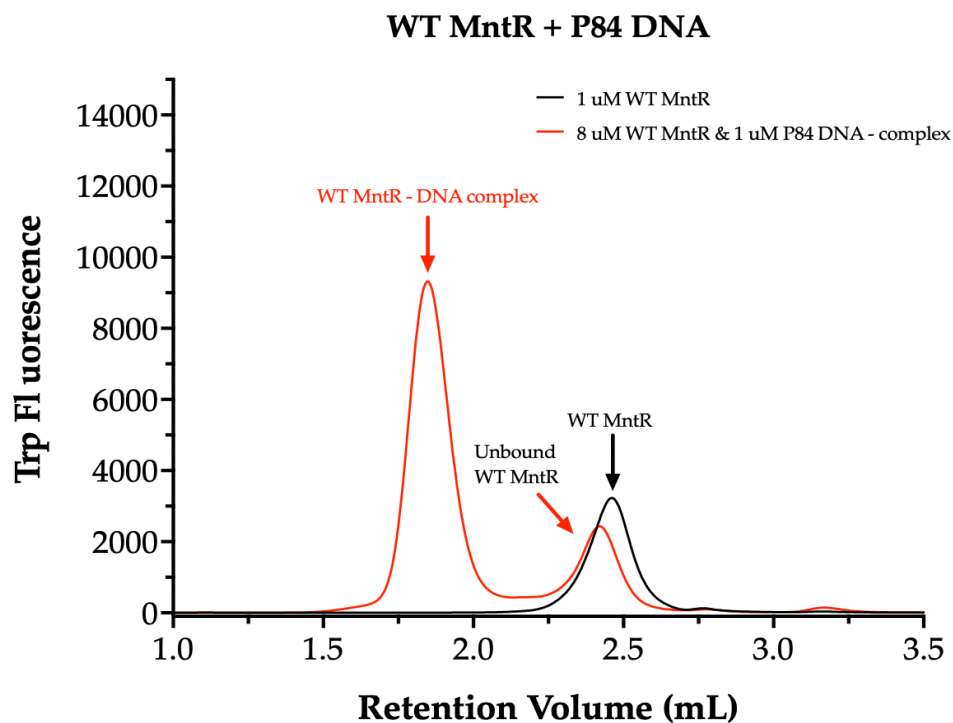


The above spectrum shows complex formation for the WT MntR and the P84 DNA at three different stoichiometries. At 41 kDa, WT MntR dimer (~34 kDa) and, at 53 kDa, P84 DNA exist freely, unbound, in solution. At 113 kDa, the 4 MntR:1 P84 *mneP* DNA appears, indicating that two dimers are bound to the *mneP* promoter sequence of the P84 DNA. At 160 kDa, the 6 MntR:1 DNA complex appears, demonstrating that a third dimer is bound. Finally, at 187 kDa, the fully saturated complex appears. Four dimers of MntR have bound to all four binding sites in the *mneP* promoter region of the P84 construct. These data that

one MntR dimer first binds and immediately recruits another dimer to bind to the DNA duplex. Furthermore, once the two MntR dimers bind to the DNA, an allosteric response is initiated, facilitating the binding of the other MntR dimers, one by one, to the *mneP* promoter.

To further confirm these complexation trends, FSEC was run on all three mutants with the P84 DNA. FSEC was run on the same samples that were prepared for the mass photometry experiments described above.

Figure 33. FSEC chromatogram showing complexing behavior between P84 DNA duplex and WT MntR.



The above spectrum shows the FSEC results for wild type MntR complexed with the P84 DNA (red), with pure wild type MntR run as a control (black). The peak at 2.45 mL (black) indicates the presence of free dimerized MntR. The wild type MntR complexed with the DNA at a high oligomeric ratio is a heavier species, so the main peak is shifted to the left (~1.8 mL). The left-most peak likely indicates an 8 MntR:1 P84 species, which is the dominant stoichiometry as verified in the mass photometry data (Figure 32). The small red peak on the right (~2.4) indicates excess MntR. It appears shifted to the left in

relation to the free wild type MntR (black) (2.45 mL). This may be due to 1-2 dimers of MntR having bound to the DNA, resulting in a slightly heavier species. These data once again raise the inquiry of whether one or two MntR first bind to the *mneP* promoter to initiate the allosteric recruitment of the other MntR dimers to the promoter sequence.

Tyr57Ala – MntR DNA coordination

Figure 34. Mass photometry chromatogram showing complexing behavior between P84 DNA duplex and Tyr57Ala MntR mutant.

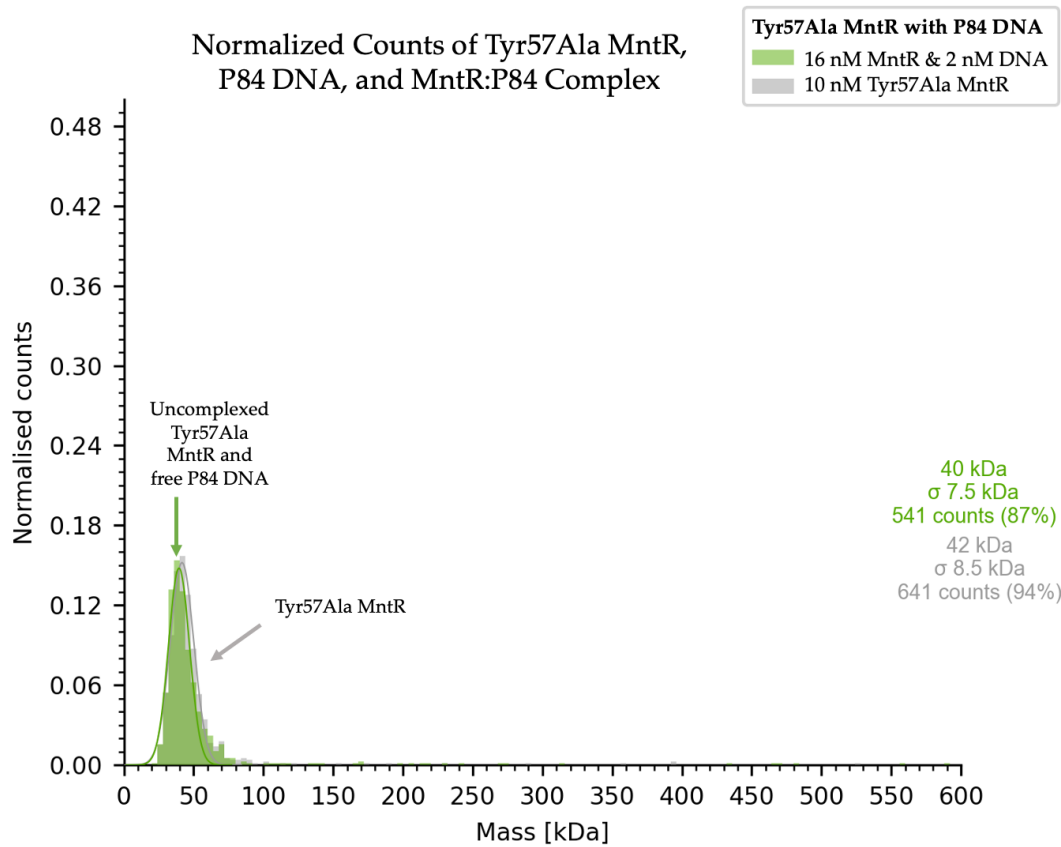


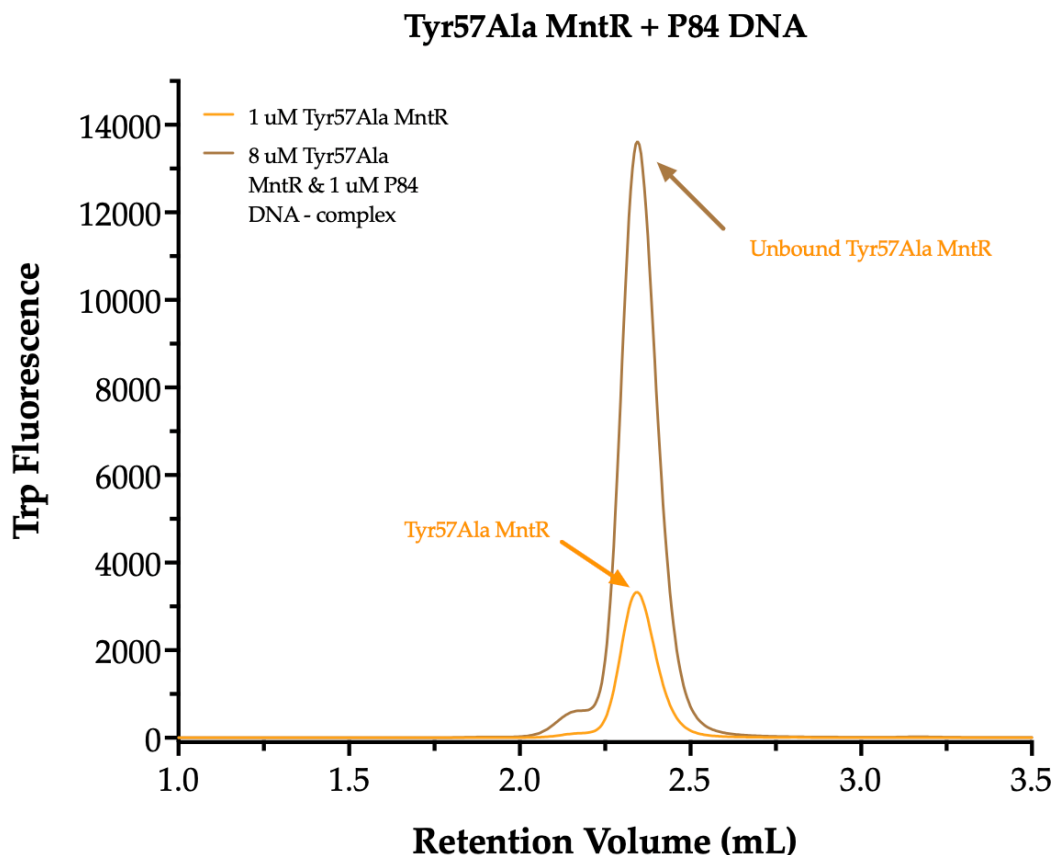
Figure 34 shows the Tyr57Ala mass photometry chromatogram. Only one peak appears for the complex sample (green), suggesting that this mutated MntR entirely fails to complex with the DNA. The complex sample (green) appears at 40 kDa, the same place as the free Tyr57Ala MntR. Therefore, it seems that the MntR dimer (34 kDa) does not bind to the P84 DNA (52 kDa).

The Tyr57Ala mutation disrupts the ability for the DNA recognition helix domain of MntR to properly rotate once bound to Mn⁺². By mutating tyrosine to

an alanine, it is apparent that the residue at site 57 plays an instrumental role in stabilizing the coordination between the MntR dimer and the DNA.

These data provide evidence that two MntR dimers do not first complex together and then bind to the DNA. Because the Tyr57Ala mutation preserves inter-dimer contacts, if two MntR dimers do first complex together and then bind to the DNA, a peak at ~64 kDa would be expected in the Tyr57Ala mass photometry chromatogram, showing that two MntR dimers can complex together in a stable manner. Because this peak is not present, it is more likely that one MntR dimer first binds to the *mneP* promoter, and the complex is not stable until another dimer immediately binds alongside the first MntR dimer to the promoter. The inter-dimer contact, preserved in this mutation, seems crucial for the initial 4 MntR: 1 DNA complex to form and stabilize.

Figure 35. FSEC chromatogram showing complexing behavior between P84 DNA duplex and Tyr57Ala MntR mutant.

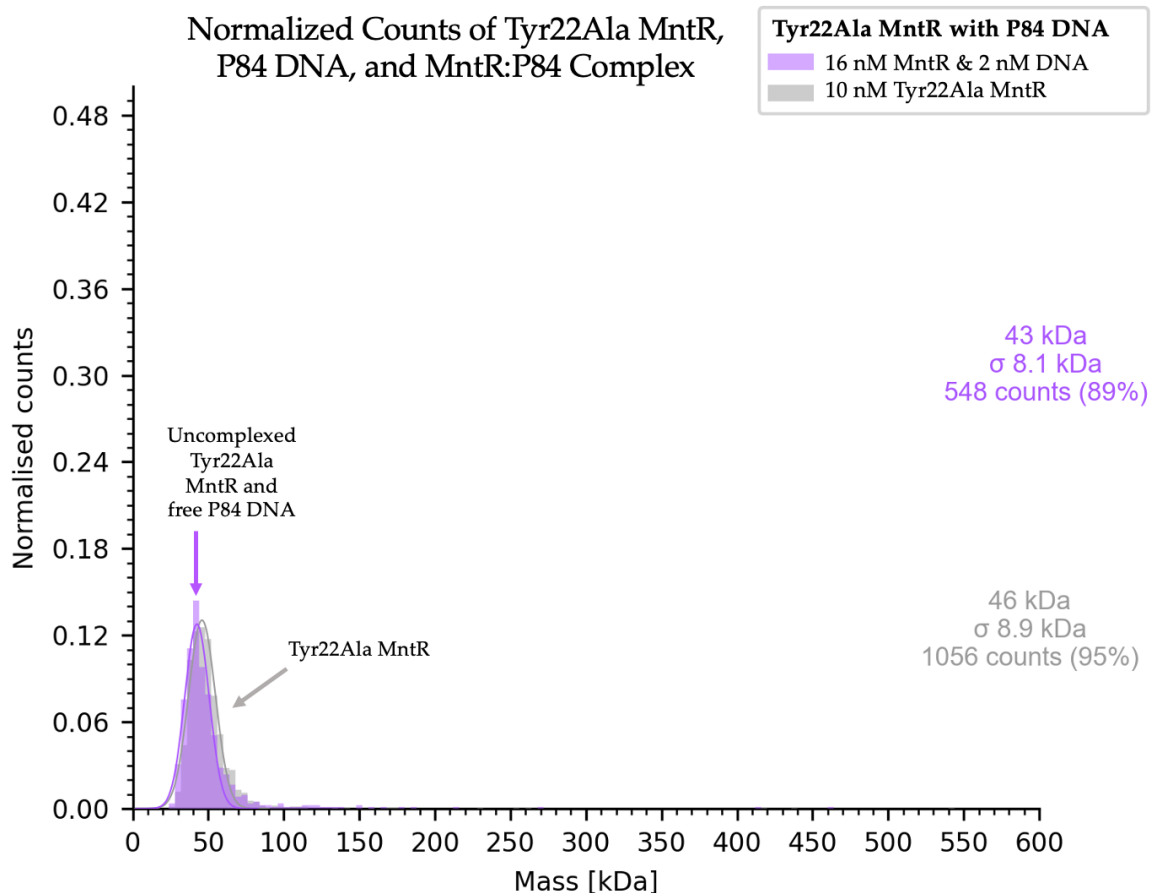


The Tyr57Ala FSEC chromatogram confirms that Tyr57Ala MntR failed to complex with the P84 DNA. The two peaks are overlayed on top of one another (2.3 mL), suggesting that these are the same species: free dimerized MntR, not bound to DNA.

Tyr57 engages in either hydrogen bonding or pi-pi stacking with the nucleotide base in the minor groove of the DNA to stabilize the coordination between the two species. The mutation to an alanine prevents this stabilization from taking the place, and as the FSEC suggests, other residues do not sufficiently supplement for the lack of this unique interaction. These data, in concurrence with the mass photometry data, indicate that tyrosine at position 57 is essential for proper MntR:DNA complex formation and that no MntR binds to the binding site in the *mneP* promoter without this crucial residue.

Tyr22Ala—Inter-dimer stabilization

Figure 36. Mass photometry chromatogram showing complexing behavior between P84 DNA duplex and Tyr22Ala MntR mutant.



In the Tyr22Ala chromatogram, only one peak appears at 43 kDa, in alignment with the free Tyr22Ala MntR dimer (46 kDa). As apparent from the absence of peaks of greater molecular weight, a complex between MntR and P84 also fails to form.

At site 22 in the wild type MntR, tyrosine engages in an ion-dipole interaction with a glutamic acid residue (site 55) on a separate dimer, which is believed to aid in holding the two MntR dimers together. Alanine contains a methyl group that fails to form any polar interaction with the glutamic acid residue on the neighboring MntR dimer, which disrupts the stabilization between the two MntR dimers. By disrupting this inter-dimer contact, MntR cannot stably coordinate with another dimer upon binding to the DNA.

Figure 37. FSEC chromatogram showing complexing behavior between P84 DNA duplex and Tyr22Ala MntR mutant.

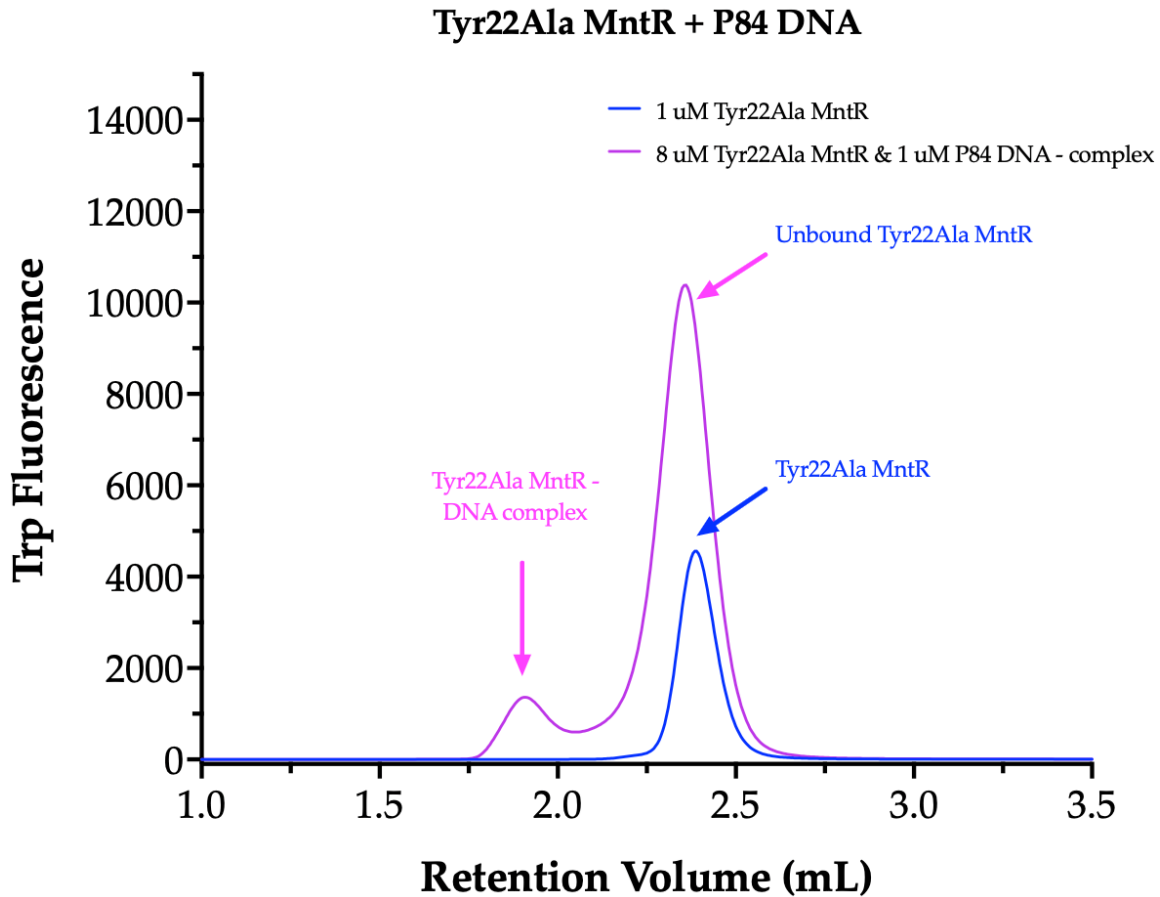


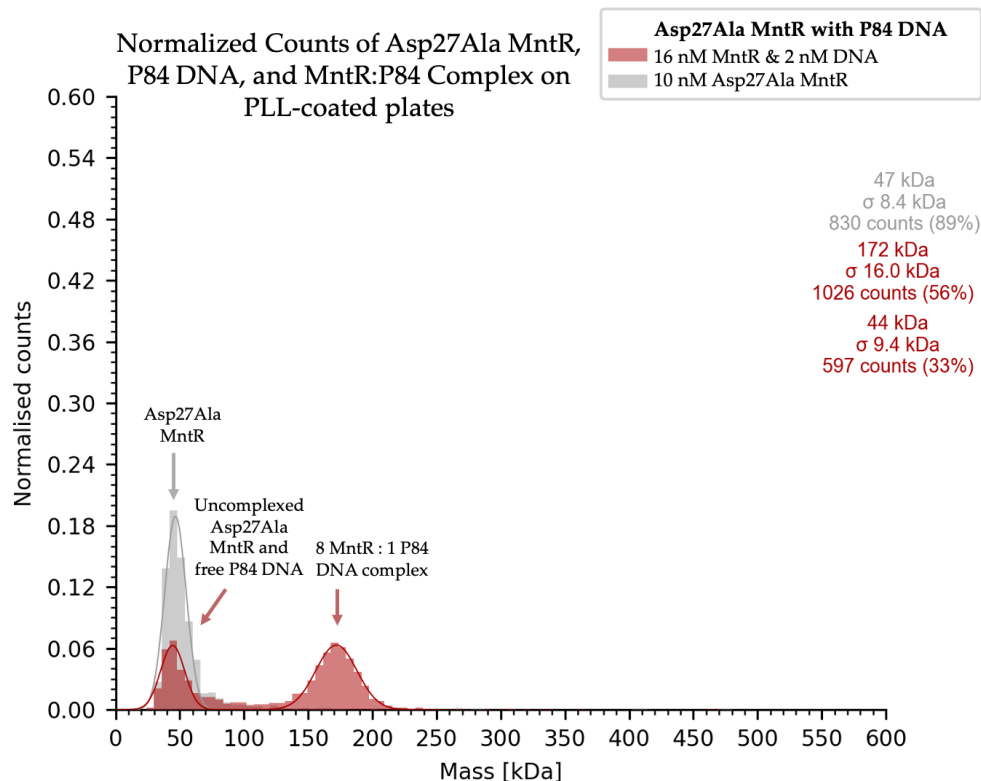
Figure 37 shows that Tyr22Ala MntR was somewhat complexed with the P84 DNA. In the mass photometry experiment, Tyr22Ala MntR completely failed to complex. The FSEC chromatogram shows that although most of the Tyr22Ala MntR does not complex with the DNA, some of it still does, evident by the small bump shifted left, where the complex peak is expected. The complex peak appears at 1.8 mL, which corresponds to the same oligomeric ratio of the 8 MntR:1 P84 seen in the wild type MntR FSEC chromatogram (Figure 32). Furthermore, the unbound Tyr22Ala MntR peak appears at ~2.4 mL, which is consistent with the unbound Tyr57Ala MntR peak at 2.4 mL (Figure 35).

These data show that MntR:P84 complexation is still possible at comparable stoichiometry to Wild Type MntR when inter-dimer contacts are disrupted, although most of the MntR stays unbound, as evident by the larger

peak shifted to the right nearly overlaying the free Tyr22Ala MntR sample peak (2.3 mL). This observation likely results from the different concentration of sample that these experiments were run with. Following several dilutions, nanomolar concentrations of sample were used for mass photometry, at the same scale with the K_d (~2 nM) of MntR for DNA. However, the original undiluted samples at micromolar concentrations were used for FSEC, way beyond the K_d of MntR for DNA. Because the reaction equilibrium was shifted far toward reactant formation, higher concentrations of reactants will push the dynamic equilibrium back towards the products, according to Le Chatelier's Principle. Therefore, some small oligomeric states of complex formation are apparent in the FSEC data for Tyr22Ala, as shown by the left-shifted peak 1.8 mL.

Asp27Ala – Intra-dimer coordination

Figure 38. Mass photometry chromatogram showing complexing behavior between P84 DNA duplex and Asp27Ala MntR mutant using PLL-coated plates.

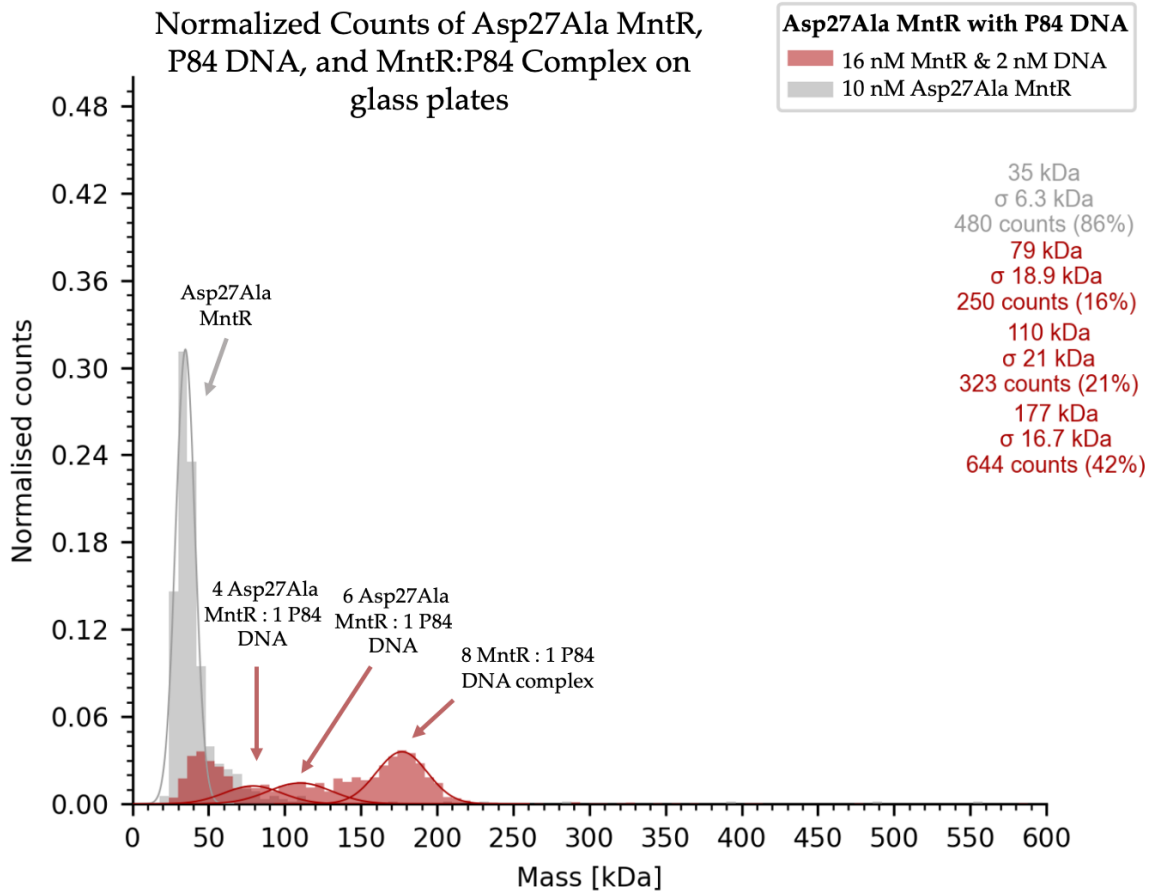


For the Asp27Ala mutant, it appears that the MntR-DNA complex successfully forms at the highest stoichiometric ratio, 8:1 MntR:P84. Unlike in

Figure 32 where many oligomeric states existed for the MntR:P84 complex, Figure 38 shows that the 8:1 MntR:P84 oligomeric state is most stable. The 172 kDa peak indicates four dimers of MntR bound to all four MntR binding sites on the *mneP* promoter. The 44 kDa peak likely represents excess MntR and indicates that all binding sites on all P84 molecules are full. These data suggest that the Asp37Ala mutation strengthened the allosteric response produced by the first MntR dimers binding.

The mutation from an aspartic acid to an alanine at site 27 de-stabilizes the salt bridges the native residue engages in with nearby lysine (site 20) and arginine (site 58). These residues (Lys20, Arg58, and Asp27Ala) are no longer tightly interlocked into a network of salt bridges. Consequently, electronegative Ser26 coordinates more tightly with the positively charged phosphate backbone of the DNA, greatly increasing the affinity of MntR for the DNA (Figure 19). Therefore, as the data from both mass photometry and FSEC show, the MntR:DNA complex readily forms, favoring the 8 MntR:1 DNA oligomeric state.

Figure 39. Mass photometry chromatogram showing complexing behavior between P84 DNA duplex and Asp27Ala MntR mutant on normal glass plates.

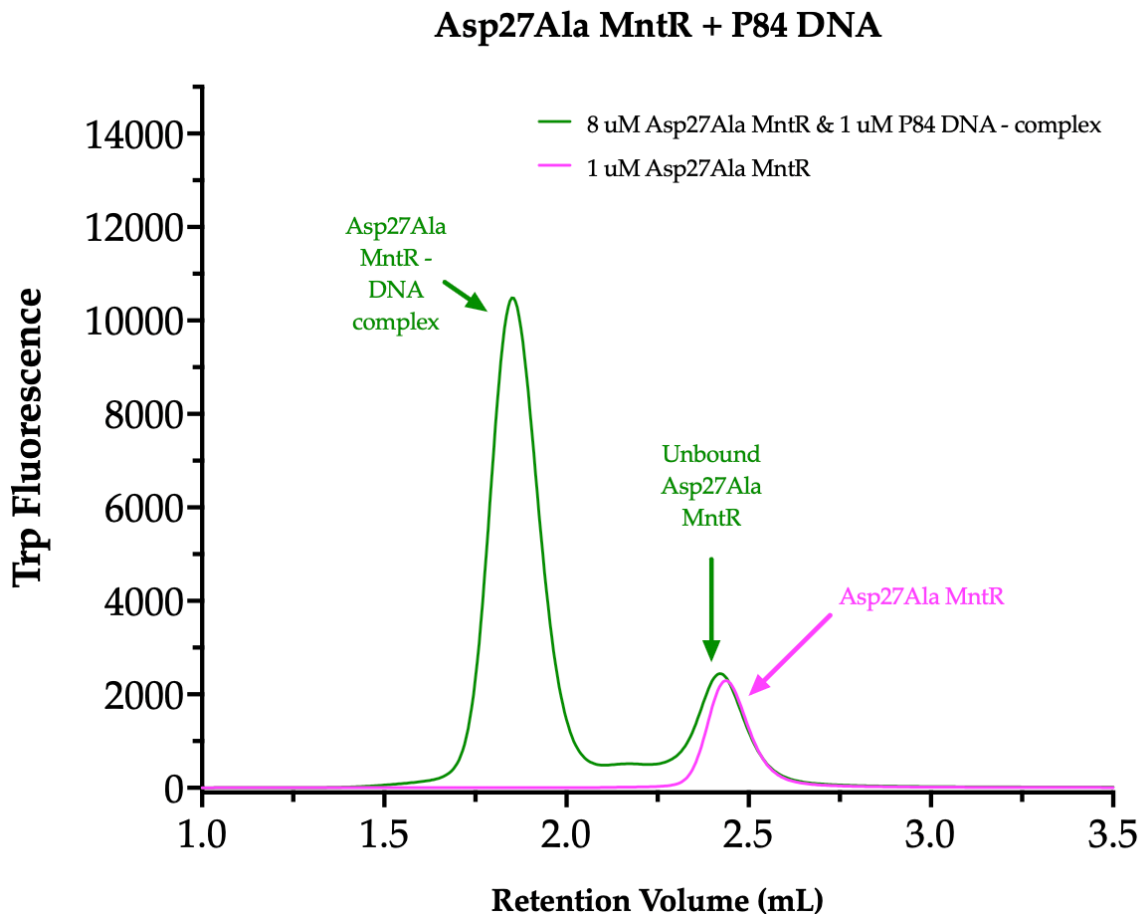


The data above show some differences from those collected when Asp27Ala samples were loaded on poly-L-lysine coated plates. Similar to the data observed for the wild type MntR (Figure 32) and unlike the Asp27Ala-PLL data (Figure 38), all oligomers are observed (4 MntR: 1 P84; 6 MntR: 1 P84; 8 MntR: 1 P84). The 8:1 stoichiometry is observed at the highest concentration, as indicated by the tallest peak shifted most right (177 kDa), which does corroborate the data observed in Figure 38.

The data should be repeated to reconcile whether Asp27Ala does only produce the 8 MntR: 1 DNA complex species. Because poly-L-lysine better coordinates DNA to the plate, it is possible that it was kinetically easier for MntR to bind to the DNA on the plate, increasing the count of 8 MntR:1 DNA species detected. When the samples were run on glass plates, more of the 4:1 and 6:1 MntR:P84 complex species are observed. Despite the samples being prepared an

hour in advance at concentrations that surpassed the K_d of MntR for the P84 DNA, it is likely that the mass photometry detector captured oligomeric states that were in process of becoming 8:1 species. Nonetheless, the Asp27Ala mass photometry collectively suggest that the 8 MntR: 1 P84 species is most favored.

Figure 40. FSEC chromatogram showing complexing behavior between P84 DNA duplex and Asp27Ala MntR mutant.



The Asp27Ala chromatogram illustrates the effect of the Asp27Ala mutation on complexing behavior between MntR and the P84 *mneP* promoter. Most of the Asp27Ala MntR complexes with the DNA, as indicated by the taller left-shifted peak (~1.8 mL). As observed in the mass photometry data (Figure 35), Asp27Ala-PLL produced a fully saturated 8 MntR:1 DNA complex, indicating that the peak at this position (~1.8 mL) corresponds to this oligomeric ratio. Some of the MntR did not bind, as represented by the smaller peak to the right. This indicates that Asp27Ala may still produce a smaller oligomeric ratio

complex, as was observed when the mass photometry experiment for Asp27Ala was repeated on normal glass plates, instead of poly-L-lysine coated plates, as discussed above.

These data reinforce the finding that Asp27Ala aids in stabilizing the complexation of the MntR dimers, likely by increasing the affinity MntR arginine residue (site 24) has for phosphate backbone of the DNA.

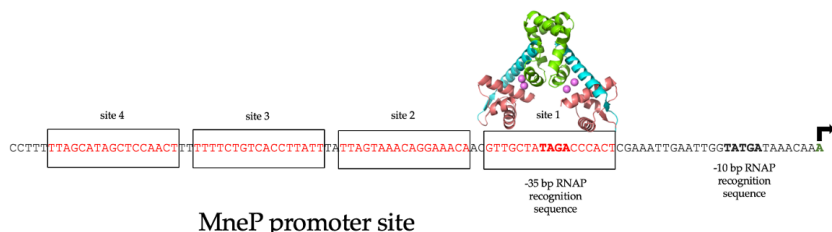
*Proposed mechanism of MntR activation of *mneP* expression*

Taking all the above mass photometry and FSEC data together, a mechanism of activation can be proposed. It seems that upon binding four Mn⁺² ions, the DNA recognition domain of the MntR dimer rotates 30 degrees, exposing the residues of that domain to the DNA. Metal binding to A and C sites allows the linker helix to adopt a more rigid confirmation, such that the N-terminal DNA-binding domain has a fixed orientation across the MntR dimer, which greatly increases the affinity for DNA (DeWitt et al., 2007). Upon rotation of this domain, Tyr57 then interacts with one or more of the DNA nucleotide base pairs in a highly stable manner.

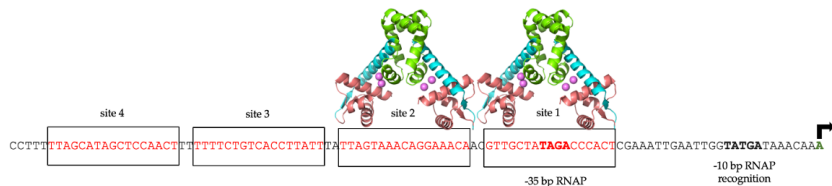
One holo-MntR dimer binds to one of the four MntR binding sites, but this complex species is relatively unstable until another MntR dimer is recruited and binds alongside the first dimer (Figure 41). The two MntR dimers stabilize one another through inter-dimer contacts, as evident by the above collected data demonstrating that minimally, only a 4 MntR:1 P84 complex forms. Upon formation, this species allosterically recruits other MntR dimers, one by one, to fill the other two MntR binding sites on the *mneP* promoter sequence. Notably, as Huang et al. have found, three binding sites must be occupied for the transcription of the *mneP* operator (Huang et al., 2017).

Figure 41. Proposed mechanism of *mneP* activation by MntR.

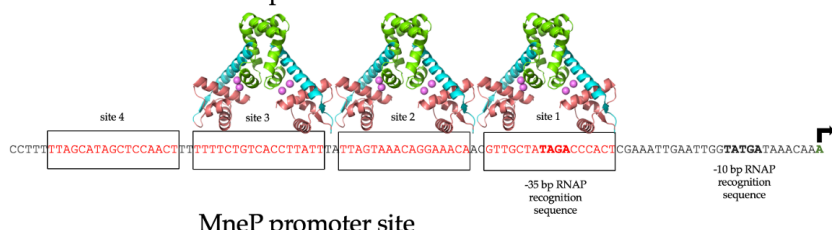
1.) Upon binding four Mn²⁺ ions, MntR binds to site 1 of the *mneP* promoter. Another MntR dimer is allosterically recruited



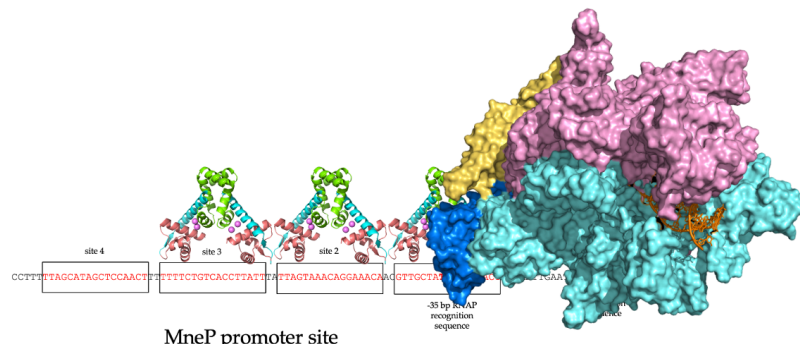
2.) A second MntR dimer binds to site 2 of the *mneP* promoter, producing a stable 4 MntR:1 DNA complex. This is yet not sufficient for *mneP* expression



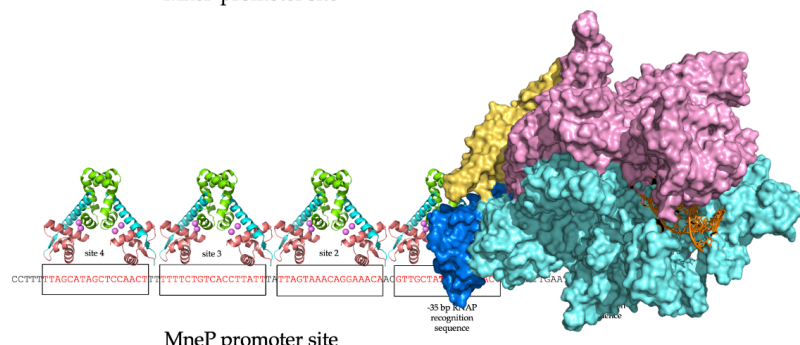
3.) A third MntR dimer binds



4.) Once three MntR dimers have bound, RNAP binds to the -35 bp recognition sequence to initiate transcription of the *mneP* operator



5.) Four MntR dimers bind for complete *mneP* expression



Furthermore, MntR binding site 1 overlaps with one of the two RNAP recognition sequences. Does the first dimer bind to MntR binding site one? Perhaps two MntR dimers bind to sites 1 and 2 and allosterically recruit MntR dimers to fill sites 3 and 4. It has been established that at least three MntR

binding sites should be filled before *mneP* is expressed (Huang et al., 2017). This may mean that three MntR dimers should bind before RNAP is recruited to transcribe the operator. However, it may be that RNAP physically interacts with the first MntR dimer once it binds to site 1 to stabilize the MntR:RNAP:DNA complex, which initiates the allosteric recruitment of the other MntR dimers. The interaction between RNAP and MntR at binding site 1 to activate specific expression of *mneP* remains elusive and is the focus of future research on this project.

Conclusions and Future Directions

Metal ion regulation is a key component contributing to bacterial virulence. This thesis focuses on the Mn⁺² transcription regulator, MntR, which features a fascinating ability to control the transcription of both Mn⁺² importer and exporters in *Bacillus subtilis*. By producing mutations to key conserved amino acid residues, the molecular mechanism of transcriptional activation of the *mneP* operator site is studied. Mass photometry, in addition to size exclusion chromatography, was used to study the oligomer stoichiometry of mutant MntR complexed with the P84 DNA construct, which features four MntR binding sites.

We validated our 4 MntR:1 DNA cryo-EM structure and verified complex formation or absence between multiple MntR dimers and the native *mneP* operator sequence. Mass photometry, a new technique for the Ahuja lab, was used to determine the oligomeric state of mutant MntR complexes with P84 DNA. Future studies should perform complexing experiments between RNAP, sigma factor *a*, the MneP106 DNA construct, and wild type MntR to identify possible oligomeric states, using both mass photometry and cryo-EM as possible techniques. This will help further elucidate the mechanism of transcriptional activation by MntR. Overall, this thesis contributes to closing the gap in our understanding of the mechanisms of regulation of manganese homeostasis in bacteria.

Appendix A: MntR Mutagenesis Reaction Protocols

Table A1. Q5 Site Directed Mutagenesis PCR Reagents

Reagent	Volume Added	Final Concentration
Q5 High-Fidelity 2X Master Mix	12.5 uL	1X
10 uM Forward Primer	1.25 uL	0.5 uM
10 uM Reverse Primer	1.25 uL	0.5 uM
Template DNA (1-25 ng/uL pSMT3)	0.338 uL (of 29.5 ng/uL)	10 ng
Nuclease-free Water	9.6 uL (fill to 25 uL)	-

Table A2. Q5 Site Directed Mutagenesis PCR Thermocycler Conditions

Step #	Instructions
1	Preheat for initial denaturation at 98 °C for 30 s
2	Denaturation at 98 °C for 10 s
3	Annealing at 57 °C for 30 sec
4	Extension at 72 °C for 3 min (30s per 1 kbp)
5	GoTo Step 2 and cycle 25 times
6	Final Extension at 72 °C for 10 min
7	Hold Temperature at 4 °C
	Stop and take out the sample any time after Step 6.

Table A3. KLD Incubation Reaction Reagents and Protocol

Reagent ¹	Volume Added	Final Concentration
PCR Product	1 uL	-

KLD Reaction Buffer 2X (NEB #B0554A)	5 uL	1X
KLD Enzyme Mix 10X (NEB #M0554S)	1 uL	1X
Nuclease-free Water	3 uL (fill to 10 uL)	-

¹ Mixed well by pipetting. Let stand at room temperature for 5 min. Incubated at 37 °C for 1 hour.

Table A4. Qiagen MiniPrep Protocol for Plasmid Purification.

Step	Instructions
1	Centrifuge ¹ cells at 5000 xg at 18 °C for 15 min.
2	Resuspend each cell mixture with 500 uL of Buffer P1 ² . Transfer 250 uL into a microcentrifuge tube. Repeat for another tube.
3	Add 250 uL Buffer P2 and mix by inverting 4-6 times. Do not allow lysis reaction to occur longer than 5 min. Reaction should turn blue.
4	Add 350 uL of Buffer N3 ³ . Mix by inverting 4-6 times. Reaction should become colorless.
5	Centrifuge at 17,900 xg (13,000 rpm in tabletop) at 18 °C for 10 min.
6	Apply 800 uL of supernatant from Step 5 to QIAprep 2.0 Spin Column by pipetting.
7	Centrifuge at 13,000 rpm at 18 °C for 30-60 s. Discard flow-through.
8	Wash column by adding 500 uL of Buffer PB ⁴ and centrifuging at 13,000 rpm at 18 °C for 30-60 s.
9	Wash column by adding 750 uL Buffer PE ⁵ and centrifuging at 13,000 rpm at 18 °C for 30-60 s.
10	Discard flow-through, and centrifuge at full speed for an additional 1 min to remove residual wash buffer.
11	Place column into a clean 1.5 mL microcentrifuge tube. To elute DNA, add 50 uL Buffer EB ⁶ to the center of the column, let stand for 1 min, and centrifuge at 13,000 rpm at 18 °C for 1 min. Nanodrop ⁷ at Abs260 to measure the DNA concentration.

¹Hettich Universal 320 R benchtop centrifuge was used.

²RNase A (final concentration of 100 ug / mL) and LyseBlue reagent (color indicator; 1:1000) should be added to Buffer P1 prior to use, and the buffer should be stored at 4 °C. Buffer P1 is stable for 6 months.

³Buffer N3 and Buffer PB contain guanidine hydrochloride, which can form highly reactive compounds when combined with bleach. If spilled, clean with appropriate laboratory detergent and water.

⁴Buffer PB removes endonucleases, ensuring that the plasmid DNA does not get degraded. If spilled, clean with appropriate laboratory detergent (must not contain bleach) and water.

⁵Buffer PE removes salts. 96-100% ethanol should be added before use.

⁵Buffer EB can be otherwise replaced with TE Buffer (10 mM Tris-Cl; 1 mM EDTA; pH 8.0) or water for DNA elution. If using water, ensure DNA is stored between -30 and -15 °C.

⁶ND-1000 Spectrophotometer was used to measure absorbance.

Table A5. Sanger Sequencing Reaction Components

Reagent	Volume Added	Final Concentration
Purified Plasmid ¹	9 uL	-
25 uM T7 Forward Primer ²	1.5 uL	2.5 uM
25 uM T7 Reverse Primer	1.5 uL	2.5 uM
Milli-Q Water	4.5 uL (fill to 15 uL)	-

¹Mutant plasmid was purified using the Qiagen Miniprep kit.

² Either the Forward or Reverse primer was used for each sequencing reaction prepared.

Bibliography

- Coady, A., Xu, M., Phung, Q., Cheung, T. K., Bakalarski, C., Alexander, M. K., Lehar, S. M., Kim, J., Park, S., Tan, M.-W., & Nishiyama, M. (2015). The *Staphylococcus aureus* ABC-Type Manganese Transporter MntABC Is Critical for Reinitiation of Bacterial Replication Following Exposure to Phagocytic Oxidative Burst. *PLOS ONE*, 10(9), e0138350.
<https://doi.org/10.1371/journal.pone.0138350>
- DeWitt, M. A., Kliegman, J. I., Helmann, J. D., Brennan, R. G., Farrens, D. L., & Glasfeld, A. (2007). The Conformations of the Manganese Transport Regulator of *Bacillus subtilis* in its Metal-free State. *Journal of Molecular Biology*, 365(5), 1257–1265. <https://doi.org/10.1016/j.jmb.2006.10.080>
- Errington, J., & Aart, L. T. V. D. (2020). Microbe Profile: *Bacillus subtilis*: model organism for cellular development, and industrial workhorse: This article is part of the Microbe Profiles collection. *Microbiology*, 166(5), 425–427.
<https://doi.org/10.1099/mic.0.000922>
- Glasfeld, A., Guedon, E., Helmann, J. D., & Brennan, R. G. (2003). Structure of the manganese-bound manganese transport regulator of *Bacillus subtilis*. *Nature Structural & Molecular Biology*, 10(8), 652–657.
<https://doi.org/10.1038/nsb951>
- Gozzi, K., Ching, C., Paruthiyil, S., Zhao, Y., Godoy-Carter, V., & Chai, Y. (2017). *Bacillus subtilis* utilizes the DNA damage response to manage multicellular development. *Npj Biofilms and Microbiomes*, 3(1), 8.
<https://doi.org/10.1038/s41522-017-0016-3>
- Helmann, J. D. (2003). Purification of *Bacillus subtilis* RNA Polymerase and Associated Factors. In *Methods in Enzymology* (Vol. 370, pp. 10–24). Elsevier. [https://doi.org/10.1016/S0076-6879\(03\)70002-0](https://doi.org/10.1016/S0076-6879(03)70002-0)

- Helmann, J. D. (2014). Specificity of Metal Sensing: Iron and Manganese Homeostasis in *Bacillus subtilis*. *The Journal of Biological Chemistry*, 289(41), 28112–28120. <https://doi.org/10.1074/jbc.R114.587071>
- Hilgarth, R. S., & Sarge, K. D. (n.d.). *Detection of Sumoylated Proteins*.
- Honda, M., Razzaghi, M., Gaur, P., Malacaria, E., Di Biagi, L., Aiello, F. A., Paintsil, E. A., Stanfield, A., Deppe, B. J., Gakhar, L., Schnicker, N. J., Spies, M. A., Pichierri, P., & Spies, M. (2023). *Human RAD52 double-ring remodels replication forks restricting fork reversal* [Preprint]. Biochemistry. <https://doi.org/10.1101/2023.11.14.566657>
- Huang, X., Shin, J.-H., Pinochet-Barros, A., Su, T. T., & Helmann, J. D. (2017). *Bacillus subtilis* MntR coordinates the transcriptional regulation of manganese uptake and efflux systems. *Molecular Microbiology*, 103(2), 253–268. <https://doi.org/10.1111/mmi.13554>
- Inaoka, T., Matsumura, Y., & Tsuchido, T. (1999). SodA and Manganese Are Essential for Resistance to Oxidative Stress in Growing and Sporulating Cells of *Bacillus subtilis*. *Journal of Bacteriology*, 181(6), 1939–1943. <https://doi.org/10.1128/JB.181.6.1939-1943.1999>
- Jakubovics, N. S., & Jenkinson, H. F. (2001). Out of the iron age: New insights into the critical role of manganese homeostasis in bacteria. *Microbiology*, 147(7), 1709–1718. <https://doi.org/10.1099/00221287-147-7-1709>
- Jun, S.-H., Warner, B. A., & Murakami, K. S. (2013). RNA Polymerase Reaction in Bacteria. In *Encyclopedia of Biological Chemistry* (pp. 167–172). Elsevier. <https://doi.org/10.1016/B978-0-12-378630-2.00629-0>
- Kriegman, J. I., Griner, S. L., Helmann, J. D., Brennan, R. G., & Glasfeld, A. (2006). Structural Basis for the Metal-Selective Activation of the Manganese Transport Regulator of *Bacillus subtilis*. *Biochemistry*, 45(11), 3493–3505. <https://doi.org/10.1021/bi0524215>
- Kroos, L., Zhang, B., Ichikawa, H., & Yu, Y. N. (1999). Control of σ factor activity during *Bacillus subtilis* sporulation. *Molecular Microbiology*, 31(5), 1285–1294. <https://doi.org/10.1046/j.1365-2958.1999.01214.x>

- Kysela, D. T., Brown, P. J. B., Huang, K. C., & Brun, Y. V. (2013). Biological Consequences and Advantages of Asymmetric Bacterial Growth. *Annual Review of Microbiology*, 67(1), 417–435. <https://doi.org/10.1146/annurev-micro-092412-155622>
- Lieser, S. A., Davis, T. C., Helmann, J. D., & Cohen, S. M. (2003). DNA-Binding and Oligomerization Studies of the Manganese(II) Metalloregulatory Protein MntR from *Bacillus subtilis*. *Biochemistry*, 42(43), 12634–12642. <https://doi.org/10.1021/bi0350248>
- Martin, R. B. (1987). A stability ruler for metal ion complexes. *Journal of Chemical Education*, 64(5), 402. <https://doi.org/10.1021/ed064p402>
- Murdoch, C. C., & Skaar, E. P. (2022). Nutritional immunity: The battle for nutrient metals at the host–pathogen interface. *Nature Reviews Microbiology*, 20(11), 657–670. <https://doi.org/10.1038/s41579-022-00745-6>
- Newing, T. P., Oakley, A. J., Miller, M., Dawson, C. J., Brown, S. H. J., Bouwer, J. C., Tolun, G., & Lewis, P. J. (2020). Molecular basis for RNA polymerase-dependent transcription complex recycling by the helicase-like motor protein Held. *Nature Communications*, 11(1), 6420. <https://doi.org/10.1038/s41467-020-20157-5>
- Partridge S.R., Foulger D., Errington J. (1991). The role of sigma F in prespore-specific transcription in *Bacillus subtilis*. *Molecular Microbiology*, 11(3), 757–67. doi: 10.1111/j.1365-2958.1991.tb00746.x. PMID: 1904527.
- Que, Q., & Helmann, J. D. (2000). Manganese homeostasis in *Bacillus subtilis* is regulated by MntR, a bifunctional regulator related to the diphtheria toxin repressor family of proteins. *Molecular Microbiology*, 35(6), 1454–1468. <https://doi.org/10.1046/j.1365-2958.2000.01811.x>
- Sazykin, I. S., & Sazykina, M. A. (2023). The role of oxidative stress in genome destabilization and adaptive evolution of bacteria. *Gene*, 857, 147170. <https://doi.org/10.1016/j.gene.2023.147170>
- Seshasayee, A. S. N., Sivaraman, K., & Luscombe, N. M. (2011). An Overview of Prokaryotic Transcription Factors: A Summary of Function and

Occurrence in Bacterial Genomes. In T. R. Hughes (Ed.), *A Handbook of Transcription Factors* (Vol. 52, pp. 7–23). Springer Netherlands.

https://doi.org/10.1007/978-90-481-9069-0_2

Swint-Kruse, L., & Matthews, K. S. (2013). Lac Operon. In *Encyclopedia of Biological Chemistry* (pp. 694–700). Elsevier. <https://doi.org/10.1016/B978-0-12-378630-2.00249-8>

Tikhomirova, A., Rahman, M. M., Kidd, S. P., Fererro, R. L., & Roujeinikova, A. (2024). Cysteine and resistance to oxidative stress: Implications for virulence and antibiotic resistance. *Trends in Microbiology*, 32(1), 93–104. <https://doi.org/10.1016/j.tim.2023.06.010>

Turrens, J. F. (2003). Mitochondrial formation of reactive oxygen species. *The Journal of Physiology*, 552(2), 335–344. <https://doi.org/10.1113/jphysiol.2003.049478>

White, A., Ding, X., vanderSpek, J. C., Murphy, J. R., & Ringe, D. (1998). Structure of the metal-ion-activated diphtheria toxin repressor / tox operator complex. *Nature*, 394(6692), 502–506. <https://doi.org/10.1038/28893>